INVESTIGATION OF METAL-ION BINDING IN THE FOUR-WAY JUNCTION CONSTRUCT OF THE HAIRPIN RIBOZYME

A Thesis

by

AURELIE L. BUCKELEW

Submitted to the Office of Graduate Studies of
Texas A&M University
in partial fulfillment of the requirements for the degree of

MASTER OF SCIENCE

May 2005

Major Subject: Chemistry

INVESTIGATION OF METAL-ION BINDING IN THE FOUR-WAY JUNCTION CONSTRUCT OF THE HAIRPIN RIBOZYME

A Thesis

by

AURELIE L. BUCKELEW

Submitted to the Office of Graduate Studies of
Texas A&M University
in partial fulfillment of the requirements for the degree of

MASTER OF SCIENCE

Approved as to style and content by:

Victoria J. DeRose
(Chair of Committee)

Kim R. Dunbar
(Member)

David P. Giedroc
(Member)

Donald J. Darensbourg
(Member)

Emile A. Schweikert
(Head of Department)

May 2005

Major Subject: Chemistry

ABSTRACT

Investigation of Metal-Ion Binding in the Four-Way Junction Construct of the Hairpin Ribozyme. (May 2005)

Aurélie L. Buckelew, B.A., Texas A&M University

Chair of Advisory Committee: Dr. Victoria J. DeRose

The hairpin ribozyme is a small catalytic RNA that cleaves a phosphodiester bond. In order for cleavage to occur, the hairpin ribozyme must properly fold into its docked conformation, in which the two loops interact to form the active site. Metal ions and the four-way junction play critical roles in the stabilization of the docked conformation. The work presented in this thesis attempts to investigate the metal-ion dependence of the docking of the four-way junction construct of the hairpin ribozyme. In addition, the activity of the hairpin ribozyme in the presence of Mn^{2+} was observed. Initially, a four-stranded four-way junction construct of the hairpin ribozyme and a loopless mutant were characterized by native gel electrophoresis and thermal denaturation to verify ribozyme formation.

A novel interaction between the sulfur of a phosphorothioate-substituted mononucleotide, such as adenosine thiomonophosphate (AMPS) or adenosine thiotrisphoshate (ATPγS), and Cd^{2+} has been characterized by UV-vis spectroscopy. A feature at 208 nm was identified to be a result of sulfur-to-Cd^{2+} transfer. The apparent binding affinities, the apparent extinction coefficients, and the binding ratios were determined for each complex.

ACKNOWLEDGEMENTS

First and foremost, I would like to thank my advisor, Dr. DeRose, as well as my committee members, for their support and guidance throughout the hurdles of graduate school.

I would like to acknowledge the DeRose group members as well, particularly Matt, Murali, Nak-Kyoon, and Edith, for their helpful scientific discussions and for their guidance.

As for my friends, you all have been so supportive and understanding over the years. I'll never forget you guys and we'll always keep in touch. In particular, Dr. Rockcliffe, I won't forget our many conversations about our experiences traveling the world and I'll miss our dinners. Murali, please continue sending us pictures of your adorable daughter. And Shayna, I'll truly miss you.

Of course, I cannot forget to thank my parents who have been there for me all my life. Throughout all our moves, you have been my constant comfort, my constant support. Thank you for always believing in me during these challenging years in graduate school as well. I'm so fortunate to have you!

Matt, when I'm with you, I feel I can accomplish anything. Your inspiring talks, visions, and hopes are contagious and I look forward to our happy future together.

TABLE OF CONTENTS

CHAPTER Page

Page

LIST OF FIGURES

FIGURE Page

FIGURE Page

LIST OF TABLES

CHAPTER I

INTRODUCTION

Nucleic Acids

The ability of nucleic acids to store genetic information and then, to express this information highlights the fundamental value of these macromolecules. There are two types of nucleic acids: deoxyribonucleic acid (DNA) and ribonucleic acid (RNA). DNA has the critical role of storing an organism's genetic information whereas RNA molecules have a multitude of functions, most of which are involved in translating the genes into proteins.[1]

The primary structure of nucleic acids arises from a chain of nucleotides all of which are linked by a negatively-charged phosphodiester backbone. (Figure 1-1) Three basic "building blocks" form a nucleotide: a five-membered sugar, a nitrogenous base, and a negatively-charged phosphate group. The sugar found in RNA is a ribose, which has a hydroxyl group located in the 2' position while DNA is composed of the sugar deoxyribose, which lacks the 2' hydroxyl group. The hydrogen bond donor/acceptor characteristics of the 2'OH contribute greatly to the diversity and complexity of RNA structures, which leads to the variety of functions of RNA. The five nitrogenous bases are adenine, cytosine, guanine, thymine, and uracil. Adenine and guanine are purine bases since they possess two fused heteroatom rings whereas cytosine, thymine, and uracil are pyrimidine bases, which have only one heteroatom six-member ring. Another difference between DNA and RNA arises from the presence of thymine in DNA and uracil in RNA. Besides the two non-bridging oxygens, the other two oxygens of the

---

This thesis follows the format of *Journal of American Chemical Society.*

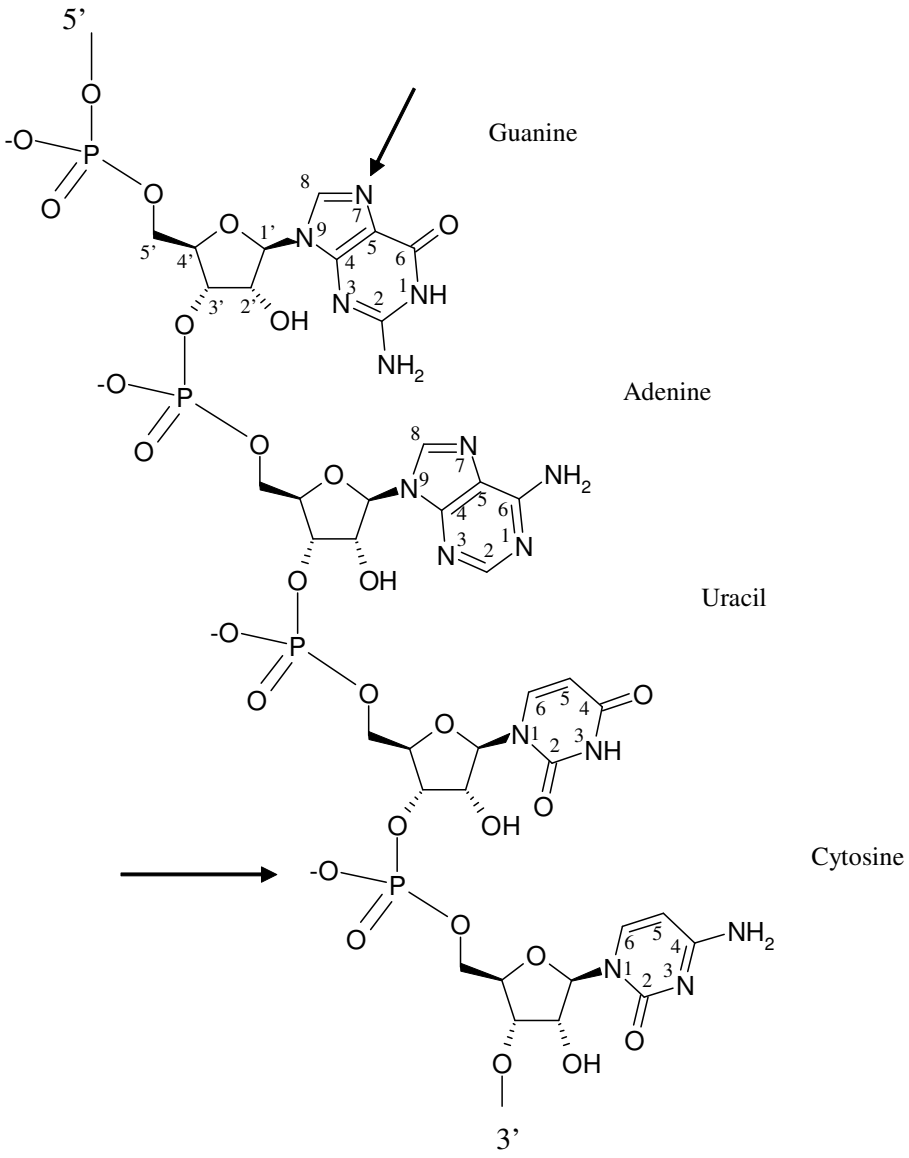

Figure 1-1: The primary structure of an oligonucleotide. The nitrogenous base is attached to the 1' position of the ribose sugar. The hydroxyl group is located at the 2' position. One oxygen of the phosphate group is linked to the 3' position of one sugar while the other is attached to the 5' position of the adjacent sugar, resulting in a phosphodiester bond.

phosphate group links the 3' position of one sugar to the 5'position of the adjacent sugar, resulting in a phosphodiester bond (Figure 1-1).[1]

The secondary structure of nucleic acids arises from canonical Watson-Crick base pairing, which is hydrogen bonding between adenine and thymine (in DNA), adenine and

uracil (in RNA), and cytosine and guanine. The A-T and A-U bases pair through two hydrogen bonds whereas the C-G bases pair via 3 hydrogen bonds (Figure 1-2).

Guanine

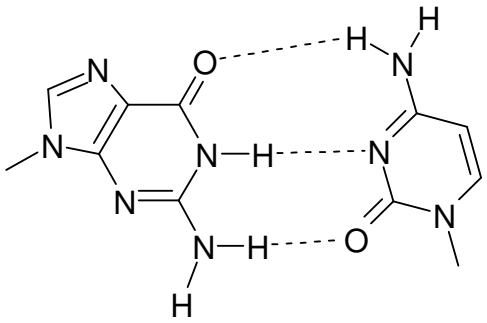

Cytosine

Adenine

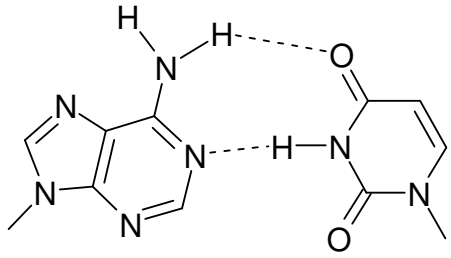

Uracil

Figure 1-2: Canonical Watson-Crick base pairs forming secondary structure.

The stacking of base pairs forms a double helix, within which the planes of the bases are approximately perpendicular to the helical axis, and the phosphodiester groups are exposed to the solvent. The driving force of this double-helical structure is the burial of the hydrophobic bases (Figure 1-3). Differing sugar conformations leads to three major double helices: the A form, B form, and Z form. The 2'OH of the ribose sugar favors the

C3'-*endo* conformer, resulting in the A-form helix. In contrast, the deoxyribose favors the C2'- *endo* puckering, which leads to the most common form of DNA, the B form.[1] DNA is generally found to be composed of two strands that form a double helix while RNA is often a single strand that folds to form secondary structures such as helices, loops, bulges, and junctions.[2]

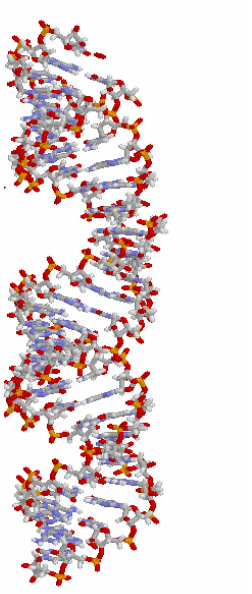

Figure 1-3: An example of secondary structure: a base-paired helical duplex. The driving force of the helical structure is the burial of the hydrophobic bases. The crystal structure of this RNA duplex is from the PDB with code of IQC0.

Tertiary structure arises from interactions between the secondary structural elements, thereby leading to more complex structures. In contrast to DNA, RNA molecules tend to form folded structures that are highly complex, compact, and stable.[3] The folding of RNA systems into their distinctive proper conformations is a prerequisite

for functionality. The folding pathway is hierarchical as the secondary structure forms, and then the RNA molecule proceeds to collapse into its compact tertiary structure (Figure 1-4).[4, 5] The intricate tertiary structure of RNA is attributed to the 2'OH of the ribose, which accommodates hydrogen bond donating/accepting abilities. An example of a distinctive tertiary structure is that of tRNA, which resembles an "L".[6] The complexity of the RNA folding pathway is due to a more rugged energy landscape, allowing for multiple folding pathways and intermediates. [7, 8]

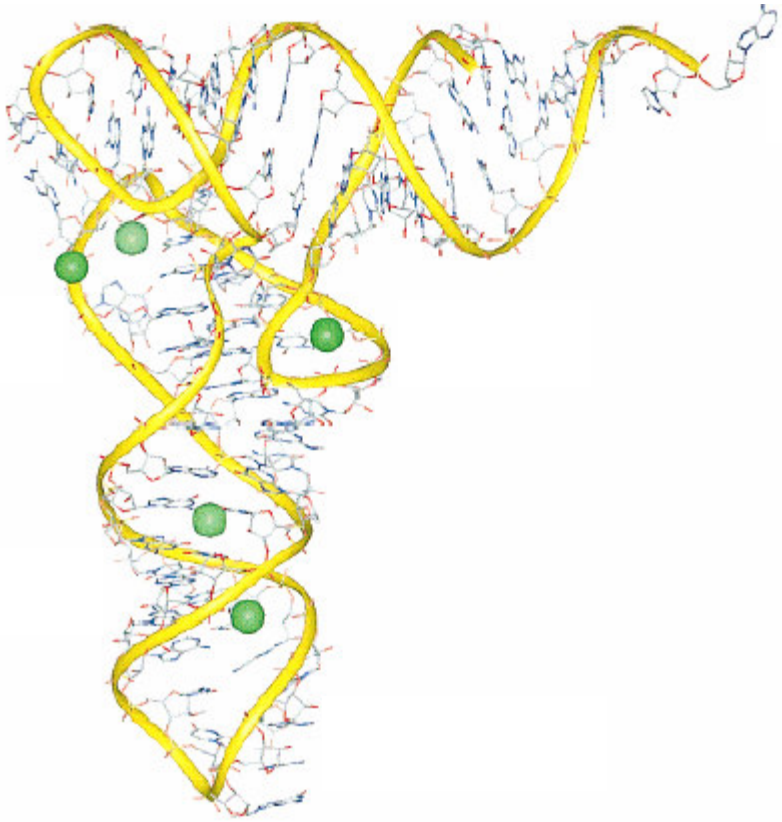

Figure 1-4: An example of tertiary structure: tRNA has a distinctive "L"shape. Tertiary contacts, arising from complex hydrogen bond networks, leads to a functional structure. The green spheres represent bound magnesium ions.[6]

Metal Ion – RNA Interactions

The folding of RNA molecules is highly dependent on metal ion concentrations. Negatively-charged non-bridging oxygens along the phosphodiester backbone render nucleic acids polyanionic. Metal ions stabilize the RNA structure allowing the backbone to fold back on itself since they electrostatically shield the anionic phosphate groups from each other.[9] Monovalent cations (the most common of which are Na^+ and K^+ *in vivo*) tend to be involved in diffuse, or "territorial" binding, which is the association of a mobile charged layer of hydrated cations with the polyanionic nucleic acid.[2] (Figure 1-5) During

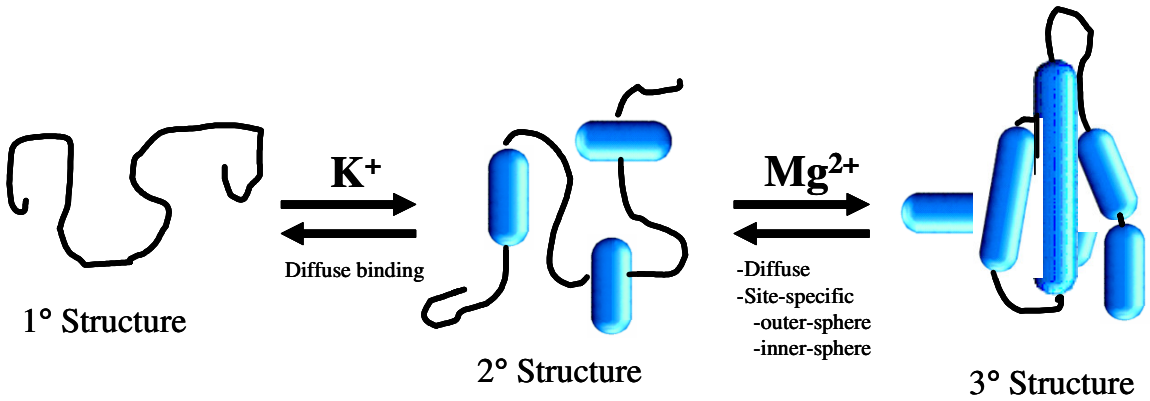

Figure 1-5: The role of metal ions during the folding pathway of an RNA molecule. Monovalent cations interact with the polyanionic RNA molecule electrostatically to promote formation of secondary structure. Divalent cations may bind with the RNA diffusely or specifically to encourage the collapse of the RNA molecule into its properly folded conformation.[3]

the formation of the tertiary structure, divalent cations, such as Mg^{2+} *in vivo*, are often required and may bind specifically or non-specifically. In specific binding, one or more water ligands are replaced by a ligand from the RNA, resulting in inner-sphere coordination. Another case of specific binding is outer-sphere coordination, from which

the divalent metal ion is bound to the RNA by through-water contacts. In contrast, nonspecific binding is described by the association of fully-hydrated cations with regions of negative electrostatic potential of the RNA.[1]

It is proposed that structurally and catalytically important metal ions in RNA tend to remain either fully or partially hydrated.[9, 10] Metal ion- RNA interactions are typically

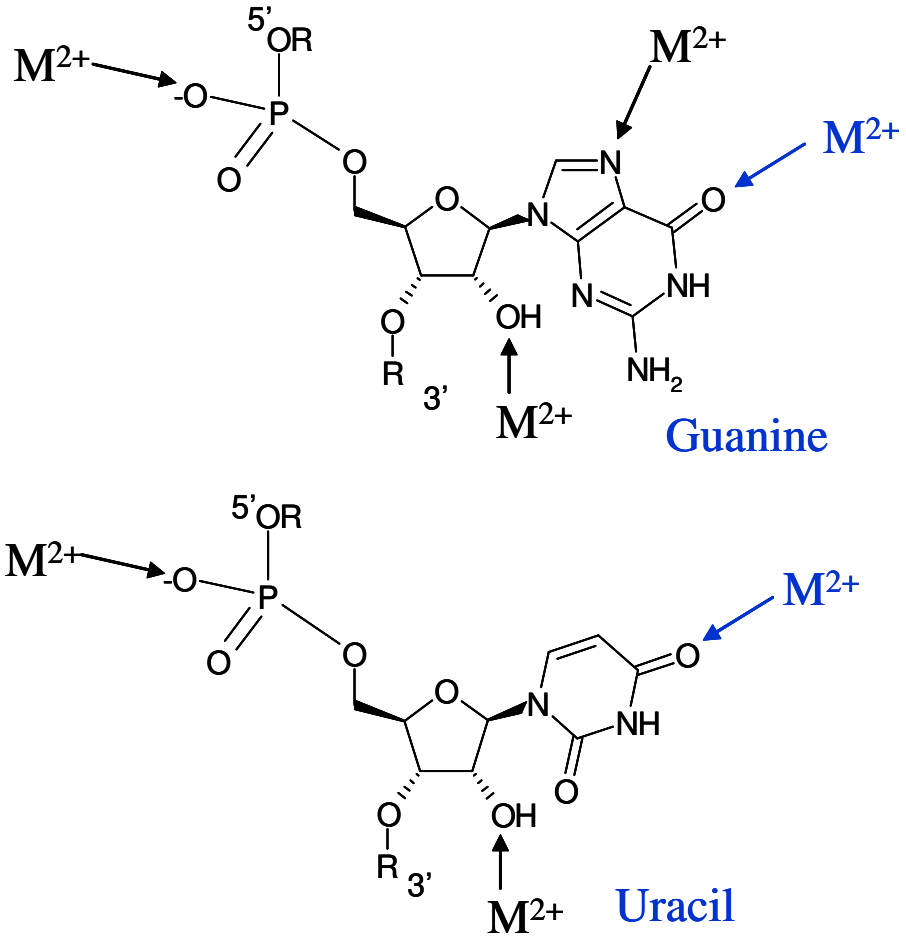

Figure 1-6: Common sites for specific metal-ion binding. They are the phosphoryl oxygens, the guanine N7 heteroatom, the O6 keto oxygen atom, and even the 2'OH of the ribose sugar.[3]

in regions of highly negative potential, which allows for favorable electrostatic interactions to compensate for the high energetic penalty of dehydration of the metal ion sphere.[10] Some common RNA ligands include the phosphoryl oxygens, the guanine N7 heteroatom, the O6 keto oxygen atom, and the 2'hydroxyl of the ribose sugar (Figure 1-6).[2] Numerous crystal structures of RNA molecules and even isolated nitrogenous bases have revealed these typical metal-RNA interactions.[1]

Metal ions, such as Mn^{2+}, $[Co(NH_3)_6]^{3+}$, Cd^{2+}, Hg^{2+}, Tb^{3+} and other lanthanides have served as structural probes in RNA molecules.[1, 2] Due to the similar charge-to-radius ratios, coordination preferences, and enthalpy of hydration between Mg^{2+} and Mn^{2+} ions, the latter serves as an effective substitute for Mg^{2+} ions in spectroscopic studies. Therefore, the paramagnetic Mn^{2+} can be utilized as a probe for divalent metal sites when monitored by EPR spectroscopy.[1, 11, 12] In addition, metal ion binding sites may be located by NMR paramagnetic line broadening induced by bound Mn^{2+} ions.[2] Cobalt(III) hexammine, $[Co(NH_3)_6]^{3+}$, is a substitution-inert complex, in which the ammine ligands are not exchanged with aqua molecules, thereby enabling one to probe for outer-sphere metal-ion binding.[1] The thiophilicity of Cd^{2+} promotes a stronger interaction than Mg^{2+} for the sulfur of a phosphorothioate-substituted RNA and this interaction can be detected by ^{31}P NMR. For example, Cd^{2+} has been observed by ^{31}P NMR to bind to the pro-R and pro-S sulfur of a phosphorothioate at the functionally important A9 site of the hammerhead ribozyme.[13] UV-vis spectroscopy has revealed a charge transfer band resulting from the coordination of a thiophilic Hg^{2+} ion to a sulfur in samples that contain a phosphorothioate modification placed at the active site.[14] Tb^{3+} has been found to inhibit the function of RNA systems by displacing critical Mg^{2+} ions.[15] In

addition, the luminescence of Tb^{3+} and other lanthanides have been used to locate metal binding sites and to determine relative affinities of other metal ions by competition studies.[16]

RNA Systems

During the process of protein synthesis directed by genetic instructions simply encoded from the four-base "language" of DNA, each type of RNA molecule functions to achieve its designated purpose, without which life would not be sustained. First of all, messenger RNA (mRNA) relays the information specifying amino acid sequences of proteins from DNA in the nucleus to the ribosome, the RNA-protein complex in which proteins are synthesized. However, in eukaryotes, before it leaves the nucleus for a ribosome, mRNA must be processed by the spliceosome, which is a complex assembly of small nuclear RNA (snRNA) and proteins. Each transfer RNA molecule (tRNA) serves as a translator between an amino acid and three RNA nucleotides (codon) of the mRNA, and transports the amino acid to the ribosome. The ribosome is composed of ribosomal RNA (rRNA) as well as proteins. It is now believed that the rRNA is enzymatic as it catalyzes peptide bond synthesis. In addition, short interfering RNAs (siRNAs) down-regulates gene expression upon binding to complementary mRNA by either causing RNA interference or stopping mRNA translation into protein.[17]

Ribozymes

Prior to 1982, RNA was known mainly for its role as passive carriers of genetic information and amino acids. The discovery of the self-splicing catalysis of the rRNA of the ciliate *Tetrahymena*, led to the eventual discoveries of more of these "ribozymes", or catalytic RNA.[18] The following year, Altman reported that the RNA component of RNase

P is the catalytically active unit.[19] Since then, the functions of RNA have broadened to include ribosomal peptide bond formation, RNA splicing and ligation, and translational regulation.[2] Ribozymes have been found in plants, bacteria, viruses, lower eukaryotes, and prokaryotes. In addition, rRNA of the ribosome is now believed to be catalytic as mentioned earlier.[20, 21] Ribozymes increase rates of phosphoryl transfer reactions by up to 10^{11}-fold and promote reaction efficiencies, k_{cat}/K_M, up to 10^8 $M^{-1}min^{-1}$.[21]

Ribozymes may be classified into one of two categories based on their size and reaction mechanism. Large ribozymes, ranging from 200-3000 nucleotides in length, include the group I intron, group II intron, and RNase P. They catalyze phosphodiester

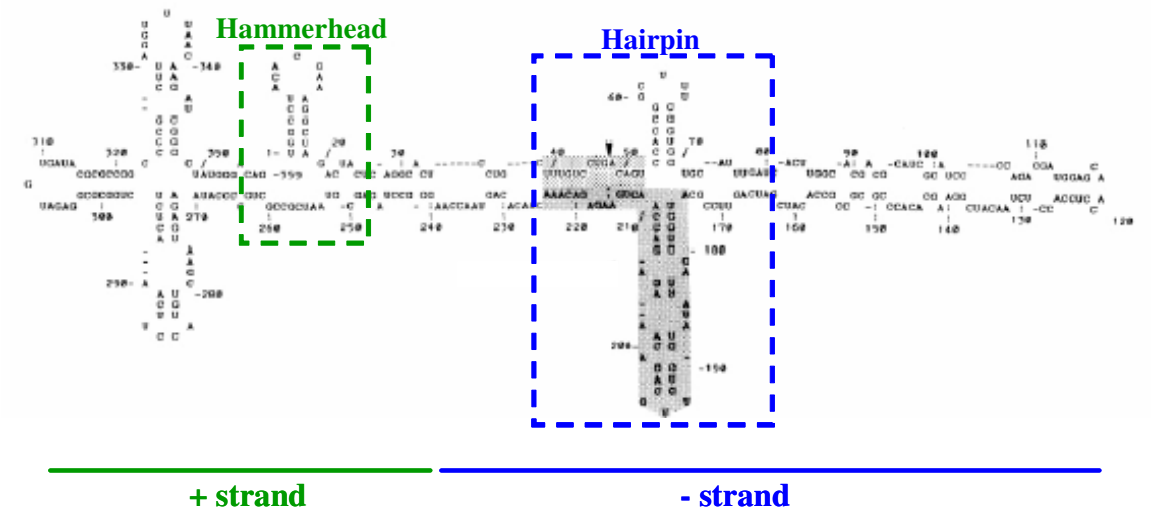

Figure 1-7: sTRSV RNA genome, 359 nucleotides in length. The hammerhead resides in the positive strand whereas the hairpin ribozyme is located in the negative strand.[24]

bond cleavage, resulting in 3'hydroxyl and 5'phosphate termini.[21] On the other hand, small ribozymes include the truncated motifs of the hairpin, hammerhead, hepatitis delta virus and *Neurospora* VS ribozymes and the size ranges from 35 -100 nucleotides. These small catalytic RNAs catalyze a reversible cleavage reaction, generating 2', 3'-cyclic phosphate and 5' hydroxyl termini.[22]

The hammerhead ribozyme has been extensively studied and is the best characterized small ribozyme. The hammerhead ribozyme is located in the positive strand of an RNA genome, which harbors the hairpin catalytic motif as well, but in its negative strand (Figure 1-7). [23] Both ribozymes are found in the satellite tobacco ringspot viral RNA genome, involved in processing RNA replication intermediates via cleavage and ligation reactions.[24] However, the two ribozymes are structurally unrelated, and therefore, each has its own catalytic strategy, including the role designated for metal ions. In the truncated versions most extensively studied, the equilibrium of the hairpin ribozyme between the two reactions favors ligation compared to the hammerhead, which favors the cleavage reaction.[24]

The Hairpin Ribozyme

The hairpin ribozyme was originally discovered in the negative strand of satellite RNA of the tobacco ringspot virus in 1986 and can be found in the chicory yellow mottle virus type 1 and the arabis mosaic virus as well.[25] Two constructs of the hairpin ribozyme, the minimal and the native, have been utilized for studies (Figure 1-8). The minimal, or hinged, construct consists of two domains, each of which contains an internal loop in between two short base-paired helices. Domain A consists of the substrate and the substrate-binding ribozyme sequence whereas Domain B is located entirely within the

ribozyme. The single-stranded connection between the domains acts as a flexible hinge, allowing the loops to interact via tertiary interactions between their critical nucleotides. The loop-loop interaction is called "docking", a prerequisite for catalysis. The cleavage site is located within loop A, 5' to a conserved guanine. Almost all of the bases required for activity are located within these loops, indicative of their involvement in tertiary contacts or direct participation in cleavage and ligation.[23]

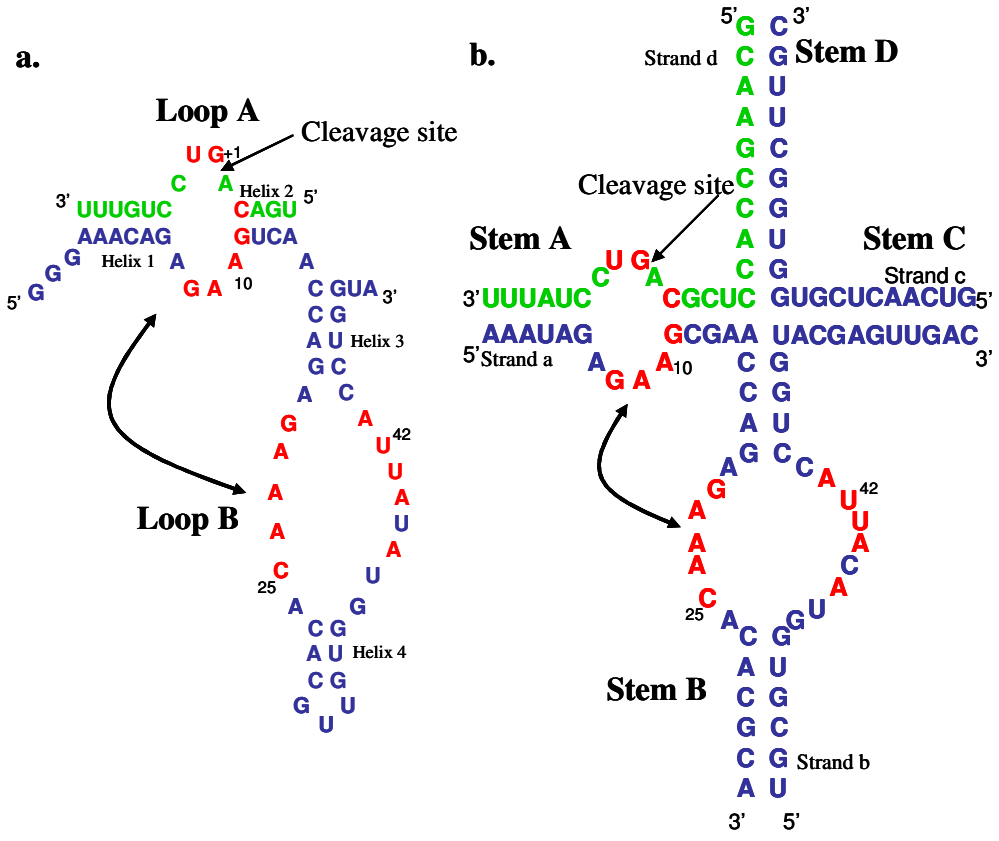

Figure 1-8: The secondary structure of two constructs of the hairpin ribozyme. (a.) the minimal, or hinged, construct and (b.) the native, or four-way junction construct. Cleavage/ligation of the substrate (shown in green) occurs 5' to G+1. Both structures contain the vital loop-carrying stems. However, the four-way junction construct contains a four-way junction and two additional base-paired helical stems.

The minimal, or hinged, structure of the hairpin ribozyme requires a maximum of only 50 nucleotides to be catalytically active (Figure 1-8(a.)). Therefore, the extensive focus on this construct has been due to its relative simplicity. However, the minimal construct requires 10-12 millimolar concentrations of Mg^{2+} to be functional. This requirement accounts for its drop in activity under physiological conditions (~2mM $MgCl_2$ and 150mM NaCl).[26] As a result, more focus has been shifted to the native construct, which retains full activity under cellular conditions. The native construct consists of the same two domains found in the minimal as well as two additional helices, all of which are connected via a four way helical junction. This key architectural element stabilizes the folded tertiary structure and increases the rate of folding at lower Mg^{2+} (0.5mM) according to single-molecule FRET studies. Upon addition of divalent metal ions, the four-way junction efficiently positions the loops such that they are primed for interaction by rotation into an antiparallel intermediate closer in structure to the folded conformation (Figure 1-9).[28] The antiparallel conformation arises from the stacking of

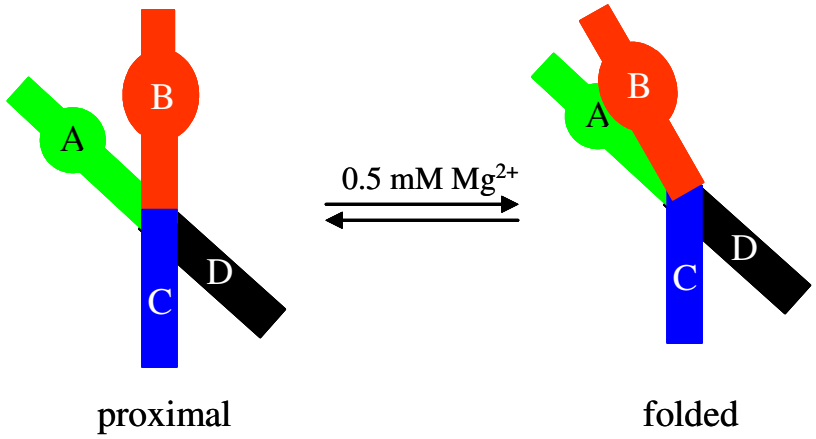

Figure 1-9: Loop-loop interaction facilitated by the four-way junction rotating the arms into a proximal state in Mg^{2+}.[27]

stem C onto stem B and stem D onto stem A allowing for the loops A and B to come into close proximity. The discovery of an antiparallel intermediate is consistent with a more recent study by Millar and coworkers employing single-pair FRET measurements. This study determined that the formation of the hydrogen bonding network between the two docked loops is facilitated by the four way junction stabilizing the arms in a "quasi-docked" state.[29]

Once in the docked state during which tertiary contacts have formed between the loops, catalysis is initiated by the abstraction of the proton of the 2'hydroxyl group, which subsequently attacks the adjacent scissile phosphorus. This attack by the 2'oxygen results in a negatively-charged trigonal bipyramidal transition state. The cleaved products, a 2', 3' cyclic phosphate and 5'OH termini, are then formed with an inversion of configuration, indicative of an S_N2 in-line attack mechanism (Figure 1-10).[30] It is

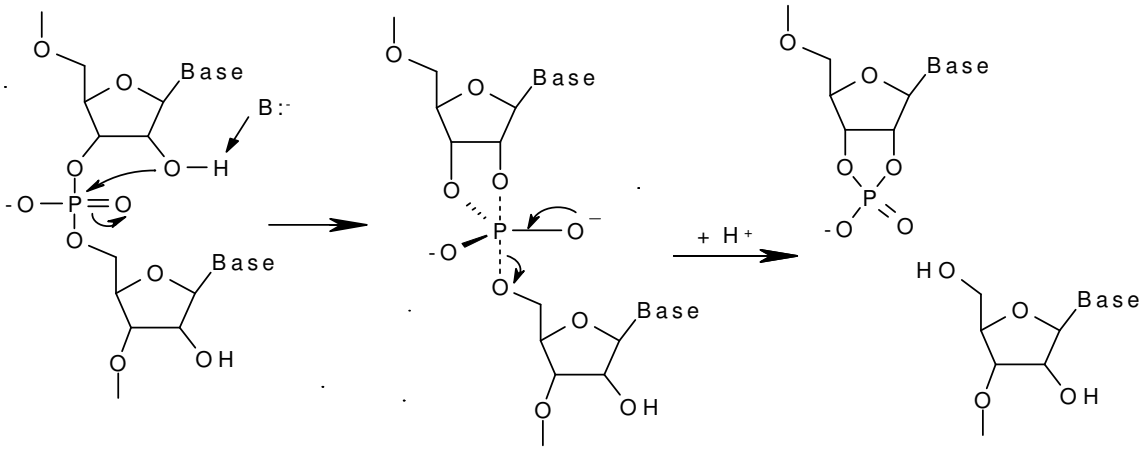

Figure 1-10: The mechanism for site-specific phosphodiester bond cleavage.

proposed that some ribozymes, such as the hammerhead and the group I intron, use water-bound metal ions to facilitate proton abstraction, to electrostatically stabilize the transition state, or to protonate the 5'oxygen leaving group.[31] In addition, unlike amino acids, nucleosides do not have pK_a's near physiological pH, making them unlikely candidates in general acid-base catalysis.[20] However, in the case of the hairpin ribozyme, its lack of both pH dependence and ionic preference on activity indicates that metal ions do not have a direct catalytic role (This will be discussed more later.) Therefore, the catalytic mechanism of the hairpin ribozyme must require nucleotide bases with perturbed pK_a values in the active site. The ability of RNA to perform general acid-base catalysis without the aid of proteins or metal ion cofactors has been previously proposed in the active sites of the HDV ribozyme and the peptidyl-transferase of the 50S ribosomal subunit.[20]

The hairpin ribozyme requires metal ions to electrostatically stabilize its structure and to facilitate docking into the active conformation, indicative of their structural role. Using FRET, Lilley *et. al.* determined that docking of the four-way junction construct occurs subsequent to the binding of polyvalent metal ions in the presence of Mg^{2+}, Mn^{2+}, Ca^{2+}, Sr^{2+}, or $[Co(NH_3)_6]^{3+}$.[32]

At this point, research has excluded direct catalytic involvement from the role of metal ions in hairpin catalysis. Phosphorothioate substitutions at the active site of the hinged construct display only a small effect on cleavage and ligation activity compared to the hairpin with unmodified phosphates.[33] In addition, NMR solution structures of the isolated domain A of the hairpin show a complete absence of metal ions.[34] The lack of metal-ion binding within the active site in domain A is confirmed by a 2.4Å-resolution

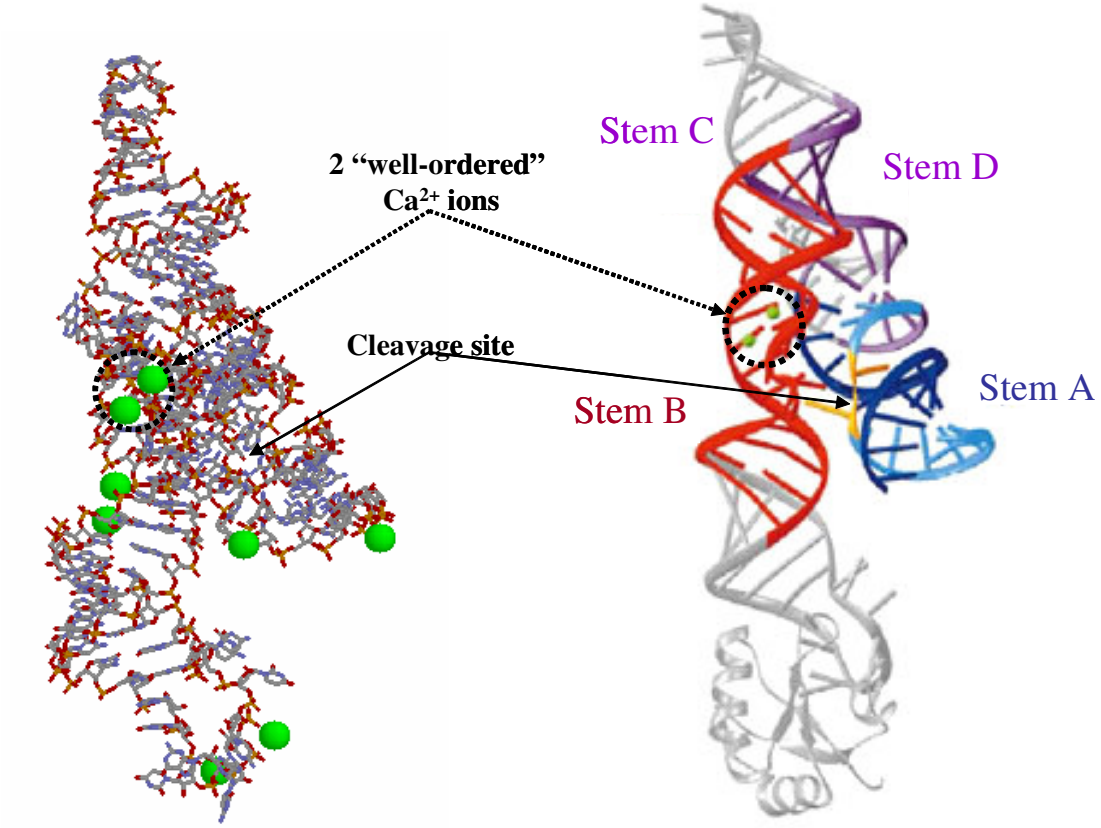

Figure 1-11: 2.4 Å resolution crystal structure of the four-way junction of the hairpin ribozyme. Eight Ca^{2+} ions (green spheres) are reported, two of which are "well-ordered". The crystallization conditions were 5 mM Spermine, 20 mM $CaCl_2$, 200 mM NH_4Cl, 30% MPD.[36] PDB # 1M5K

crystal structure of the docked complex of the four-way junction construct with a 2'O-methyl inhibitor in place of the 2'OH nucleophile (Figure 1-11).[35]

As mentioned earlier, a wide array of divalent metal ions enhance folding into the active conformation and hence, the rate of activity. However, the minimal construct of the hairpin ribozyme maintains high levels of cleavage/ligation activity independent of divalent metal ions, as well. Some studies indicate that high concentrations of monovalent metal ions, such as Na^+ or Li^+, are sufficient to promote catalysis.[36, 37] In fact,

catalysis is supported in the presence of cations in general, including NH_4^+, aminoglycoside antibiotics, and organic polyamines, such as spermine.[33, 37, 38] A study using micromolar concentrations of the aqueous complex, $Tb(OH)(aq)^{2+}$, demonstrated that the Tb^{3+} complex reversibly inhibits the ribozyme.[15] In the same study, a surface charge potential of loop B was constructed, revealing an unusually highly negative "binding pocket" in the major groove, into which Tb^{3+} is proposed to bind. Phosphorothioate modifications of the phosphates lining the pocket resulted in no change in Tb^{3+} inhibition constants, suggestive of outer-sphere cation binding. In addition, the kinetically inert complex, $Co(NH_3)_6^{3+}$, which is structurally similar to the hexahydrated Mg^{2+}, supports cleavage and ligation even more effectively than Mg^{2+}. These findings strongly suggest that inner-sphere coordination of these cations is not required.[15] However, the high-resolution crystal structure of the docked four-way junction construct saturated in 20mM Ca^{2+} reveals that in the wide minor groove of stem B, two "well-ordered" metal ion binding sites exist and the Ca^{2+} ions coordinate the RNA through both inner- and outer-sphere contacts.[35] In contrast, paramagnetic line broadening, chemical shift mapping, and intermolecular NOEs indicate that domain B contains four to five metal binding sites, all of which may be bound by Mn^{2+}, Mg^{2+}, and $Co(NH_3)_6^{3+}$.[39]

Previous optical melt studies of 2-way, 3-way, and 4-way junction constructs of the hairpin ribozyme show only a single transition, suggesting simultaneous, cooperative disruption of all helical structures.[40] However, more recently, derivative analysis of optically-detected thermal denaturation as well as differential scanning calorimetry (DSC) of the 2-way junction, or hinged, construct reveal the presence of at least two distinct peaks, each of which has been correlated to the independent unfolding of each

domain. The results show that domain A clearly unstacks before domain B. In addition to the two major transitions, there is a broad low-temperature feature, the identity of which is uncertain.[41] No transitions had been correlated to the unfolding of tertiary interactions between the loops.

The research described in this thesis focuses on the four-way junction construct, as it is a better representation of the native conformation in the viral RNA genome, it is catalytically active under physiological conditions, and it is more stable. Based on previous studies, metal ions bind to the major groove of domain B just opposite to its docking face. In addition, to induce the conformational transition into the active form, divalent ions are absolutely required.[42] More specifically, the key role of the four-way junction to orientate the loops for interaction in the docked state is aided by the presence of divalent metal ions. This could arise from a potential catalytically/structurally-important metal-binding site within the four-way junction that has not been investigated before. A recent FRET study determined a cooperativity coefficient of 1.02 ± 0.14, which suggests that docking is coupled to the binding of one Mg^{2+} ion. However, the location of the Mg^{2+}-binding site has not been identified.[29] Although the crystal structure of the four-way junction construct of the hairpin ribozyme did not reveal a metal ion within the four-way junction, the solution conditions for crystallization are very different and not necessarily representative of solution conditions in nature.[35, 43] Therefore, the hypothesis of the work presented in this thesis is the requirement of a tightly-bound metal-ion within the four-way junction to induce the stems to rotate into the ribozyme's active antiparallel position. A mutant hairpin ribozyme lacking both loops A and B was

employed in this work to eliminate all other potentially tight metal-binding regions, thereby isolating the four-way junction as the sole region of interest. (Figure 1-12)

In brief, the goals of the work presented in this thesis involve the characterization of the four-way junction construct of the hairpin ribozyme and consequently, the investigation of a putative metal-binding site within the four-way junction to further clarify the catalytic/structural role of metal ions in the hairpin ribozyme. Native gels, thermal denaturation, kinetics, and EPR spectroscopy were employed to achieve these goals.

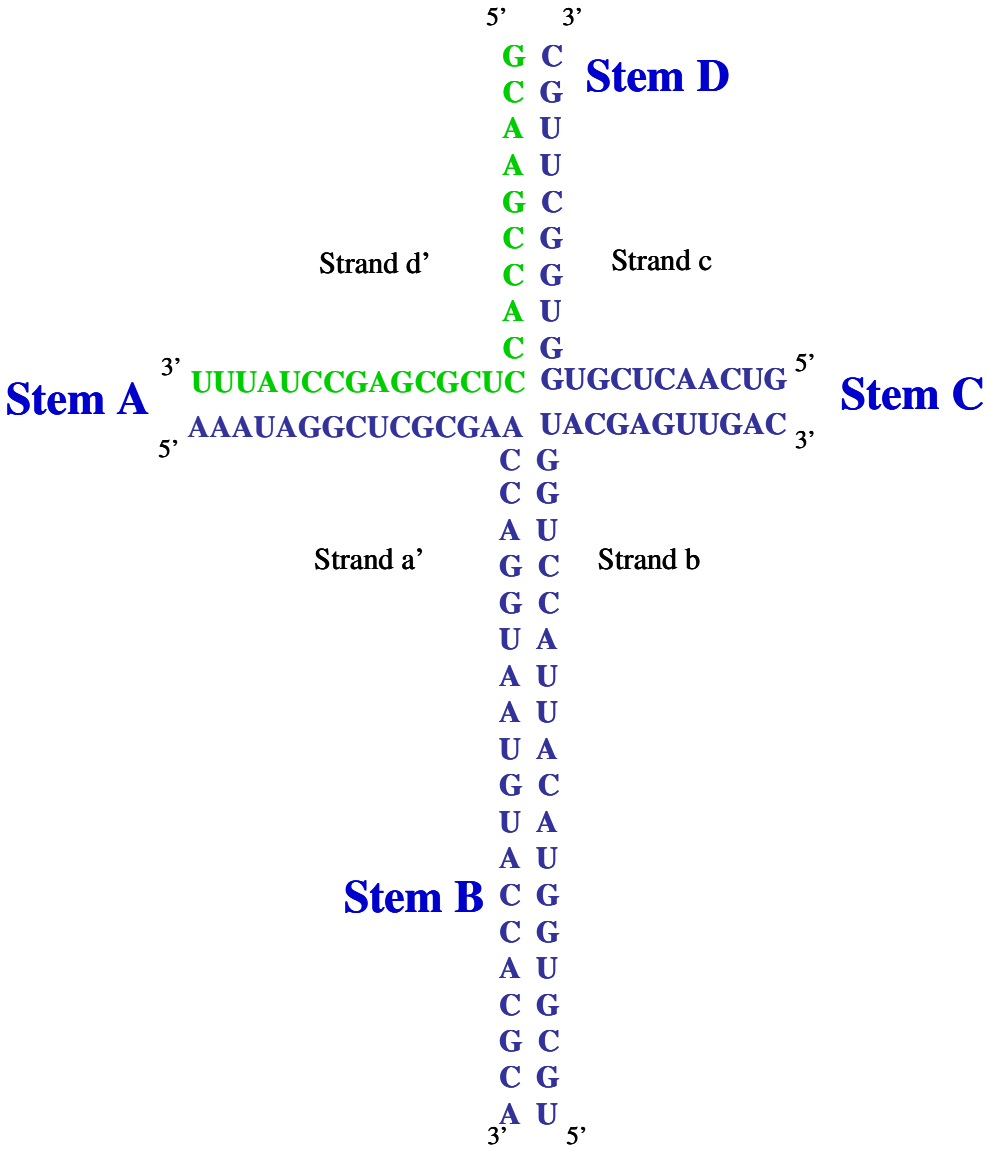

Figure 1-12: The sequence of the mutant hairpin ribozyme. The mutant is composed solely of base-paired helical stems connected via the same four-way junction.

CHAPTER II

MATERIALS AND METHODS

RNA Preparation

RNA was ordered from Dharmacon, where it was synthesized by phosphoroamidite chemistry. The RNA pellet was deprotected upon incubation in 400 µL of acetic acid buffer for 30 minutes at 60°C and then purified by polyacrylamide (20%) gel electrophoresis. The RNA was electroeluted to collect the purified RNA and dialyzed against 5 mM triethanolamine (TEA), 100 mM NaCl, pH 7.8 buffer at 4°C with five reservoir changes for 72h. The RNA was concentrated to 300 - 400 µL and then ethanol-precipitated upon the addition of 1 mL of ethanol and 30 µL of 3 M sodium acetate. After spinning down and drying, the RNA was resuspended in a solution of 40 µL of 5 mM TEA, pH 7.8, and 100 mM NaCl for the hinged contruct and 25 mM NaCl for the native construct. Concentrations were determined by employing a Cary 300 Bio UV/Vis spectrometer to measure the absorbance of the RNA in solution at 260 nm.

The hinged construct consisted of two strands: the 53-mer and the 14-mer. The 14-mer was deoxymodified on the adenine 3' to the cleavage site to prevent cleavage. The extinction coefficients of the 53-mer and 14-mer are 558,100 $Lmol^{-1}cm^{-1}$ and 134,900 $Lmol^{-1}cm^{-1}$, respectively. On the other hand, the native construct was composed of four strands: strand a, strand b, strand c, and strand d. (Figure 2-1) With the exception for activity studies, strand d was deoxymodified at the adenine, 3' to the cleavage site to prevent cleavage. The extinction coefficients for strands a, b, c, and d are 344,800 $Lmol^{-1}cm^{-1}$, 297,700 $Lmol^{-1}cm^{-1}$, 187,200 $Lmol^{-1}cm^{-1}$, 224,000 $Lmol^{-1}cm^{-1}$,

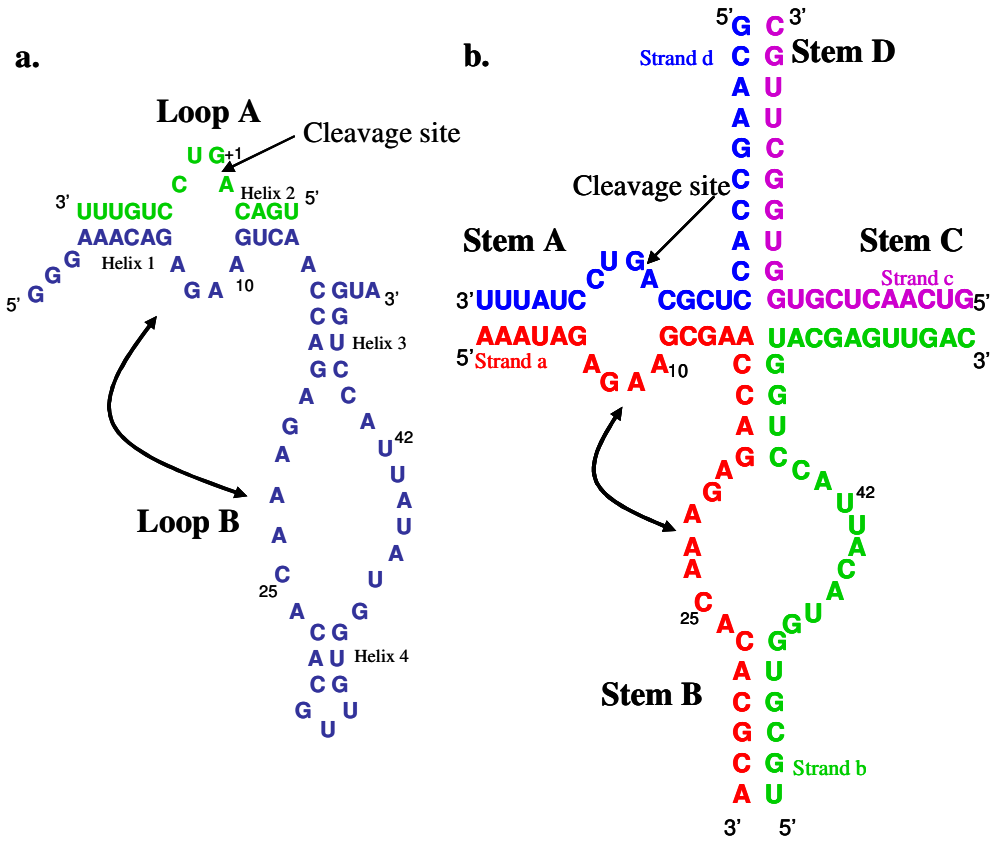

Figure 2-1: The RNA sequences of two constructs of the hairpin ribozyme. (a.) the minimal, or hinged, construct and (b.) the native, or four-way junction construct. Strands a, b, c, d, and d' of the four-way junction construct are a 32mer, 30mer, 20mer, 24mer, and 21mer, respectively.

respectively. The extinction coefficient for a shortened cleavage d strand (21-mer) used for activity studies is 196,000 $Lmol^{-1}cm^{-1}$. The purified RNA was stored at -30°C.

Nondenaturing (Native) Gel Electrophoresis

Gels were prepared with 1 x Tris/boric acid/EDTA (TBE) buffer (89 mM Tris and 89 mM boric acid, pH ~ 8.5) and 8% acrylamide:bisacrylamide (29:1, Fisher 40% stock). Gels were typically polymerized upon the addition of 600 µL of 10% ammonium persulfate and ~ 30 µL of TEMED. For the experiments with 1 mM $MgCl_2$ in the gels and the running buffer, 1 x TB buffer without EDTA was utilized instead of 1 x TBE

buffer. A solution of 1 mM $MgCl_2$ was added to gels before polymerization as well as to the running buffer.[44] Samples of the four-way junction construct of the hairpin ribozyme were made from the addition of 2 µL of a 10 µM stock solution of each strand in a 1:1:1:1 stoichiometric ratio of the four strands in 5 mM TEA, either 25 mM or 100 mM NaCl, and pH 7.8. In addition, a 1 µL spike of a 5' ^{32}P radiolabeled RNA strand was added to each sample in order to observe later on a phosphoroimaging screen whether this strand complexes with the other three nonradiolabeled strands. The annealing protocol involves heating the four strands with spiked RNA at 65°C for 10 minutes and then slow-cooling for one hour. Once the ribozyme was annealed, the desired concentration of Mg^{2+} was added to the designated samples. Before loading into the gel wells, 1 µL of 50% glycerol was added for every 10 µL of each sample. Gels were run in a 4°C cold room at 100 – 220V for about 2.5 – 5 h. The gels were dried and exposed to a phosphoroimaging screen. Images were scanned by a FUJIX BAS 2000 phosphoroimaging system.

Activity Studies

Strand d was 5'^{32}P radiolabeled by T4 polynucleotide kinase (PNK). The activity of the four-way junction construct of the hairpin ribozyme was determined by using a 60 µM stock solution of strands a, b, and c and a 50 µM stock solution of the substrate, the cleavable strand d. Therefore, these studies were under single-turnover condition, in which the enzyme strands are in excess of the substrate strand. A spike of the radiolabeled cleavable strand d was added to each sample as well. The RNA strands were annealed in 5 mM TEA, pH 7.8, and either 25 mM or 100 mM NaCl at twice their final concentration by heating for 10 minutes at 65°C, slow cooling for 1h, and

equilibrating at 20°C for 10 minutes. Ribozyme reactions were initiated by the addition of equal volume of RNA to a solution of M^{2+} ($M^{2+} = Mg^{2+}$ or Mn^{2+}) and were incubated at 20°C for a set time, ranging from 10 seconds to 12 h. To end the reactions at each time point, a quenching buffer, consisting of 90% formamide and 40 mM EDTA, was added and mixed thoroughly in the reaction solution. The completed reaction was then immediately stored in dry ice until the substrate was able to be separated from the product by gel electrophoresis on 20% polyacrylamide gels. Phosphoroimaging analysis was employed to quantify radiolabeled substrate and product strands.

Once the intensities of the substrate and product bands on the gels were quantitated, a background was subtracted. Then, the quantity of substrate cleaved, P, was divided by the summation of the cleaved substrate and the quantity of uncleaved substrate, S, in order to determine the fraction cleaved (Equation 2.1).

$$\text{Fraction cleaved} = (P/(P+S)) \qquad [2.1]$$

Kinetic traces were obtained by plotting fraction cleaved as a function of time in minutes. Reaction rate constants (*k*) were determined by non-linear least squares analysis using Equation 2.2: [45]

$$P_t = (1-e^{-kt}) * P_f \qquad [2.2]$$

in which P_t is the product yield at time t, P_f is the product yield at $t = \infty$ or reaction completion. For biphasic rates, Equation 2.3 was employed.

$$P_t = [(1-e^{-k1t}) * P_{f1}] + [(1-e^{-k2t}) * P_{f2}] \qquad [2.3]$$

UV-Melt Studies

A Cary 300 double-beam UV-Vis spectrometer equipped with a six-cell block and a variable temperature controller was employed for UV melt experiments. The four-way junction construct and the mutant hairpin ribozyme were prepared at a concentration of 2 μM RNA, annealed at 65°C for 10 min, and slow-cooled on ice for 20 min. A specified amount of divalent cation was added from stock solutions. Samples were then loaded into the cells, sealed, placed in the spectrometer, and equilibrated to 5 °C for 15 min prior to running. A temperature probe was inserted into a sample containing no metal ions. The temperature controller was ramped at a rate of 0.3 deg °C/min from 5 to 90 °C and data points were collected every 0.3 degree. Absorbance was monitored at 260 and 280 nm as the temperature was raised.

The melt profile was derived from plotting the first derivative of absorbance with respect to temperature (dA/dT) as a function of temperature. The program, T-melt, which runs on a UNIX workstation, was used to fit the thermal denaturation profiles.[46] The data were fit using a nonlinear least squares fitting algorithm to a sequential folding model described by Theimer and Giedroc.[47] This model assumes that each optical melt transition is two-state, during which the molecule can be either fully folded or fully unfolded.

Effect of Alternative Annealing Procedures for Thermal Denaturation Studies

The annealing procedures of the four strands of the hairpin ribozyme were modified to identify conditions optimal for the proper folding of the four-way junction construct. Initially, the procedure involved the heating of the stoichiometric quantities of

the four strands at 90°C and slow-cooling from a 75°C water bath. During another annealing procedure, the four strands were incubated at 65°C for 10 minutes and then, slow cooled for one hour.[48] The second alternative annealing procedure was identical to the first with the exception that the slow-cooling in the water bath was from 65°C to room temperature. The next two procedures involved the annealing of paired strands first by heating for 90°C for 2 minutes and slow-cooling for 10 minutes. The two annealed pairs were then combined together, annealed by heating at 37°C, and finally slow-cooled on the benchtop.

The first combination involved the annealing of pairs of strands: strand a with strand b, and strand c with strand d. The two pairs were then annealed together and thermally denatured. The next combination resulted from the pairing of strand a with strand d and strand b with strand c. Once annealed together, the pairs were thermally denatured. Upon comparison of the melt profiles of the four strands annealed under different conditions, the variation was insignificant. Therefore, it appeared that any procedure was adequate to form the four-way junction construct and the first alternative annealing procedure was chosen to be employed for the remainder of the experiments.

Metal-Dependent Thermal Denaturation Studies

The melting temperatures at different concentrations of divalent cations were plotted as $1/T_m$ vs. [Metal] (M) and fit to Equation 2.4:[49]

$$1/T_m = 1/T_o - (R/\Delta H_o) \ln [(0.5 + 0.5 (1 + 4K_fL)^{1/2})^m/(0.5 + 0.5 (1 + 4K_uL)^{1/2})^m] \quad [2.4]$$

in which T_m is the melting temperature at specific metal ion concentration, T_o is the melting temperature in the absence of metal ion concentration, R is the gas constant, ΔH_o is the van't Hoff enthalpy, K_f and K_u are the equilibrium binding affinities for the folded and unfolded forms of the RNA, respectively, L is the free metal ion concentration, and finally m is the number of phosphates involved in the unfolding event under study. The two-state model assumes that one divalent cation for every two phosphates is assumed to have an electrostatic interaction.[47, 49]

Electron Paramagnetic Resonance Spectroscopy

Electron paramagnetic resonance (EPR) spectroscopy is a branch of spectroscopy in which microwave radiation is absorbed by molecules, ions, or atoms possessing electrons with unpaired spins as a function of magnetic field. The magnetic field interacts with unpaired electron spin moments, resulting in different energy states. For example, an ion with an S value of ½ will have energy states that can have a value of either –½ or +½ , which aligns with or against the magnetic field, respectively. The difference in energy between the two states is in the range of microwave frequencies. This unpaired electron-magnetic field interaction can be described by the Zeeman Hamiltonian in Equation 2.5:

$$\mathcal{H} = \beta_e H \bullet g \bullet S \qquad [2.5]$$

in which g is the landé factor, β_e is the electron Bohr magneton, S is the spin operator, and H is the applied field strength.

The nuclear moment of an atom's nucleus interacts with the magnetic field as well, which is described by another Hamiltonian equation, the nuclear Zeeman term shown in Equation 2.6:

$$\mathcal{H} = \beta_e H \bullet g \bullet S - \beta_n H \bullet g_n \bullet I \qquad [2.6]$$

in which the nuclear spin operator is represented by I and β_n is the nuclear Bohr magneton.

The next term describes the electron-nuclear hyperfine interaction revealed in Equation 2.7.

$$\mathcal{H} = \beta_e H \bullet g \bullet S - \beta_n H \bullet g_n \bullet I + S \bullet a \bullet I \qquad [2.7]$$

in which a is the hyperfine coupling tensor, defined as the magnitude of the interaction

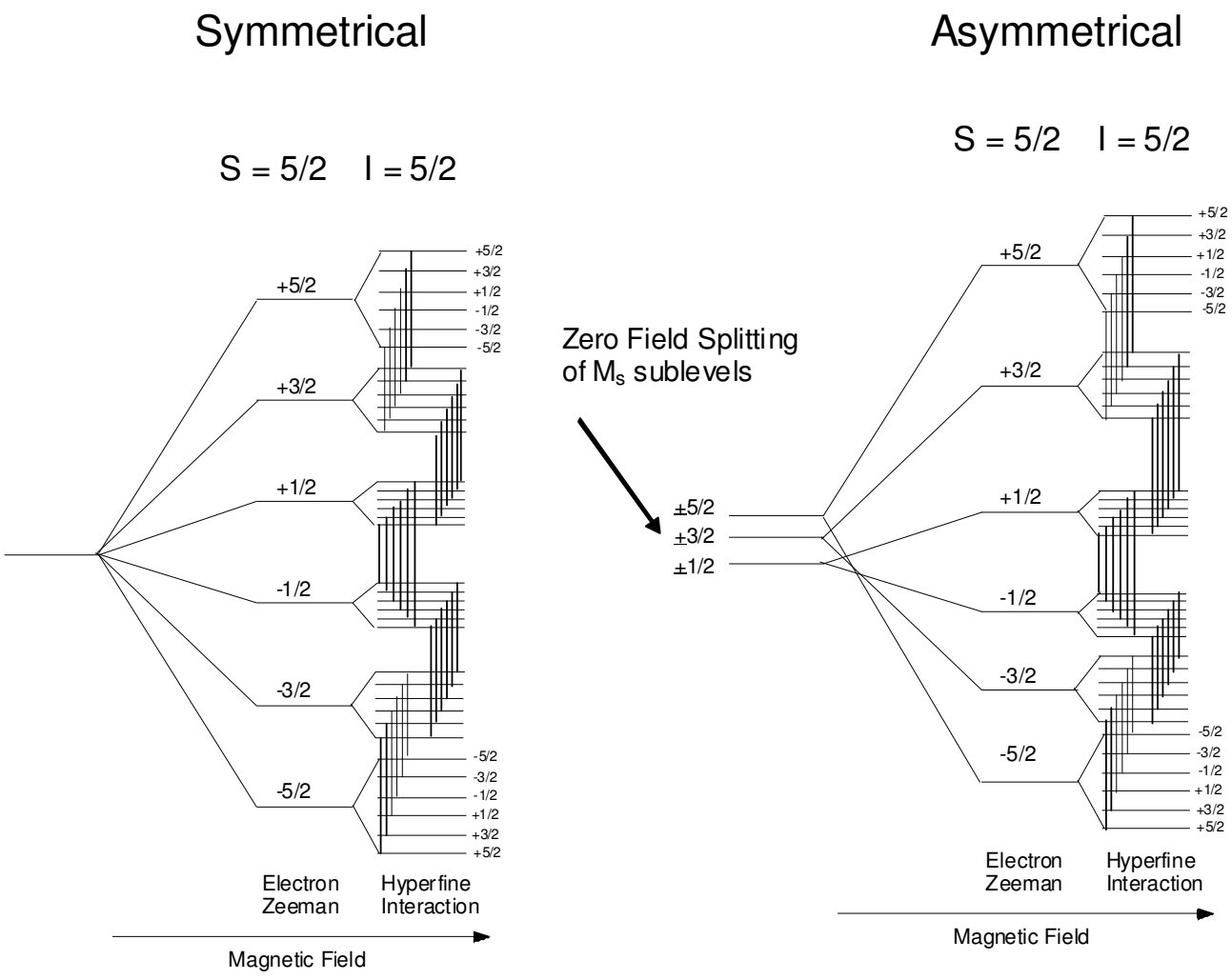

Figure 2-2: EPR splitting diagrams for a Mn^{2+} ion in two types of environments.

between the electron spin and the nuclear spin.

Finally, there is one additional term in the overall Hamiltonian equation for ions with as S value greater than ½ (such as Mn^{2+} S = 5/2). This term is the zero-field splitting (zfs) of electronic states shown in Equation 2.8.

$$\mathcal{H} = \beta_e H \bullet g \bullet S - \beta_n H \bullet g_n \bullet I + S \bullet a \bullet I + S \bullet D \bullet S \qquad [2.8]$$

in which D is the zero-field splitting tensor. Zero-field splitting is defined as the removal of the degeneracy of the spin states in the absence of an applied field.

For a high spin d^5 Mn^{2+} ion, the electron-splitting diagram in two different types of environments is shown in Figure 2-2. When the Mn^{2+} ion is in a symmetrical environment, the EPR spectrum is a six-line hyperfine pattern centered at g ~ 2 resulting from a superposition of all 30 allowed $\Delta m_s = \pm 1$, $\Delta m_I = 0$ transitions as seen in Figure 2-2. The signal intensity of a Mn^{2+} ion broadens beyond detection at room temperature when bound to an RNA molecule due to the lower symmetry of the bound Mn^{2+}, an increase in the rotational correlation time, and changes in electron relaxation pathways.[12] Therefore, the difference in signal intensities arising from free Mn^{2+} with and without the RNA in solution can be correlated to the number of bound Mn^{2+} ions per RNA molecule. (Figure 2-3) The binding isotherm results from a plot of the number of Mn^{2+} ions bound per RNA molecule as a function of free Mn^{2+} ions in solution (μM), which is then fit to an equation to yield a K_d and the total number of bound metal ions using KaleidaGraph (Synergy Software).[11] Equation 2.9 involves a sum of *j* sets of n independent, non-interacting sites:

$$\left[Mn^{2+}{}_{bound}\right]/\left[hybrid\right] = \sum_{j=1}^{j} \{(n_i * \left[Mn^{2+}{}_{free}\right]) / (K_d + \left[Mn^{2+}{}_{free}\right])\} \qquad [2.9]$$

The terms [Mn^{2+}_{bound}] and [Mn^{2+}_{free}] are the concentrations of bound and free Mn^{2+} ions in the sample, respectively, and finally K_d is the apparent dissociation constant.

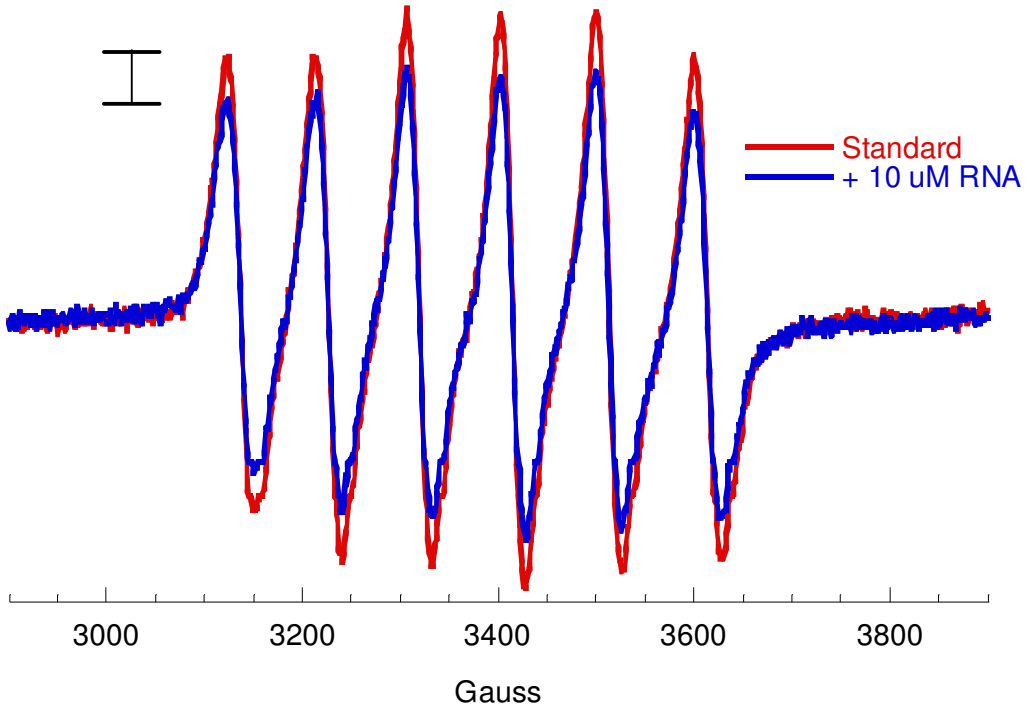

Figure 2-3: Comparison of EPR signal intensities of free Mn^{2+} in solution and free Mn^{2+} in the presence of RNA.

On the other hand, at lower temperatures (4 - 20 K), small additional features are apparent in the six-line hyperfine of the EPR spectrum and they mainly arise from semiforbidden $\Delta m_I = \pm 1$ transitions. Decreased symmetry and therefore, zero-field splitting, contributes to the presence of these semiforbidden transitions.[12,50] Because low temperatures allow for the detection of more details in the EPR spectrum, any deviations

from a standard Mn^{2+} EPR spectrum when Mn^{2+} is in the presence of RNA can indicate a different Mn^{2+} ligand environment.

A Bruker EMX X-band EPR spectrometer operating at a frequency of 9.44 GHz equipped with a TE_{102} rectangular cavity was used. Generally, the acquisition parameters were 100 kHz modulation frequency, a microwave power of 0.2 mW, and an average of 1 to 4 scans. The modulation amplitude was 25 G for room temperature and 15 G for data collected at liquid He temperatures. An Oxford continuous flow liquid helium cryostat was employed for low temperature EPR studies. The Bruker WinEPR program software allowed for the examination of EPR spectra and for the determination of the signal intensities.

Samples were prepared by combining and annealing equal concentrations of each hairpin ribozyme strand. The annealing procedure involved heating the solution for 10 minutes at 65ºC, and then slow cooling for 1h. To minimize metal hydroxide formation, $MnCl_2$ was added from a freshly-made stock solution prepared from a 1 M $MnCl_2$. The room temperature EPR samples contained 10 μM RN and a range of Mn^{2+} ion concentrations (0.02 – 0.7 mM) in a total volume of 75 μL prepared in quartz capillary tubes, which were placed into a standard 4 mm EPR tube.

CHAPTER III

CHARACTERIZATION OF THE FOUR-STRANDED FOUR-WAY JUNCTION CONSTRUCT OF THE HAIRPIN RIBOZYME AND ITS MUTANT

Introduction

There are three possible constructs of the hairpin ribozyme: the 2-way junction, or the hinged, construct, the 3-way junction construct, and finally, the four-way junction construct, or the native construct (Figure 3-1).[40] As the names imply, these constructs differ in the number of stems and therefore, the type of junction linking these stems. For

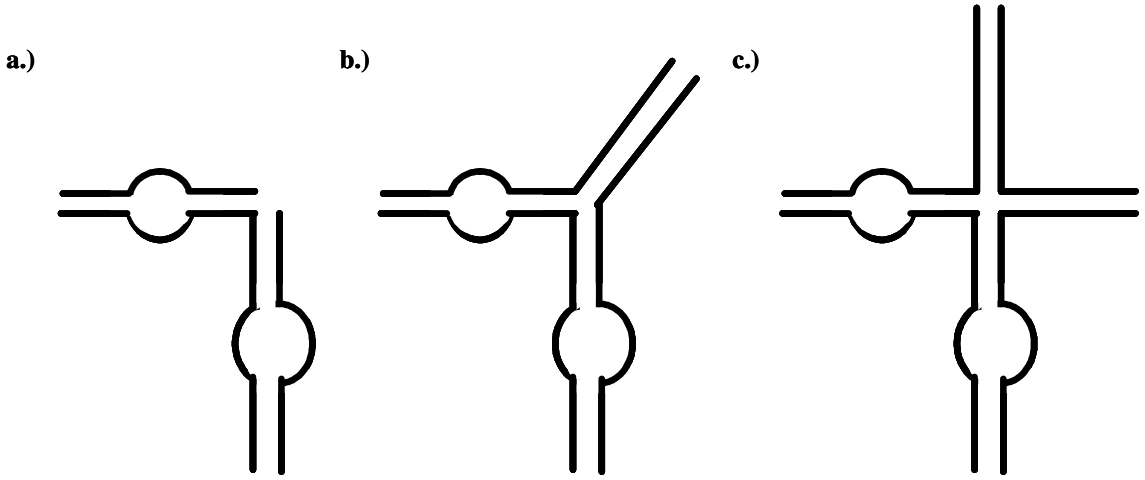

Figure 3-1: The three types of constructs of the hairpin ribozyme based on the type of junction. The a.) two-, b.) three-, and c.) four-way junction constructs of the hairpin ribozyme are shown. The four-way junction construct is the most stable since this junction is the key architectural element which positions the loop-carrying stems into close proximity.

each type of construct, there are variations in the number of strands used to form the hairpin ribozyme. For example, the literature reports studies employing native constructs of the hairpin ribozyme, consisting of only one strand, two strands, or four strands.[43, 51]

The construct chosen for the studies presented in this thesis is the four-way junction construct, which is a better representation of the native conformation in the viral RNA genome, is catalytically active under physiological conditions, and is more stable than the hinged construct. It was initially proposed that this greater stability of the four-way junction construct may enhance a tertiary signature in thermal denaturation profiles, thereby facilitating the study of the effect of metal ions on tertiary structure. In addition, the four-way junction plays a critical metal-dependent role in orientating the two loop-carrying stems into close proximity to promote tertiary contacts between the essential loops.[28, 29]

Ultimately, the goal of this work was to locate catalytically/structurally significant metal binding sites within the hairpin ribozyme by site-specific modifications, such as phosphorothioate substitutions, deoxymodifications, and base modifications. Examples of base modifications include abasic modifications, substitution with another base, or substitution with a modified base. Phosphorothioate substitution into a nucleic acid involves the replacement of a non-bridging phosphate oxygen with a sulfur atom in either the pro-R or pro-S position, resulting in a site with a high affinity for Cd^{2+} or Hg^{2+}. Phosphorothioate metal-rescue experiments have been used extensively as a biochemical probe for locating metal-binding sites in functional RNAs. If a critical Mg^{2+} ion was directly coordinated to the oxygen that was replaced by the sulfur of the phosphorothioate, the activity should decrease. Activity may then be restored upon addition of a soft, thiophilic metal ion, such as Cd^{2+} or Hg^{2+}.[31] For example, Cd^{2+} has been observed by ^{31}P NMR to bind to the pro-R and pro-S sulfur of a phosphorothioate substitution at the functionally important A9 site of the hammerhead ribozyme.[13]

Phosphorothioate-substitution in conjunction with ^{31}P NMR would be an ideal technique for specifically locating metal-binding sites in the phosphodiester backbone in the hairpin ribozyme. The separation of the Rp and Sp diastereomers is achieved by HPLC and is only practical for strands that do not exceed 40 nucleotides. As a result, a hairpin construct was chosen that meets this critical limitation.

The particular four-way junction construct employed in these experiments is that used in a trFRET study by Millar and coworkers, and the sequence is similar to that found in the viral RNA genome.[48] This construct consists of four strands: strand a (a 32-mer), strand b (a 30-mer), strand c (a 20-mer), and strand d (a 24-mer), or the substrate. (Figure 3-2) Stem A arises from the base-pairing of strand a and strand d, Stem B from

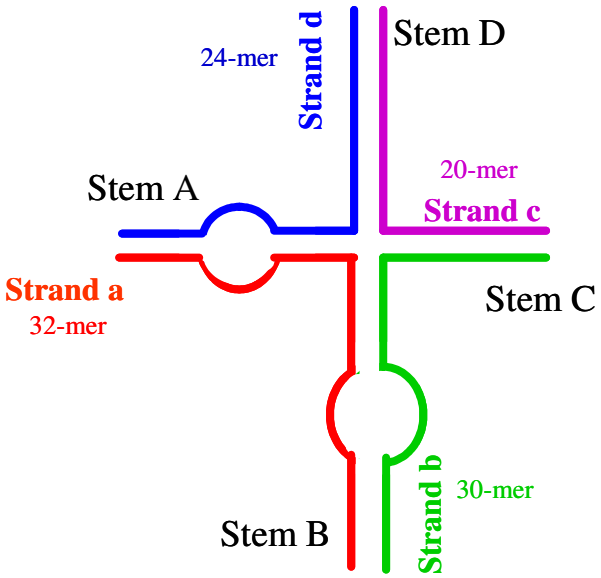

Figure 3-2: The four-stranded four-way junction construct of the hairpin ribozyme. Stem A arises from the base-pairing of strand a and strand d, Stem B from strand a and strand b, Stem C from strand b and strand c, and finally, Stem D from strand c and strand d.

strand a and strand b, Stem C from strand b and strand c, and finally, Stem D from strand c and strand d.

The first step in these studies is to characterize formation of the hairpin ribozyme from four individual strands. Conditions to improve the yield of the hairpin complex and to minimize subcomplexes were determined by monitoring complex formation by native gel electrophoresis and thermal denaturation.

Nondenaturing (Native) Gel Electrophoresis

Introduction

Nondenaturing gels are electrophoresis gels in which RNA complexes are not denatured and therefore, remain folded while traveling through the gel. The mobility of different complexes and conformations is dependent on both size and compactness. Therefore, folded RNA may be separated from another conformation, uncomplexed RNA strands, or dimers based on differences in mobility.[44, 52] Hence, this technique is amenable to applications that distinguish the four-way junction construct of the hairpin ribozyme from uncomplexed single-stranded RNA, or from two-stranded, or three-stranded complexes. In addition, the intensity of the band of the four-way junction construct should indicate the extent of hairpin ribozyme formation. Each native gel presented in this chapter has one lane loaded with a single-stranded ^{32}P- radiolabeled RNA, used as a "marker", the mobility of which serves as a guide for other lanes of several bands. For example, Figure 3-3(a.) reveals radiolabeled strand a in the first lane and this strand can be observed in the other lanes within the same gel as bands of identical mobility.

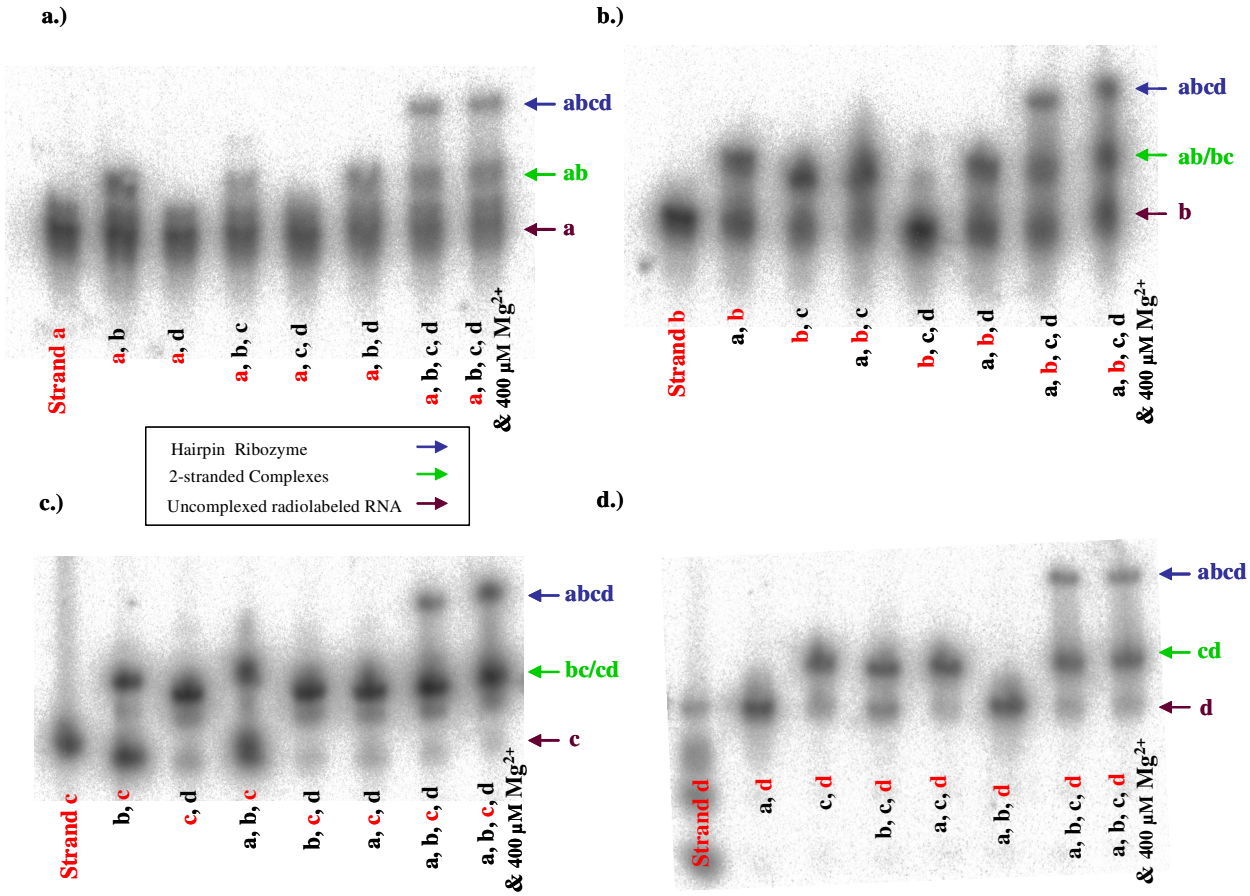

Figure 3-3: Four 8% native gels in which samples contain a ^{32}P-radiolabeled strand. (a.) ^{32}P-radiolabeled strand a, (b.) ^{32}P-radiolabeled strand b, (c.) ^{32}P-radiolabeled strand c, and (d.) ^{32}P-radiolabeled strand d. The solution conditions were 1.5 µM RNA, 5 mM TEA, pH 7.8, 100 mM NaCl. The RNA strands were heated at 65°C for 10 min. and slow-cooled for 1 hour. The radiolabeled strands are indicated in red. Together, these native gels indicate that all four strands are going into the band of lowest mobility.

Ribozyme Complex Formation Revealed by Native Gels without Mg^{2+}

All native gels reveal three distinct bands in the lane containing all four annealed strands. The "lowest" band always displayed the same high mobility as the marker band, or the uncomplexed strand, whereas the other two bands were located "higher" than any

of the marker bands (Figure 3-4). Therefore, if the four-way junction construct of the hairpin ribozyme was indeed forming, then either one or both of these bands with lower mobility should be the hairpin ribozyme, in one or two possible conformations. This is consistent with the principle that a complex, particularly composed of four strands, would have a lower mobility in the gel than that of a single, uncomplexed strand.

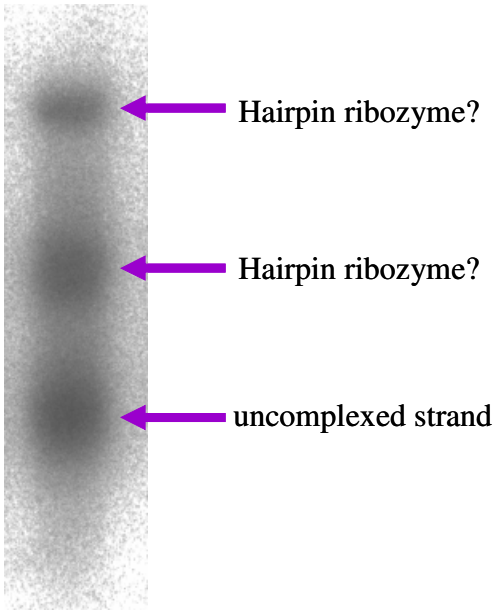

Figure 3-4: A lane of three bands arising from all four strands in an 8% native gel. In this case, ^{32}P-radiolabeled strand b is added to the sample. The highest-mobility band is uncomplexed strand b based on the mobility of the "marker" on the same gel (not shown). The two bands with lower mobility are identified by further experiments. The solution conditions were 1.5 μM RNA, 5 mM TEA, pH 7.8, 100 mM NaCl.

The lanes of three-strand combinations were compared with those of four strands in solution in an initial effort to determine the identity of the bands. It was found that the band of lowest mobility was only apparent in the presence of all four strands and not in the lanes containing three strands. This indicates that a unique complex is only forming

in the presence of the four strands and rules out the possibility of the middle band as the hairpin ribozyme.

In another experiment, samples of all four annealed strands were run on a native gel. Each sample had been spiked with all four radiolabeled strands. The objective was to determine the number of strands that contributed to the formation of the complex manifested in the lowest-mobility band. This band was then excised from the native gel, cut into smaller pieces, and loaded into wells of a denaturing gel. Ideally, if all four strands did combine to form the hairpin complex, then four bands of differing mobility should be revealed. The band with the fastest mobility was assigned as strand c, a 20-mer, whereas strand d, a 24-mer, was assigned to the band of intermediate mobility. Finally, the band with the lowest mobility was less defined and broader, which suggests that strand a and strand b, a 32-mer and 30-mer, respectively, were difficult to resolve. Although the outcome of the experiment was not conclusive, the possibility of four strands originating from the excised native gel band could not be ruled out.

To further this investigation, a methodical procedure, in which samples consisting of various combinations of the four strands were loaded into the same gel, was utilized for each radiolabeled strand. (Figure 3-3) For example, radiolabeled strand a served as the marker for one gel, and the mobility of the marker could be compared with the bands arising from the interaction (or lack of interaction) between strands a and b; a and d; a, b, and c; a, b, and d; a, c, and d; all four strands; and all four strands in the presence of 400 μM Mg^{2+}. This was repeated for each gel in which only one radiolabeled strand served as a marker for clarity. Therefore, there were four native gels, each of which contained samples with one radiolabeled strand, one of a, b, c, or d (Figure 3-3).

The lanes with the paired strands in the four native gels were revealed to have a high-mobility band from uncomplexed RNA as well as one low-mobility band, indicative of an interaction between the two strands. This was observed for all pairs except for the strand a and d combination. Only one band of uncomplexed strand a or strand d, depending on which was radiolabeled, could be observed (Figure 3-3(a.)(d.)). In contrast, the native gels highlight the strong affinity between the strand c and d pair as revealed by the intense band with lower mobility than that of uncomplexed RNA (Figure 3-3(c.)(d.)). With regard to strands a and b and strands b and c, 50% of each component forms complex (Figure 3-3(a.)(b.)(c.)). The lanes of samples containing three strands also exhibited the same bands, with related intensity and mobility, as those of the paired strands. Generally, in 100 mM NaCl, one strand was excluded from the interaction of the other two strands.

However, in the presence of all four strands, an additional band with the lowest mobility is apparent, which is absent in the lanes with the other strand combinations. A final result to note is the indistinguishable intensity of this lowest-mobility band in the absence and presence of Mg^{2+}. This is not consistent with the idea that Mg^{2+} should stabilize the hairpin ribozyme, thereby, promoting the formation of the hairpin and the intensification of its band. Therefore, the Mg^{2+} ions must not be traveling through the gel with the negatively-charge hairpin ribozyme, which becomes destabilized and more temperature-sensitive.

An additional experiment was performed to verify that the lowest-mobility band apparent only in the presence of all four strands had the same low mobility regardless of the radiolabeled strand. The native gel revealed that the lowest-mobility band observed

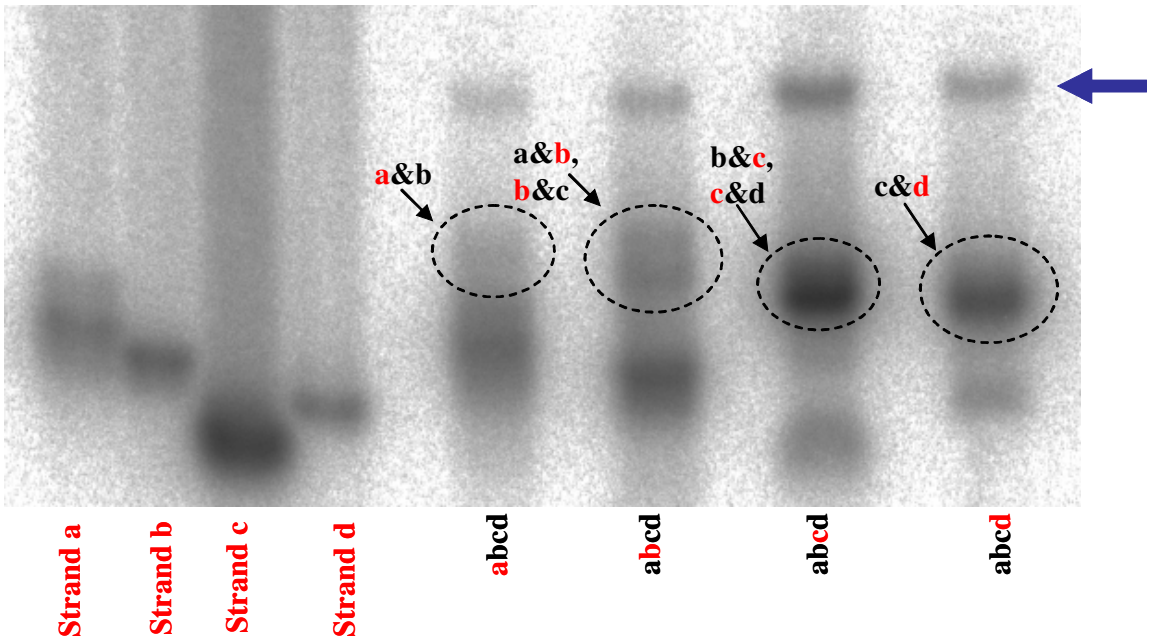

Figure 3-5: The band of lowest mobility observed by each radiolabeled strand has the same mobility. An 8% native gel revealed that the lowest-mobility band (denoted by the arrow) does have the same mobility, indicating that all four strands go into the same complex. The solution conditions were 1.5 μM RNA, 5 mM TEA, pH 7.8, 100 mM NaCl. The RNA strands were heated at 65°C for 10 min. and slow-cooled for 1 hour. The radiolabeled strands are indicated in red.

by each radiolabeled strand has identical mobility, indicating that all four strands comprise the same complex, the four-way junction construct of the hairpin ribozyme (Figure 3-5).

Ribozyme Complex Formation in Native Gels Containing Mg^{2+}

Once the formation of the four-way junction construct of the hairpin ribozyme was confirmed, its homogeneity in solution became the next concern. Based on the lack of intensity of the band, it became apparent that under these conditions the solution was not composed primarily of the hairpin ribozyme. The fact that the T_m of the major large-enthalpy peak is only ~ 25°C in the absence of Mg^{2+} in 25 mM NaCl underscored the

high sensitivity of the hairpin ribozyme to temperature. Although the native gels were run in a cold room at 4°C, the running temperature of the native gels increases with voltage and current. Based on its band's lack of intensity, the hairpin ribozyme with Mg^{2+} present in the samples was destabilized, most likely due to the diminished ability of the Mg^{2+} ions to remain electrostatically associated with the RNA as it migrates through the gel. As a result, gels were prepared by the addition of 1 mM Mg^{2+} to the native gel before polymerization as well as to the tris-borate running buffer, containing no EDTA.

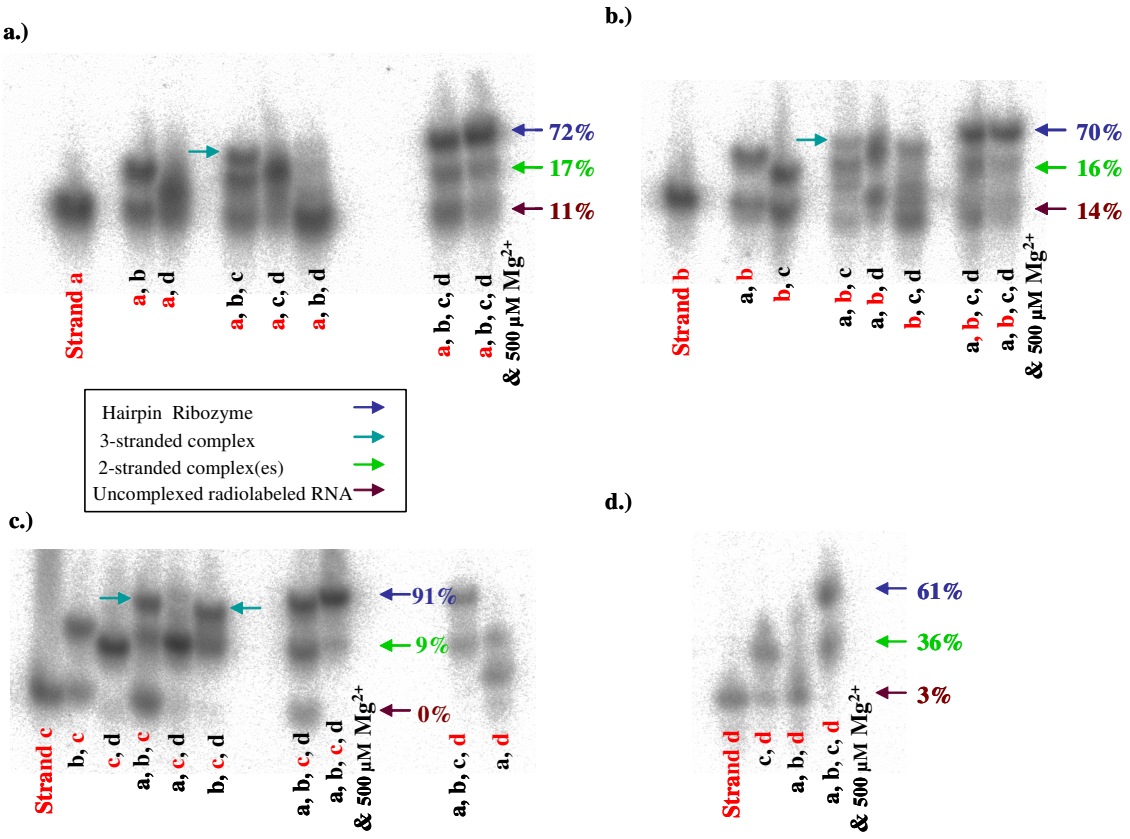

Figure 3-6: Four 8% native gels polymerized with 1 mM Mg^{2+} in which samples contain one ^{32}P-radiolabeled strand. (a.) ^{32}P-radiolabeled strand a, (b.) ^{32}P-radiolabeled strand b, (c.) ^{32}P-radiolabeled strand c and ^{32}P-radiolabeled strand d, and (d.) ^{32}P-radiolabeled strand d. The solution conditions were 1.5 µM RNA, 5 mM TEA, pH 7.8, 25 mM NaCl. The RNA strands were heated at 65°C for 10 min. and slow-cooled for 1 hour. The radiolabeled strands are indicated in red. Together, these four native gels revealed that the majority of all four strands interact with each other to form the hairpin ribozyme.

The Mg^{2+} within the gel and in the running buffer should stabilize the ribozyme. Another stabilizing factor was the use of near-freezing water flowing through the gel box as the native gels were run to maintain the temperature below 25°C.

The "methodical procedure" was repeated under these new gel conditions and the results were as expected. The intensity of the band of the hairpin ribozyme ranged from 50 – 60 % depending on the radiolabeled strand in comparison with the intensities of the other two bands within the same lane. In comparison, the intensity of the same band was greater, ranging from 60 - 90 %, in the presence of 500 µM Mg^{2+} (Figure 3-6).

Despite these promising results, the native gel containing Mg^{2+} also stabilized the formation of three three-stranded complexes. The three-strand combinations of a, b, and c; a, b, and d; as well as b, c, and d, have an additional third band with lower mobility

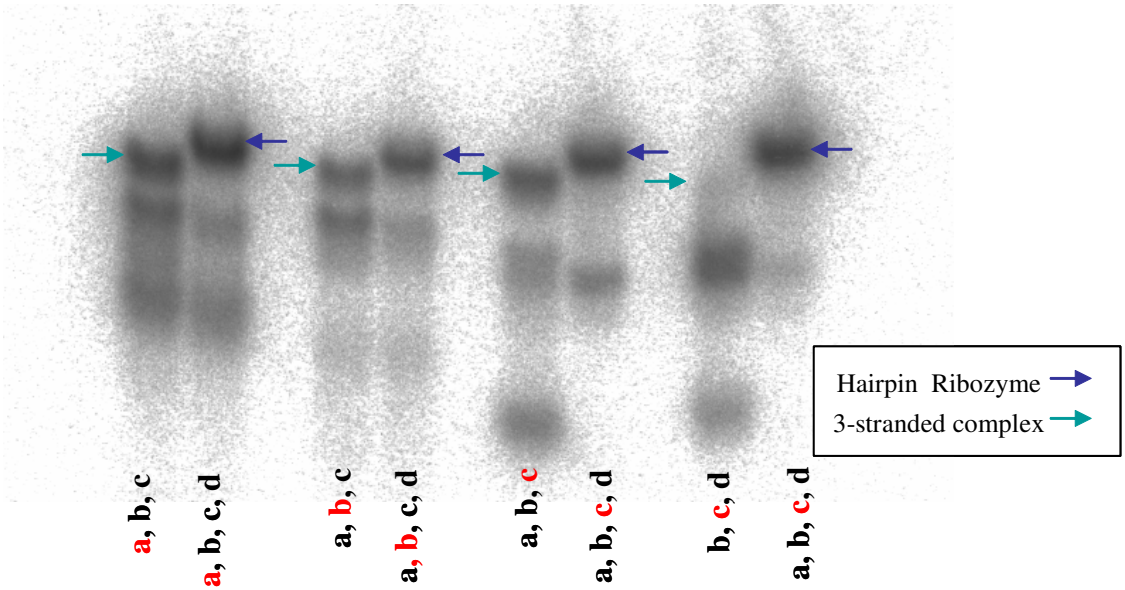

Figure 3-7: An 8% native gel containing 1 mM Mg^{2+} to discriminate between the bands of lowest mobility of the three-stranded complex and hairpin ribozyme. This native gel confirms that the lowest-mobility band of a three-stranded complex and that of the hairpin ribozyme arises from two unique complexes. The solution conditions were 1.5 µM RNA, 5 mM TEA, pH 7.8, 25 mM NaCl. The RNA strands were heated at 65°C for 10 min. and slow-cooled for 1 hour. The radiolabeled strands are indicated in red.

than the other two bands within their lanes. However, this new band appears to be more mobile than that of the hairpin ribozyme, which may be due to a slight "smiling" in the gel. The term, "smiling", refers to the uneven running of the gel such that the samples loaded in the middle of the gel run faster than those loaded on the ends. In order to effectively distinguish the mobility of the two bands of lowest mobility, an additional native gel, loaded with alternating samples of the three-stranded complexes and the hairpin ribozyme, was run. Direct comparison of these bands does reveal that they have different mobility, and therefore, are two unique complexes (Figure 3-7).

Mutant Complex Formation in Native Gels Containing Mg^{2+}

A mutant hairpin ribozyme lacking both loops A and B was employed in this work to eliminate all potentially tight metal-binding regions, thereby isolating the four-

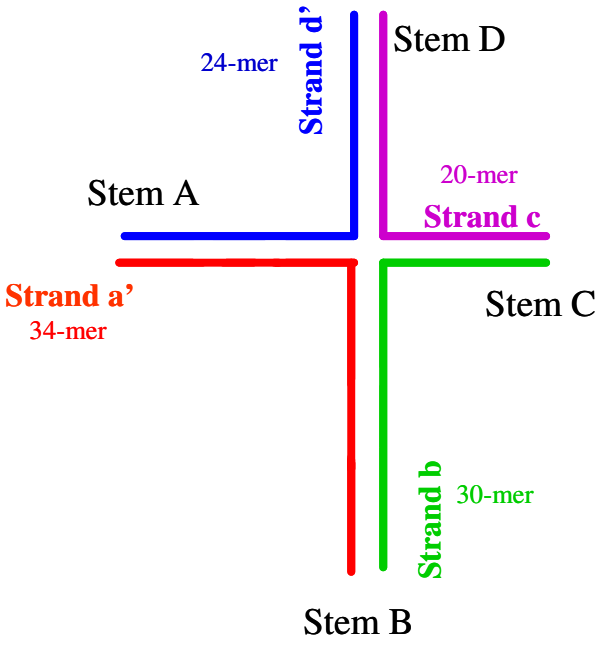

Figure 3-8: The four-stranded isolated four-way junction mutant. Stem A arises from the base-pairing of strand a' and strand d', Stem B from strand a' and strand b, Stem C from strand b and strand c, and finally, Stem D from strand c and strand d'.

way junction as the sole region of interest. Like the ribozyme, the loopless mutant is composed of four strands all of which are connected to each other by an identical four-way junction (Figure 3-8). The sequences of the strands are also identical to those of the hairpin ribozyme, except for the base-paired regions that replaced the loops (Figure 1-12). More specifically, strands b and c are exactly the same strands that contribute to the structure of the hairpin ribozyme. However, strands a and d are designed differently to accommodate the new base-paired regions and are denoted as a' and d' in the mutant. Therefore, like the ribozyme, the mutant needed to be characterized by native gels as well.

All four strands, a', b, c, and d' were annealed using the procedure described for the ribozyme, in which the four strands were heated at 65°C and slow-cooled for one hour. Both the native gels and the TRIS-borate running buffer contained 1 mM Mg^{2+} and no EDTA. The native gels were run in a cold room at about 4°C with near-freezing water running through the gel box to maintain a lower temperature during the experiment. The solution conditions were 5 mM TEA, 25 mM NaCl, and pH 7.8.

The methodical procedure was employed for the mutant's strands as well (Figure 3-9). Each of the new mutant strands a' and d' have two conformations as shown by the two bands in the lane of each solitary strand. All the paired strands result in a band of lower mobility indicative of each pair's interaction. Three-stranded complexes are also possible for various strand combinations based on bands of even lower mobility than those of the paired complexes. Finally and more importantly, the presence of all four strands yields a band of the lowest mobility not apparent for any other strand combination. Therefore, this band can be assigned as the mutant hairpin ribozyme. One

of the two lanes of samples with all four mutant strands contained 500 µM Mg^{2+}. The intensity of the mutant's band in both lanes are very similar, indicative of a less pronounced effect of Mg^{2+} on the stabilization of the mutant than of the ribozyme. For each native gel, the hairpin ribozyme was run in the adjacent lane to serve as a guide. All four radiolabeled mutant strands are part of the mutant complex, which has a slightly lower mobility than the hairpin ribozyme. A possible explanation is the ability of the hairpin ribozyme to dock in the presence of Mg^{2+}, thereby becoming more compact and having a greater mobility than that of the more extended, undocked mutant ribozyme.

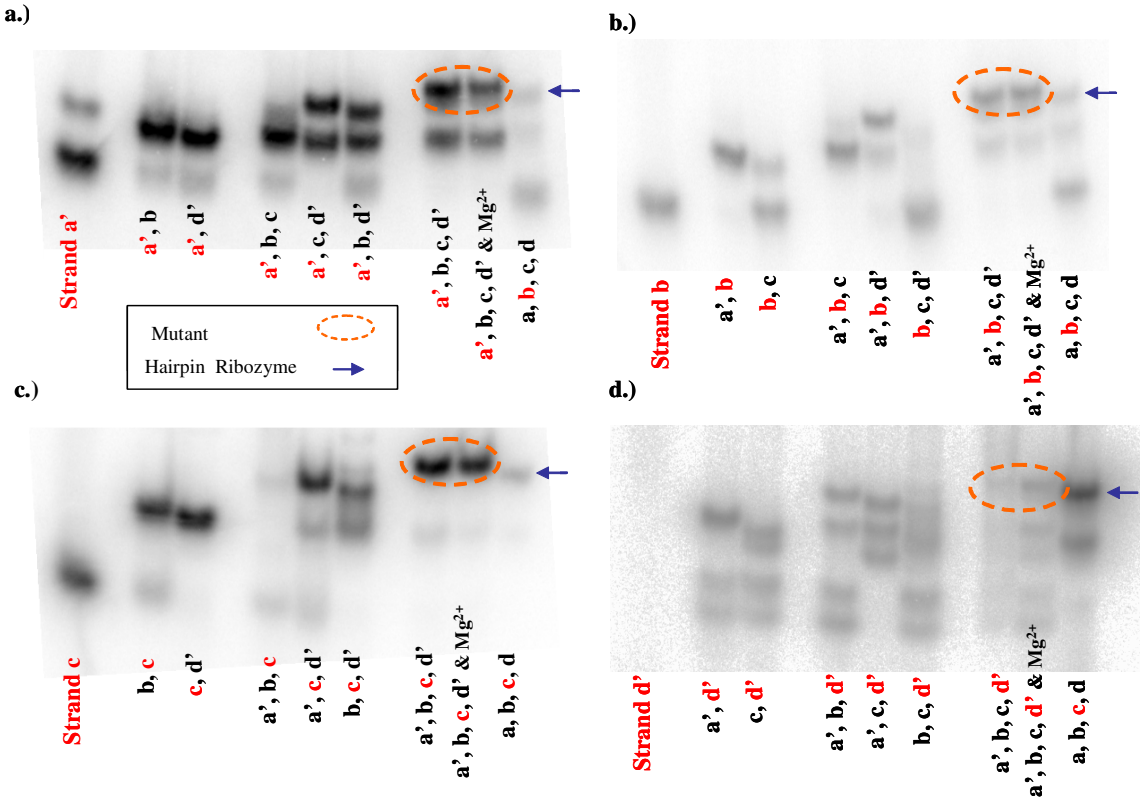

Figure 3-9: Four 8% native gels polymerized with 1 mM Mg^{2+} in which mutant samples contain one ^{32}P-radiolabeled strand. (a.) ^{32}P-radiolabeled strand a, (b.) ^{32}P-radiolabeled strand b, (c.) ^{32}P-radiolabeled strand c, and (d.) ^{32}P-radiolabeled strand d. The solution conditions were 1.5 µM RNA, 5 mM TEA, pH 7.8, 25 mM NaCl. The RNA strands were heated at 65°C for 10 min. and slow-cooled for 1 hour. The radiolabeled strands are indicated in red. Together, these four native gels revealed that the majority of all four strands interact with each other to form the mutant.

Thermal Denaturation Studies

Introduction

Thermal denaturation was employed to further characterize the hairpin ribozyme and its loopless mutant by studying their unfolding events. The assignment of each observed transition in a melt profile to the unfolding event of each stem of the hairpin ribozyme and its mutant aided in characterizing and confirming the formation of these RNA structures. Figure 3-10 shows three melt profiles of the hairpin ribozyme in the absence of divalent metal ions, in the presence of 400 μM Mg^{2+}, and in the presence of 50 μM Mn^{2+}. These concentrations were chosen based on FRET studies of Lilley *et al.,* which determined an apparent binding affinity of about 400 μM Mg^{2+}. Due to the general observation of higher binding affinities of Mn^{2+} ions for RNA structures, a lower concentration of 50 μM Mn^{2+} was chosen.

As expected, the resulting melt profiles of the hairpin ribozyme (5 mM TEA, 100 mM NaCl, pH 7.8) were broader with more absorbance and complexity than those of the simpler hinged construct (Figures 3-10 & 3-11). There was one prominent low-temperature feature as well as two less pronounced features in the higher-temperature region of the melt profile of the hairpin ribozyme. For example, in the absence of divalent metal ions, the large enthalpy feature had a T_m of ~ 35°C and more subtle features were found at ~ 52°C and ~ 62°C (Figure 3-10(a.)). In contrast, the hinged construct in identical solution conditions had two major features and one broad low-temperature feature at ~ 22°C in its simpler melt profile (Figure 3-11(a.)). The melting temperature of the first major feature is at ~ 30°C and that of the second is ~ 50°C. The change in absorbance as a function of temperature of the major enthalpy peak in the melt

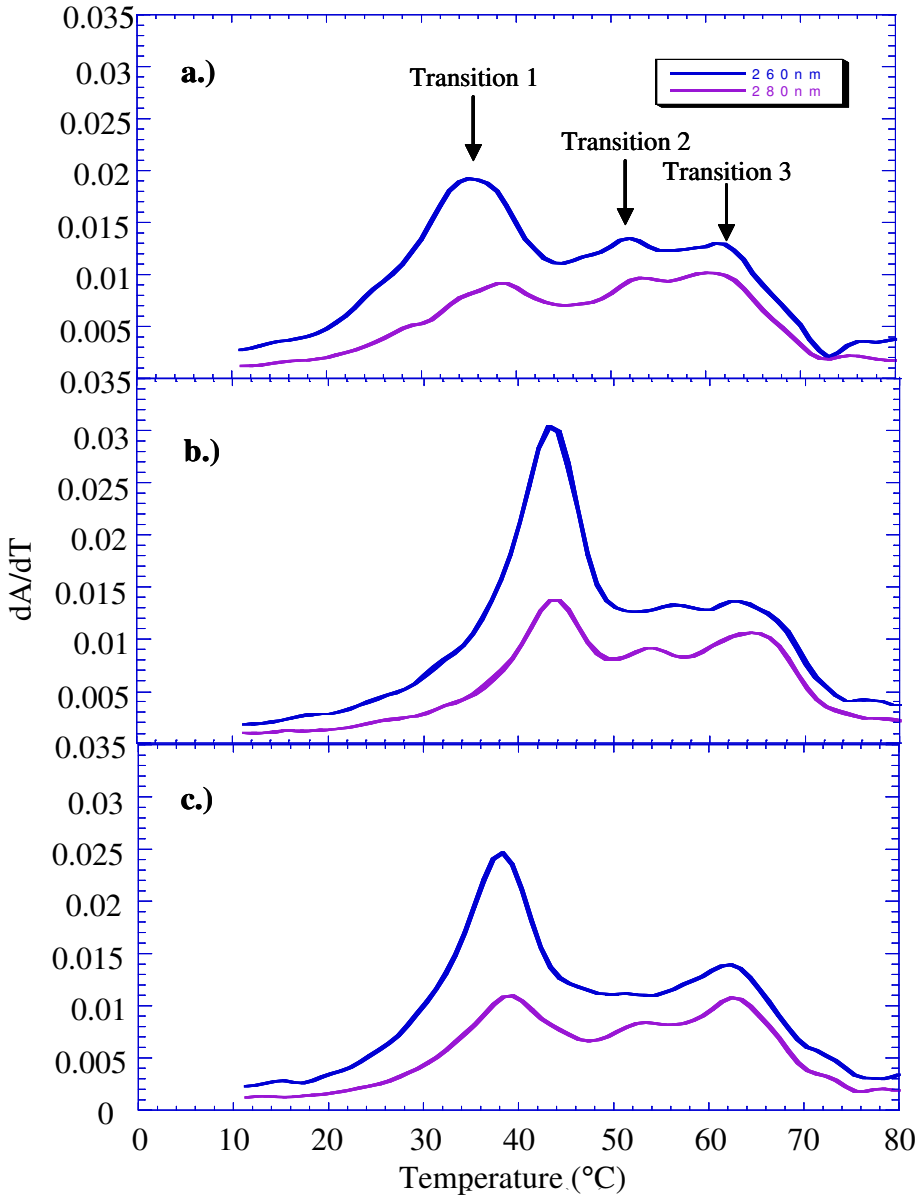

Figure 3-10: Melt profiles of the hairpin ribozyme in various concentrations of divalent metal ions. The melt profiles of strands a, b, c, and d (a.) in the absence of M^{2+} (b.) in the presence of 400 µM Mg^{2+} and (c.) in the presence of 50 µM Mn^{2+}. The solution conditions were 2 µM RNA, 5 mM TEA, pH 7.8, 100 mM NaCl.

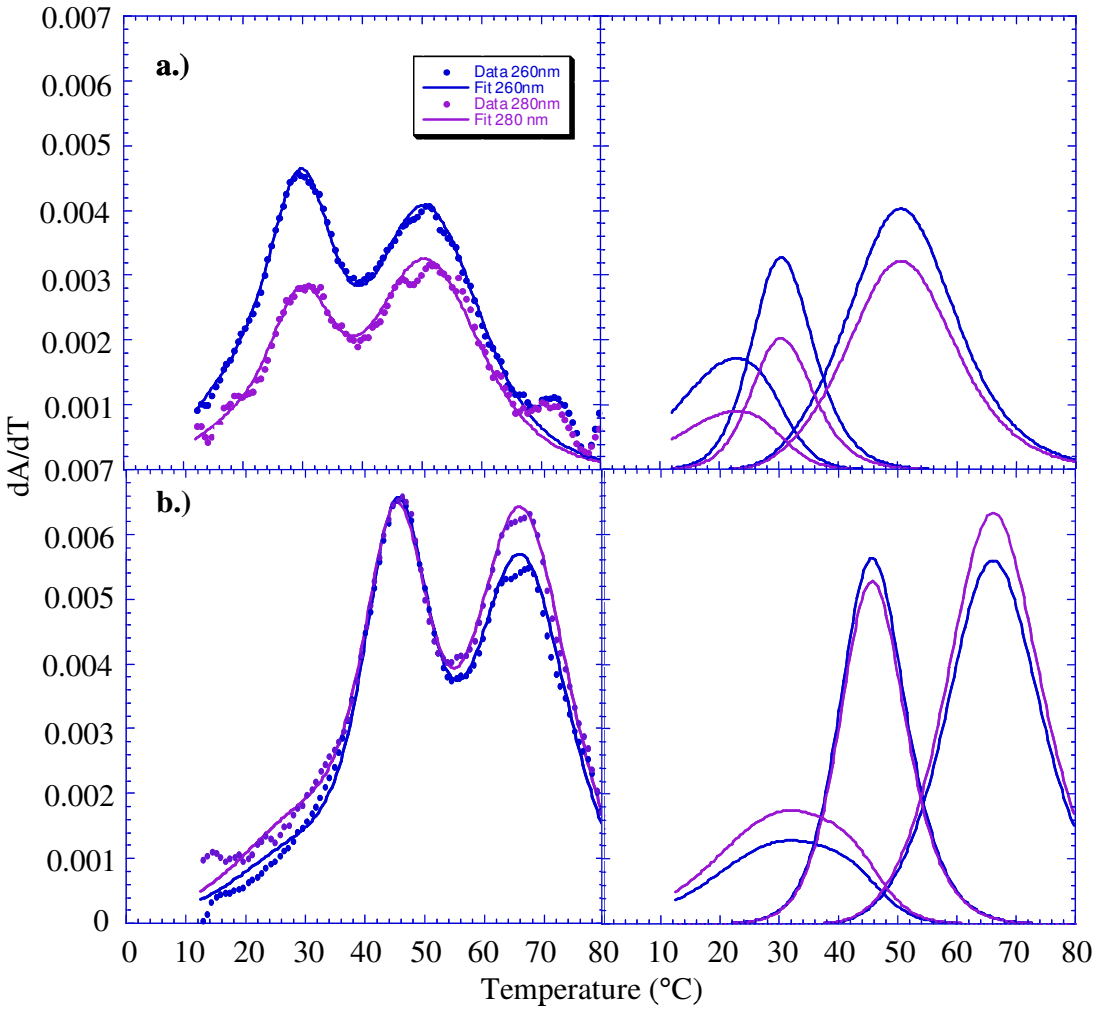

Figure 3-11: Melt profiles of the hinged construct of the hairpin ribozyme. The melt profiles in the hinged construct (a.) in the absence of M^{2+} (b.) in the presence of 10 mM Mg^{2+}. The raw data are plotted to the left and the individual fits are plotted on the right. The solution conditions were 2 μM RNA, 5 mM TEA, pH 7.8, 100 mM NaCl. The RNA strands were heated 90°C for 2 min. and fast-cooled in ice.

profile of the four-way junction construct is about six times greater in intensity than that of the two major enthalpy peaks of the hinged construct, suggestive of more extensive structure in the four-way junction construct.

Assignment of Transitions in the Melt Profile of the 4-Way Junction Construct of the Hairpin Ribozyme

The assignment of the transitions of the melt profile of the four-way junction construct of the hairpin ribozyme was accomplished by obtaining melt profiles of pairs of strands (Figure 3-12). The melt profile of strands a and d was featureless, suggesting that their interaction was not sufficient to form Stem A. On the other hand, each melt profile of the other pairs has one distinct feature. The interaction of strands a and b produce a feature at ~ 44°C, which is the same melting temperature as that of the large-enthalpy transition in the melt profile of the hairpin ribozyme. Therefore, a contributor to the prominent feature in the melt profile of the hairpin ribozyme is the unfolding of Stem B. The transition arising from the interaction between strands b and c results in a higher T_m of ~ 52°C, which is very similar to that of the low-profile peak in the melt profile of the four strands in solution. Therefore, this feature can be assigned as the unfolding event of Stem C. Finally, the two strands, c and d, in solution give rise to a feature with the highest T_m of ~ 65°C, which matches that of the final feature in the high-temperature region and is the melting temperature of Stem D. In addition, the features from each melt profile are very alike in shape. With the exception of the featureless melt profile of strands a and d, the melt profiles of the paired strands reveal features that compare well to those in the melt profile of the hairpin ribozyme.

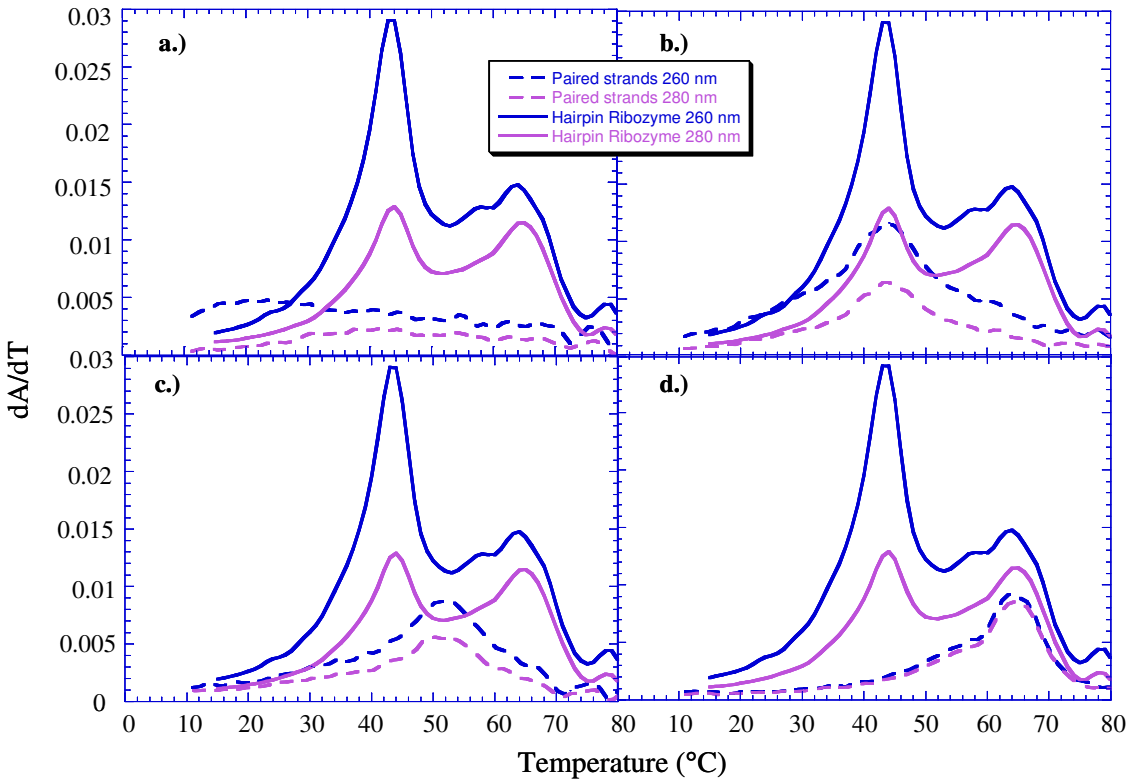

Figure 3-12: Overlay of melt profiles of hairpin ribozyme and paired strands. (a.) strands a & d (b.) strands a & b (c.) strands b & c, (d.) strands c & d. The solution conditions were 2 µM RNA, 5 mM TEA, pH 7.8, 100 mM NaCl, 400 µM Mg^{2+}. The RNA strands were heated at 65°C for 10 min. and slow-cooled for 1 hour.

Taking into account the difference between the overall melt profile of the hairpin ribozyme and the summation of the three melt profiles with transitions, a feature at about ~ 44°C was determined to be missing from the overall melt profile. Therefore, it appears that strands a and d must interact to form Stem A only in the presence of all four strands, and its unfolding event occurs at ~ 44°C. The simultaneous unfolding of both Stem A and Stem B at ~ 44°C corresponds to the large enthalpy of this transition.

Another experiment was performed to effectively eliminate the possibility that the melt profile arises from a three-strand complex, from which one of the four strands is excluded (Figure 3-13). The combination of strands examined were a, b, c; b, c, d; a, b, d; and a, c, d. None of the melt profiles was similar to that arising from all four strands in solution, thereby, precluding the formation of a three-stranded complex. The melt profile

of strands a, b, c, and d in solution was unique and reproducible. As a result, this experiment and the assignment of the transitions confirm that the four-way junction construct of the hairpin ribozyme forms.

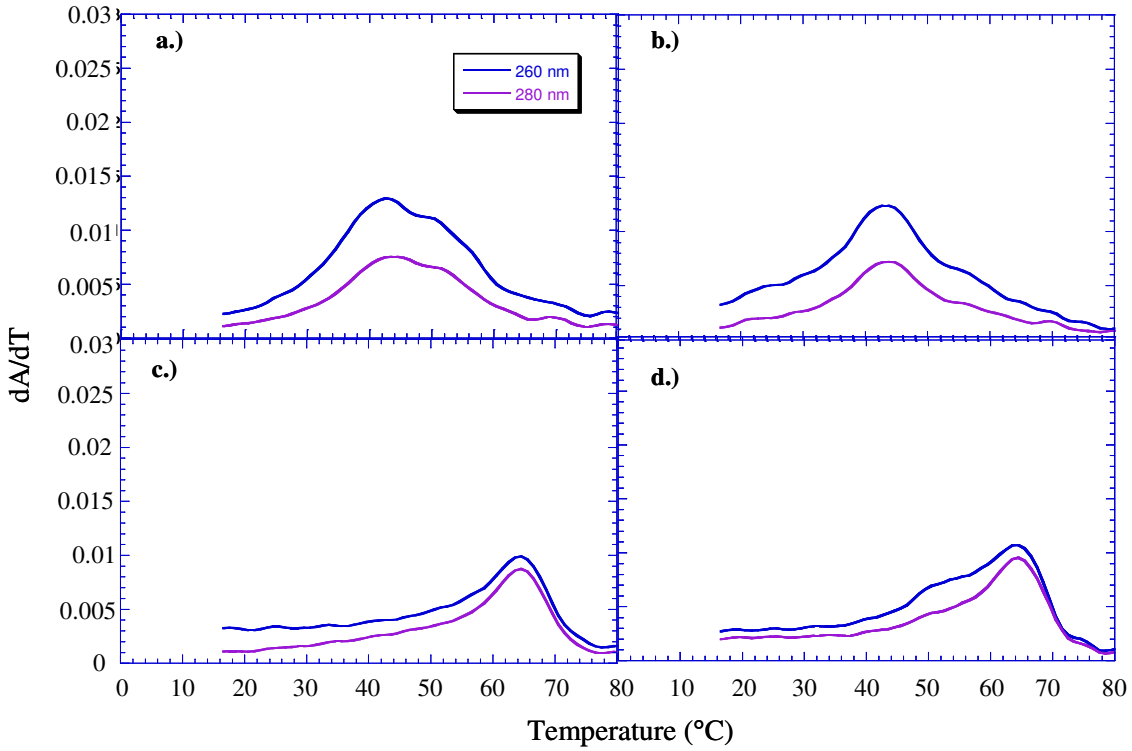

Figure 3-13: The melt profiles of solutions containing three strands. (a.) strands a, b, and c (b.) strands b, c, and d (c.) strands a, c, and d, (d.) strands a, b, and d. The solution conditions are 2 µM RNA, 5 mM TEA, pH 7.8, 100 mM NaCl, 400 µM Mg^{2+}. The RNA strands were heated at 65°C for 10 min. and slow-cooled for 1 hour.

Melt Profile of the Mutant

The melt profile of the mutant hairpin ribozyme is distinguishable from that of the four-way junction construct of the hairpin ribozyme (Figure 3-14). There are two major

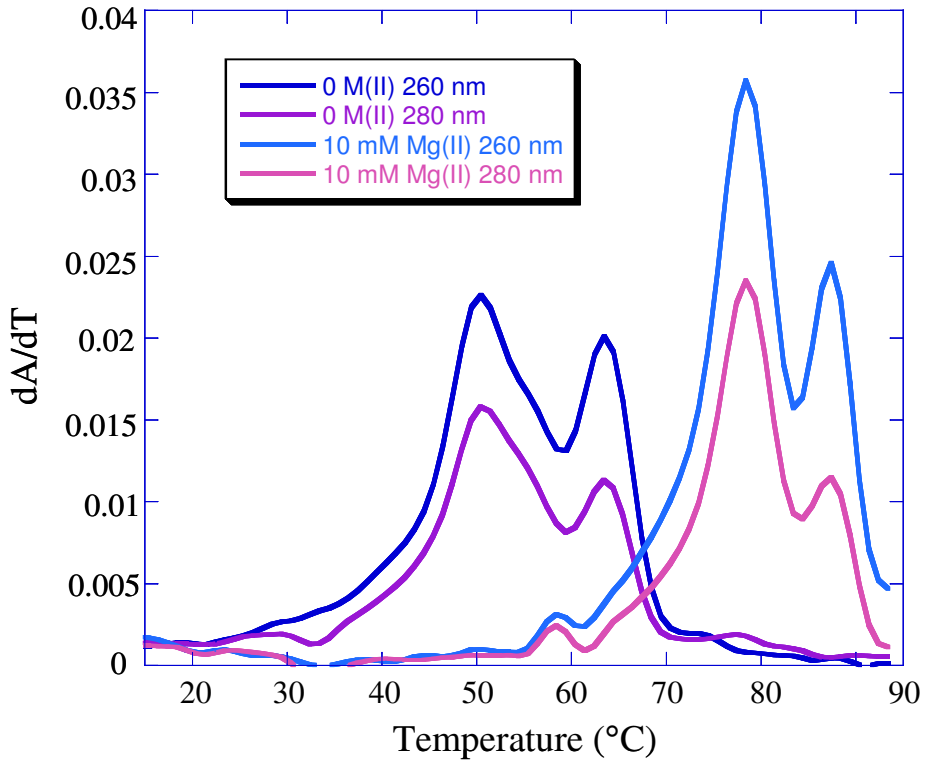

Figure 3-14: Melt profiles of the mutant without M^{2+} and in the presence of 10 mM Mg^{2+}. The solution conditions were 2 μM RNA, 5 mM TEA, pH 7.8, 25 mM NaCl. The RNA strands were heated at 65°C for 10 min. and slow-cooled for 1 hour.

enthalpy features, one of which is at ~ 50°C and the other at ~ 65°C, in 5 mM TEA, 25 mM NaCl, pH 7.8, without divalent metal ions. Even in the absence of divalent metal ions, the absorbance intensity is even greater than that of the major feature of the hairpin ribozyme. The addition of 10 mM Mg^{2+} results in a shift to higher melting temperatures and a dramatic increase in enthalpy of the peaks. The peaks corresponding to the two extreme concentrations of Mg^{2+} (0 and 10 mM) reveal the degree of shifts in the melting temperatures of the two transitions, neither of which is as great as the shift of the major enthalpy transition representing the unfolding of both loop-containing Stems A and B in the hairpin ribozyme. Internal loops tend to have greater metal-ion dependence due to its

lower stability compared to base-paired helices.[53] Therefore, base-paired RNA should not have large shifts in melting temperature, and this is observed for the two transitions in the melt profile of the mutant ribozyme. The small shifts are consistent with the presence of only base-paired helical stems. The two transitions of the melt profile of the mutant hairpin ribozyme arise from the uncooperative melting of all four stems.

The melting of individual pairs of strands overlays well with the overall melt profile of all four mutant strands (Figure 3-15). The pair of strands a' and d' is destabilized at ~ 54°C and most likely accounts for the shoulder observed in the first transition of the overall melt profile (Figure 3-15(a.)). The interaction between strands b and c is manifested as a broad low-enthalpy transition at ~ 40°C, which most likely contributes to the shoulder observed in the beginning of the overall melt profile (Figure 3-15(c.)). The strand c and d' pair has a T_m of ~ 50°C, which contributes to the first transition of the overall melt profile as well (Figure 3-15(d.)). Therefore, the a'-d', b-c, and c-d interactions all contribute to the first transition of the overall melt profile. Based on its length, Stem B, arising from the strand a' and b interaction, should have a higher melting temperature than the other stems (Figure 3-15(b.)). As expected, the strand a' and b interaction unfolds at ~ 65°C, and matches in enthalpy and temperature with the second major transition of the overall melt profile. Based on the formation of a larger extended complex in the native gels, the overall melt profile represents the thermal denaturation of the mutant hairpin ribozyme, and is not a result of a mixture of paired interactions in solution.

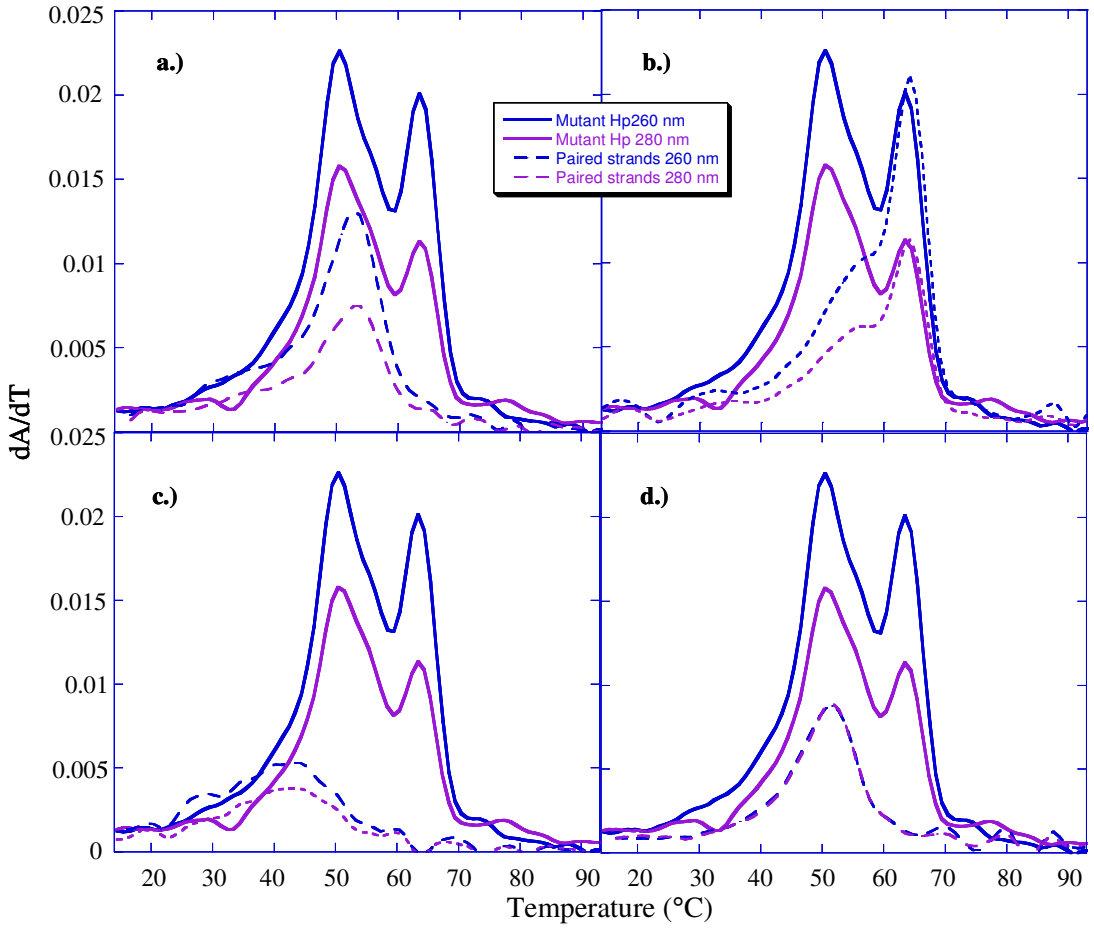

Figure 3-15: Overlay of the mutant melt profile and the melt profiles of paired strands. (a.) strands a' & d' (b.) strands a' & b (c.) strands b & c, (d.) strands c & d'. The solution conditions were 2 μM RNA, 5 mM TEA, pH 7.8, 25 mM NaCl. The RNA strands were heated at 65°C for 10 min. and slow-cooled for 1 hour. The blue lines and purple lines represent thermal denaturation detected at 260 nm and 280 nm, respectively. The melt profile shown in solid lines is that of the overall mutant hairpin ribozyme and the melt profiles shown in dashed lines are those of the paired strands in solution.

Comparison of Results of Native Gels and Thermal Denaturation

The application of native gel and thermal denaturation techniques provided consistent and valuable information. For example, both techniques point to the absence of an interaction between strands a and d. Native gels revealed only one band arising from uncomplexed strand a or strand d, depending on which was radiolabeled. This result matched the information determined from the UV melt profile, in which there were no transitions. This is consistent with the requirement for a higher background Na^+ concentration to encourage the formation of isolated Stem A for an NMR experiment.[34] The small strand-a-and-d interaction is explained by an insufficient number of base pairs in both helices that flank the internal loop to stabilize the structure. The presence of other strands is necessary to facilitate the interaction.

Both native gels and thermal denaturation highlighted the strong affinity between the strand c and d pair. The majority of strands c and d form a 2-stranded complex as indicated by an intense band with lower mobility than the marker's band. Thermal denaturation of this pair revealed its melting temperature to be the greatest in comparison to the other pairs. Therefore, more thermal energy was required to destabilize the strong, favorable interaction between strands c and d, or Stem D. In contrast, 50% of each member of the pairs of strands a and b and strands b and c form complexes and the pairs' melting temperatures are lower.

Conclusion

In conclusion, a solution composed mostly of the four-stranded four-way junction construct of the hairpin ribozyme and of the isolated four-way junction mutant hairpin ribozyme can be examined for its interactions with metal ions. This has been achieved by

a multi-lateral approach applying two techniques: native gels and thermal denaturation experiments. Activity revealed by kinetics experiments, discussed in the next chapter, also confirms the formation of the hairpin ribozyme.

The application of these techniques provided consistent and valuable information. Each thermal denaturation melt profile of the hairpin ribozyme and of the mutant was unique and complex, and the transitions were assigned as specific unfolding events for each stem. Native gels had provided insight into not only the quantity of the hairpin ribozyme and the mutant formed in solution, but the presence of other possible strand combinations as well. In fact, the results from native gels and UV melts were consistent.

The melting temperatures of the individual stems in the absence of divalent metal ions underscored the sensitivity of the ribozyme to temperature and the need for metal ions in the native gel and running buffer for stabilization. In other words, the melt profile provided valuable information for optimizing conditions in native gel electrophoresis, which was used to determine the homogeneity of the hairpin ribozyme in solution. In addition, the successful application of native gel electrophoresis for the complexation of four RNA strands may be the first to be reported. Finally, activity studies were useful in the confirmation of the homogeneity of the hairpin ribozyme in solution based on the percent of cleaved product.

CHAPTER IV

THE CATALYTIC AND STRUCTURAL ROLES OF METAL IONS IN THE FOUR-WAY JUNCTION CONSTRUCT OF THE HAIRPIN RIBOZYME

Introduction

As in any other RNA system, metal ions play a critical role in electrostatically stabilizing the structure of the hairpin ribozyme.[10] In fact, the lack of direct catalytic involvement of metal ions during cleavage and ligation of the hairpin ribozyme supports the widely-accepted view that the role of metal ions play is strictly structural. This is reinforced by the absence of both pH dependence and ionic preference on activity. In addition, phosphorothioate substitutions at the active site of the hinged construct display only a small effect on cleavage and ligation activity compared to the hairpin with unmodified phosphates. This points to an absence of metal ions bound to the phosphate groups near the active site.[33] NMR solution structures of the isolated domain A show a complete absence of metal ions.[34] This observation was confirmed in a 2.4 Å-resolution crystal structure of the docked complex of the four-way junction construct with a 2'O-methyl inhibitor in place of the 2'OH nucleophile (Figure 1-11).[35] Therefore, in the hairpin ribozyme, metal ions have a passive role in the catalytic mechanism, which is believed to require nucleotide bases with perturbed pK_a values in the active site. The ability of RNA to perform general acid-base catalysis without the aid of proteins or metal ion cofactors has been proposed already in the active sites of the HDV ribozyme and the peptidyl-transferase of the 50S ribosomal subunit.[20] As a result, numerous studies have sought the identity of the catalytic nucleotides.

Despite the absence of metal ions within Loop A of the hairpin ribozyme, there are two other regions of interest, which may have potentially tight metal-binding sites. One such region is Loop B. A surface charge potential of isolated domain B was constructed, revealing an unusually high electronegative "binding pocket" in the major groove, into which Tb^{3+} is proposed to bind.[15] Phosphorothioate modifications of the phosphates lining the pocket resulted in no change in Tb^{3+} inhibition constants, suggestive of outer-sphere cation binding. In addition, studies with the kinetically-inert complex, $Co(NH_3)_6^{3+}$, which is structurally similar to the hexahydrated Mg^{2+}, produce cleavage and ligation more effectively than Mg^{2+}. These findings strongly suggest that inner-sphere coordination of these cations is not required for catalysis.[15] In contrast, the high-resolution crystal structure of the docked four-way junction construct saturated in 20 mM Ca^{2+} reveals that, in the wide minor groove of Stem B, eight metal ion binding sites exist, two of which are "well-ordered" in that the Ca^{2+} ions are coordinated to the RNA through both inner- and outer-sphere contacts.[35] In addition, paramagnetic line broadening, chemical shift mapping, and intermolecular NOE connectivities indicate that the isolated domain B contains metal binding sites, all of which may accommodate Mn^{2+}, Mg^{2+}, and $Co(NH_3)_6^{3+}$.[39]

Another metal-binding region of interest is the four-way junction, a critical architectural element that stabilizes the folded tertiary structure and increases the rate of folding of the hairpin ribozyme at low Mg^{2+} (0.5 mM) concentrations.[28, 29] Upon addition of divalent metal ions, the four-way junction effectively orients the loops to facilitate their interaction with each other by rotation into an antiparallel intermediate, or "quasi-docked" state, preceding the completely folded conformation (Figure 1-9).[28, 29] In

addition, divalent metal ions, such as Mg^{2+}, Mn^{2+}, Ca^{2+}, Sr^{2+}, and $[Co(NH_3)_6]^{3+}$, or excess Na^{+} are required for docking of the hairpin ribozyme.[32] Based on previous FRET studies, at least one metal-binding site must be occupied to induce the four-way junction to position the stems into the "quasi-docked" state. Evidence points to the involvement of at least one metal ion at the four-way junction. However, the crystal structure of the four-way junction construct of the hairpin ribozyme did not reveal a metal ion within the four-way junction. This could be explained by the fact that solution conditions for crystallization are very different and not necessarily representative of solution conditions in nature.[35,43] Therefore, studies performed under physiological solution conditions may reveal metal-binding sites not observed in the crystal structure. The work presented in this chapter is based on the hypothesis that the critical metal binding site necessary to achieve the docked state is located within the four-way junction. This potential catalytically- and structurally-significant metal-binding site within the four-way junction was investigated using EPR spectroscopy.

Paramagnetic Mn^{2+} used in EPR spectroscopy is generally an effective substitute for Mg^{2+} due to similar charge-to-radius ratio for a wide range of biological molecules. The literature reports that the four-way junction construct of the hairpin ribozyme docks in the presence of Mn^{2+}, but is not active under these conditions.[32] Therefore, kinetics experiments were performed in a buffer different from that used in other reported studies for verification of this observation.

Metal-dependent thermal denaturation studies were employed to yield an apparent binding affinity of metal ions associated with the folding and unfolding of each stem and to aid in the characterization of the four-way junction construct of the hairpin ribozyme.

Finally, EPR spectroscopy was used to determine the number of types of metal-binding sites and the number of metal ions for each type of site and their apparent binding affinities for both the hairpin ribozyme and the mutant. A high binding affinity would indicate the involvement of metal ions in inner and/or outer sphere contacts with the RNA, highlighting the significance of the metal-binding site(s). The presence of a high binding affinity site in a region of high electronegative potential may indicate structurally-important metal ions.[31]

Low-temperature EPR experiments of both the hairpin ribozyme and the mutant were performed and discussed in this chapter to reveal a change in the lineshape of the EPR spectrum as a result of asymmetry around a Mn^{2+} ion, indicative of possible inner-sphere coordination to the RNA.

Activity Studies

Introduction

Mn^{2+} ions have proven to be an effective probe for metal binding sites in spectroscopic techniques, such as EPR spectroscopy and paramagnetic line broadening of NMR signals. In order to be an effective probe in the four-way junction construct of the hairpin ribozyme, Mn^{2+} ions, as its natural counterpart, Mg^{2+}, must promote activity. The hinged construct is functional in Mn^{2+}, however, the role of Mn^{2+} ions in the four-way junction construct is not as clear. Although Mn^{2+} induces proper global conformation, gel activity assays demonstrated an absence of cleavage.[32] This is unusual considering that numerous ribozymes, such as the hammerhead, hepatitis delta virus, *Neurospora* VS, RNase P, and the *Tetrahymena* Group I intron, are all active in the presence of Mn^{2+}.[9] Therefore, single-turnover conditions were used in a buffer of 5 mM triethanolamine

(TEA) as opposed to 50 mM Tris-HCl used in the gel activity assay reported by Lilley and coworkers. Unlike TEA buffer, Tris buffer may interfere with metal-RNA interactions, diminishing the number of Mn^{2+} ions available to achieve phosphodiester bond cleavage.[12]

Other major goals of the kinetics experiments involve the determination of the apparent binding affinity of the catalytically important metal ions and the comparison of this value to that reported in the literature for the same construct as well as for the hinged construct.

Cleavage of the Hairpin Ribozyme in 100 mM NaCl

In 5 mM TEA, 100 mM NaCl, pH 7.8, the first activity assays yielded results that contradicted the lack of activity of the four-way junction construct reported in the literature. In fact, cleavage was observed even in the absence of any divalent metal ions. Control experiments to explore the possibility of contamination were performed during which the RNA was incubated with EDTA in a TEA buffer known to have no divalent metal ion contamination. A concentration as high as 10 mM EDTA was needed to eliminate cleavage. However, another possibility was investigated in which the experiments were performed in different Na^{+} concentrations in the absence of EDTA. The four-way junction construct of the hairpin ribozyme was still slightly active in 50 mM NaCl, but cleavage was not observed in 25 mM NaCl. Therefore, the NaCl concentration of all the experiments unless otherwise specified is 25 mM.

Effect of Ligation on Percent Cleavage

The first-order rate constant (min^{-1}) for cleavage of the substrate strand was determined under single-turnover conditions. The ratios of the enzyme to substrate

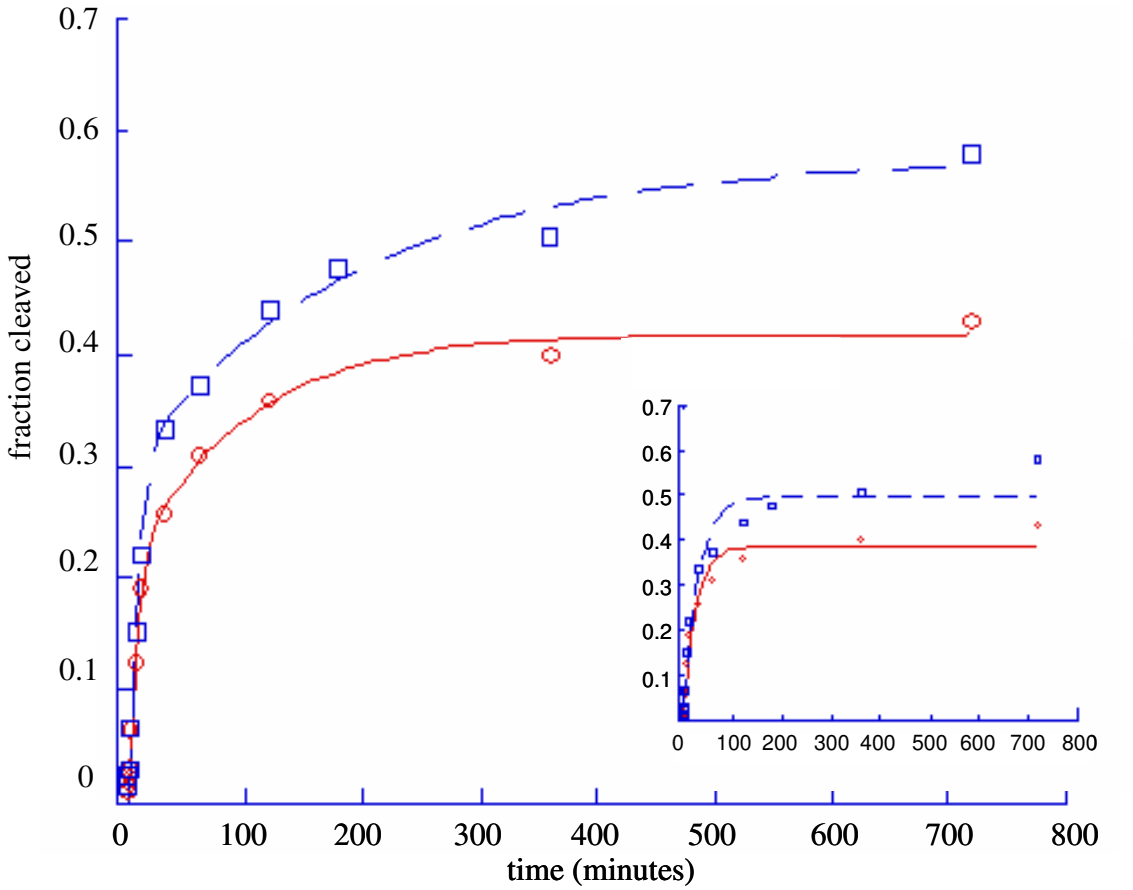

Figure 4-1: Comparison of biphasic and monophasic fits to kinetic traces in 2 mM Mg^{2+} and Mn^{2+}. The biphasic fits follow the data points more accurately than monophasic fits, which are shown in the inset. The single-turnover conditions were in 5 mM TEA, 25 mM NaCl, pH 7.8. The Mg^{2+} trace is shown in red and Mn^{2+} in blue.

concentrations were increased to 2:1 and the substrate was reduced to trace amounts. Despite these variations, the measured rates of cleavage were not affected, indicating that the rates arise from 1:1 complexes. (Data not shown.)

Figure 4-1 shows kinetic traces for the hairpin ribozyme with a shortened d strand in the presence of 2 mM Mg^{2+} and Mn^{2+}. The kinetic traces results from the plot of the fraction of the substrate cleaved as a function of time in minutes. The data were then fit by a nonlinear least-squares analysis using Equations 2.2 and 2.3. The double-

exponential fit follows the time points accurately throughout all the time points unlike the single-exponential fit. Therefore, the biphasic fit more accurately describes the data compared to the monophasic fit.

The biphasic fits yield the percent cleavage and the observed rate for both the fast- and slow-cleaving populations of the hairpin ribozyme at each M^{2+} concentration. The biphasic nature of the hairpin ribozyme catalysis is consistent with literature reports and

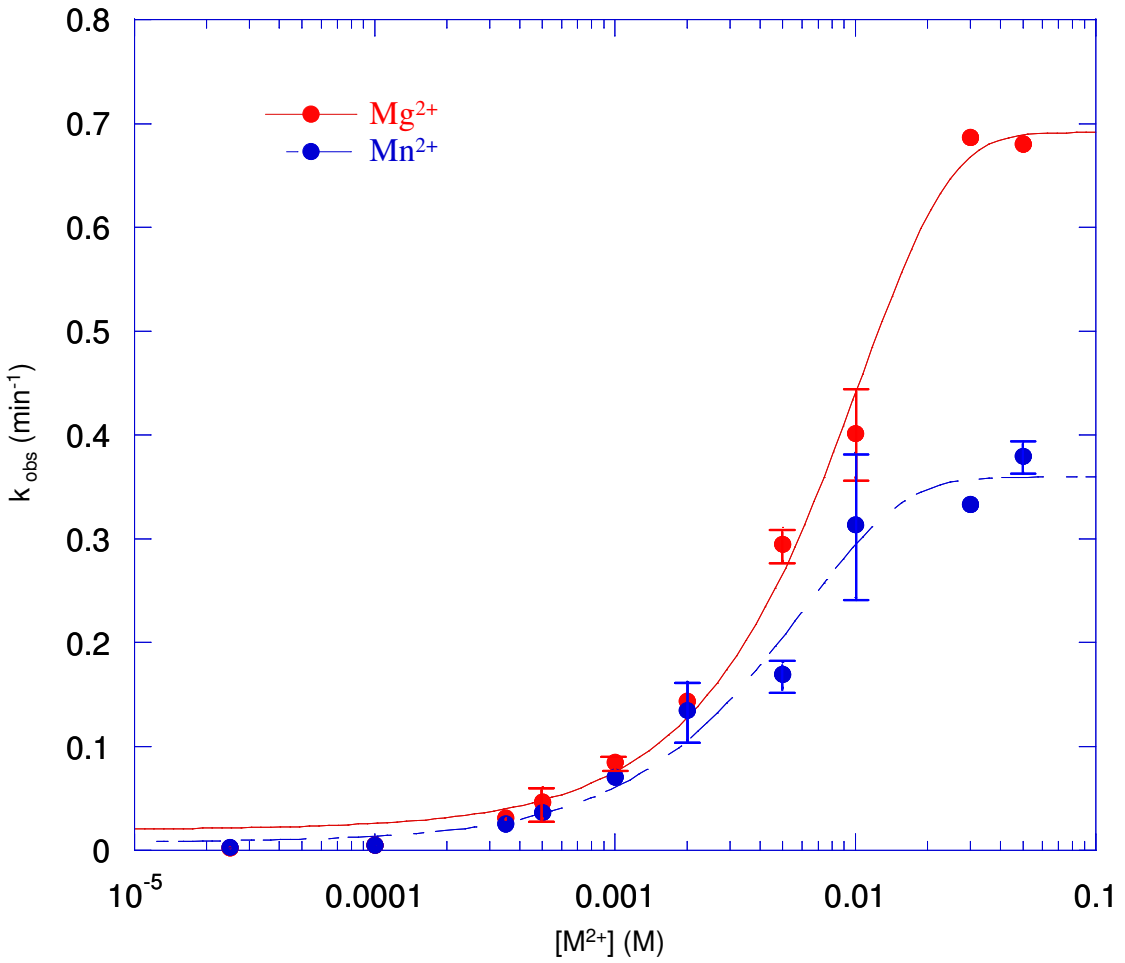

Figure 4-2: Mg^{2+}- and Mn^{2+}- dependent rate profiles of the four-way junction construct of the hairpin ribozyme with the shortened d substrate strand. The $[Mg^{2+}]_{1/2}$, the midpoint of the red sigmoidal curve, is 7 mM and $[Mn^{2+}]_{1/2}$, the midpoint of the blue sigmoidal curve, is 4 mM. The single-turnover solution conditions were 5 mM TEA, 25 mM NaCl, pH 7.8.

is proposed to arise from the various potential hydrogen bonding networks between Loop A and Loop B, some of which are correct and lead to the most efficient catalysis. [54]

The apparent binding affinity of the catalytically important divalent metal ions was determined from the midpoint of rate profiles, which were obtained from plotting the observed rate as a function of divalent metal ion concentration (Figure 4-2). But, initially, instead of resembling a sigmoidal curve as shown in Figure 4-2, the rate profile of the hairpin ribozyme in the presence of varying concentrations of Mg^{2+} displayed an increase in the observed rate from 25 μM to 5 mM Mg^{2+}, but then decreased steadily until the final concentration of 50 mM Mg^{2+}. In addition to the unusual drop in activity at higher concentrations of Mg^{2+}, the individual kinetic traces revealed a significant reduction in percent cleavage to only about 15%. (Shown in Appendix.)

The decrease in percent cleavage was most likely due to the ligation reaction, which is highly favored in the hairpin ribozyme. In other words, the percent cleavage drops as a direct result of the rapid reassociation of the cleaved products at higher Mg^{2+} concentrations. In order to circumvent this problem, the substrate (strand d) was shortened by three nucleotides to destabilize helix 1 on Stem A, to allow dissociation of the products (Figure 4-3).[43, 51] This shortened strand results in less base pairs within Helix 1, thereby enhancing the diffusion of the 3' product away from the ribozyme and reducing ligation. As a result, the percent cleavage increased to 70 – 75% at lower divalent metal ion concentrations. Since proper folding of a ribozyme leads to function, a plot of the percent of the cleaved product as a function of time can be directly correlated to the percent of the properly-folded hairpin ribozyme that formed in solution. Therefore, this high percentage of cleaved product indicates a majority of the hairpin ribozyme

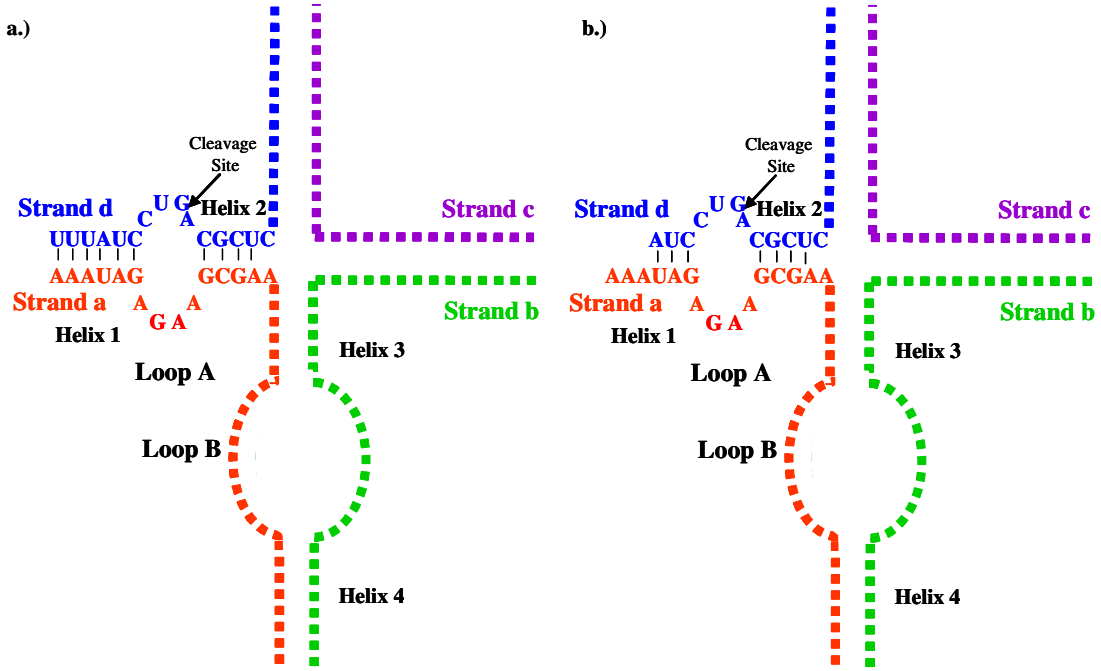

Figure 4-3: The effect of the number of base pairs in Helix 1 on ligation. (a.) 6 base pairs vs. (b.) 3 base pairs. The hairpin ribozyme greatly favors ligation, during which the cleaved products reassociate, thereby reducing the ability to accurately determine the percent of hairpin formed. To circumvent this problem, the substrate, or strand d, was shortened by three nucleotides to destabilize helix 1 on Stem A, which consequently allowed for the products to dissociate more readily.

formed in solution, consistent with results from native gel electrophoresis. However, the ligation reaction was still evident beyond Mg^{2+} concentrations of 5 mM due a gradual drop in the percent cleavage.

Activity Arises Solely From Presence of All Four Strands

A control kinetics experiment was performed to verify that two-stranded and three-stranded complexes do not contribute to the observed activity. The 2-strand combinations under examination were strands a and d, strands b and d, and strands c and d while the 3-strand combinations were strands a, b, d, strands b, c, d, and strands a, c, d.

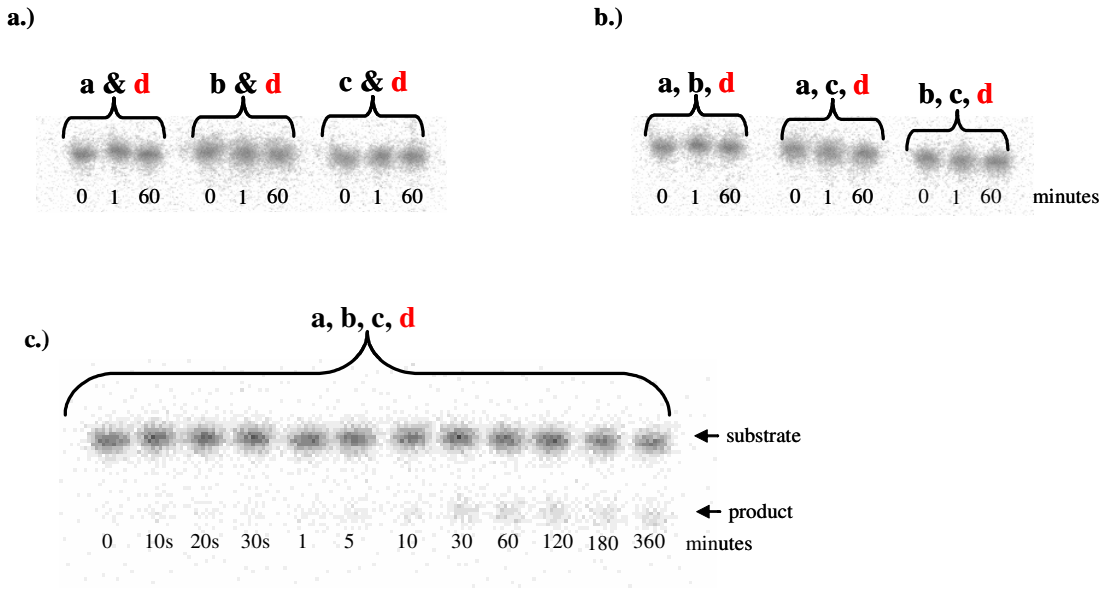

Figure 4-4: A control kinetics experiment to verify that observed cleavage activity arises solely from hairpin ribozyme. (a.) two-stranded and (b.) three-stranded complexes do not contribute to the observed activity at three time points. The reaction conditions were 3 µM enzyme, 2.5 µM d substrate, 5 mM TEA, pH = 7.8, 25 mM NaCl, and 20 °C. The four RNA strands were incubated at 65°C for 10 min., slow-cooled for 1hr, and equilibrated 10 minutes at 20°C. A 20% denaturing gel was used to separate the substrate from any cleaved product. (c.) Example of a gel activity assay revealing cleavage in 10 mM Mg^{2+}.

The absence of cleaved product demonstrates that the observed activity arises solely from the hairpin ribozyme (Figure 4-4).

Mg^{2+}- and Mn^{2+}- Dependent Rate Profiles

The Mg^{2+} - dependent rate profile for the fast cleavage activity of the hairpin ribozyme containing the shortened d strand is shown in Figure 4-2. The rate profile of the hairpin ribozyme containing the shortened d strand reveals that the maximum observed rate in 5 mM TEA, 25 mM NaCl, pH 7.8 in Mg^{2+} is 0.68 ± 0.003 min^{-1}. The midpoint of the curve is the concentration of Mg^{2+} at half maximal activity, $[Mg^{2+}]_{1/2}$, and

is regarded as an apparent binding affinity for a metal-binding site necessary for catalysis. Therefore, the apparent binding affinity of Mg^{2+} is about 7 mM.

Contrary to reports in the literature, the hairpin ribozyme is found to be active in Mn^{2+}. The ability for the hairpin ribozyme to cleave in Mn^{2+} may be affected by the TRIS buffer, which may interfere with critical Mn^{2+}-RNA interactions described in published studies. The maximum observed rate of the hairpin ribozyme in Mn^{2+} is 0.38 ± 0.015 min^{-1}, about half the maximum rate in Mg^{2+}. The apparent binding affinity, $[Mn^{2+}]_{1/2}$, in 5 mM TEA, 25 mM NaCl, pH 7.8, is 4 mM, which is similar to that of Mg^{2+}.

The similar apparent binding affinities for Mg^{2+} and Mn^{2+} are consistent with the nondiscriminatory nature of metal ions in the catalysis of the hairpin ribozyme reported in the literature. In fact, the apparent binding affinity values correspond well to 3.5 mM and 2 mM, for Mg^{2+} and Mn^{2+}, respectively in 50 mM Tris/HCl, 100 mM NaCl, pH 7.5 for the hinged construct of the hairpin ribozyme.[15] In addition, these values compare well to the binding affinities of the Mg^{2+} and Mn^{2+} of 10 mM and 4 mM, respectively, for the minimal construct in more similar buffer conditions of 5 mM TEA, 100 mM NaCl, and pH 7.8.[41] Therefore, the apparent binding affinities of the catalytically-relevant divalent metal ions for the simpler hinged construct and the four-way junction construct are similar. Based on these results, the passive role of metal ions in catalysis does not appear to change depending on the construct under examination.

Mg^{2+}- and Mn^{2+}- Dependent UV Thermal Denaturation Studies

The higher charge-to-radius ratio divalent metal ions make them more effective than monovalent ions with charge screening the phosphodiester backbone. Therefore, divalent metal ions have a greater impact on the stabilization of RNA structure.[10] The

extent by which divalent metal ions associate with and stabilize the global structure of the four-way junction construct of the hairpin ribozyme was determined by recording melt profiles over a range of Mg^{2+} (5 μM – 10 mM) and Mn^{2+} (5 μM – 5 mM) in the presence of a fixed concentration of 25 mM NaCl. From the melt profiles, the reciprocal of the melting temperature, $1/T_m$ (K^{-1}), was plotted as a function of the log concentration of divalent metal ions and fit to Equation 2.4 as seen in Figures 4-5 and 4-6.[49] This model assumes an electrostatic interaction of one divalent metal ion for every two phosphates, and two-state unfolding associated with the transition being fit. For both Mg^{2+} and Mn^{2+}, the binding affinity for the folded form (K_f) and the binding affinity for the unfolded form (K_u) were obtained from the fits for Transition 1 and Transition 3 of the melt profile of the four-way junction construct of the hairpin ribozyme shown in Figure 4-7. The apparent dissociation constant, $K_{d\ app}$, is defined as the reciprocal of K_f. Transition 1 is the major enthalpy feature resulting from the simultaneous unfolding of Stems A and B. Transition 3 is the subtle highest-temperature feature arising from the unfolding event of Stem D. The binding affinities of Mg^{2+} for the folded form is 4,603 ± 400 M^{-1} and for the unfolded form is 1,456 ± 150 M^{-1} for Transition 1, while K_f is 3,998 ± 200 M^{-1} and K_u is 660 ± 50 M^{-1} for Transition 3. The apparent dissociation constants of Mg^{2+} are 217 ± 20 μM and 250 ± 13 μM for Transition 1 and Transition 3, respectively. The binding affinities of the folded and unfolded forms of Stem C cannot be clearly determined since it is obscured by the more prominent transitions of the melt profile.

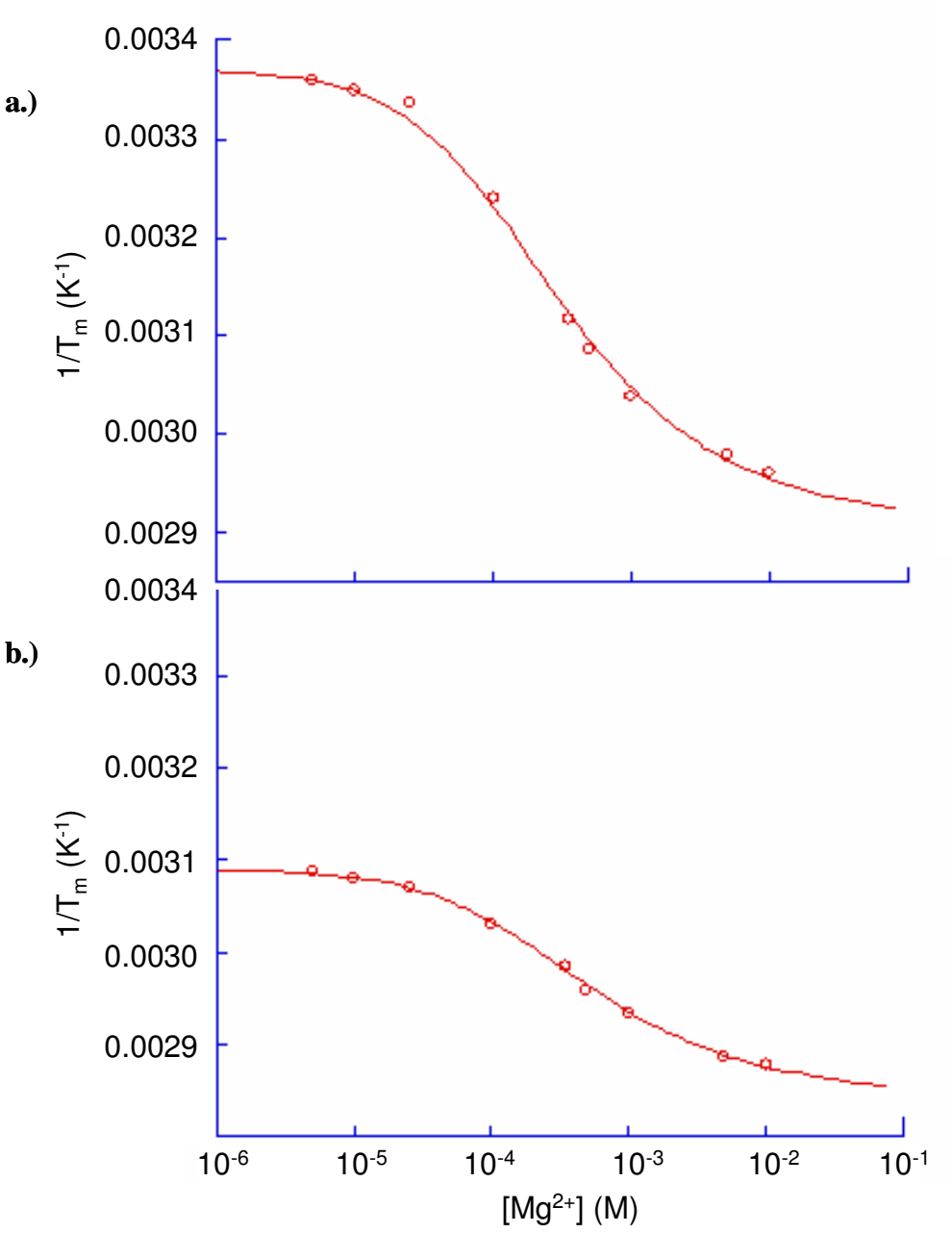

Figure 4-5: Mg^{2+}- dependent UV thermal denaturation of the four-way junction construct of the hairpin ribozyme. The metal-dependent shift in melting-temperature is shown for a.) Transition 1 and b.) Transition 3. The solution conditions were 5 mM TEA, 25 mM NaCl, pH 7.8.

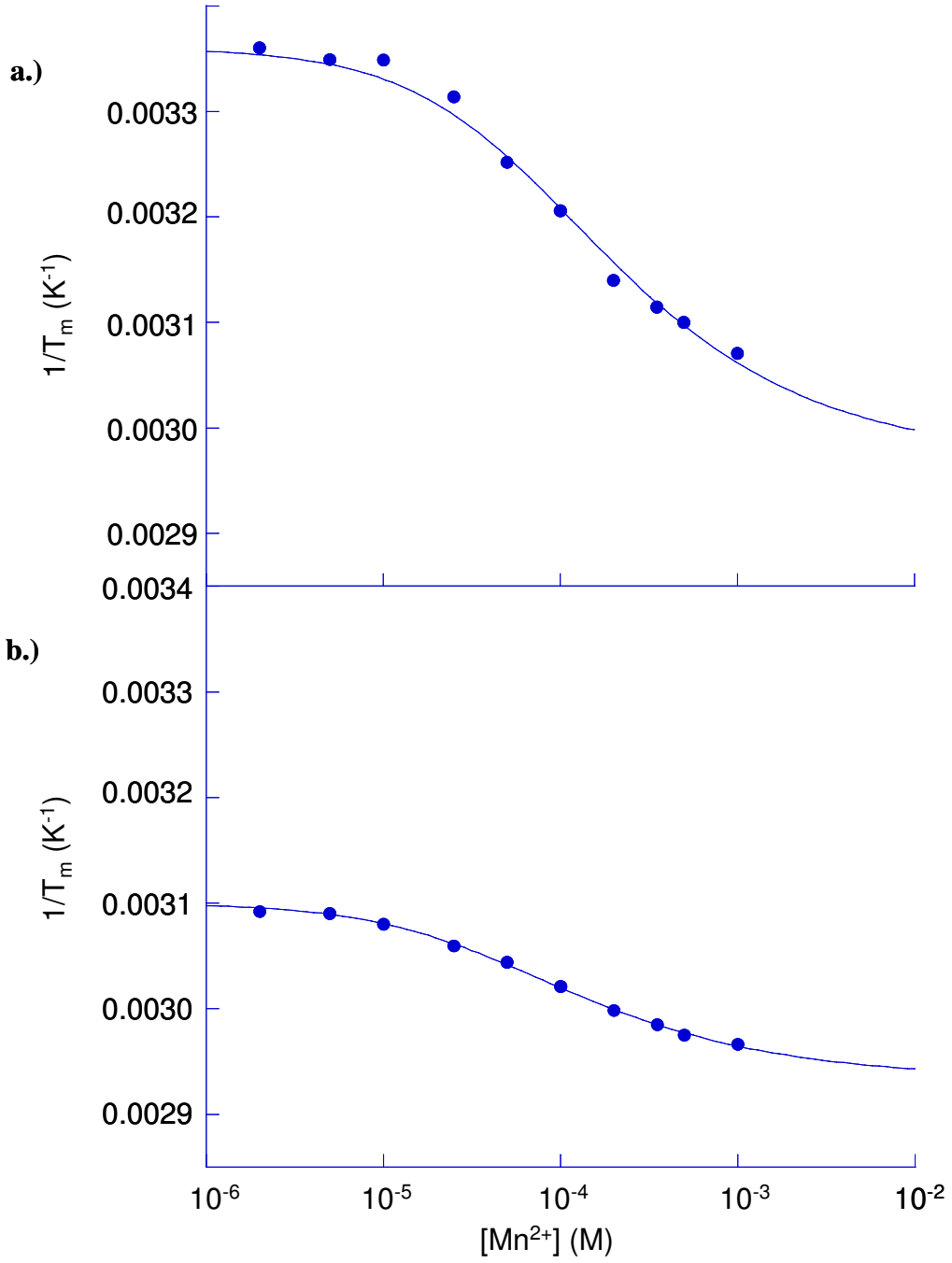

Figure 4-6: Mn^{2+}- dependent UV thermal denaturation of the four-way junction construct of the hairpin ribozyme. The metal-dependent shift in melting-temperature is shown for a.) Transition 1 and b.) Transition 3. Solution conditions were 5 mM TEA, 25 mM NaCl, pH 7.8.

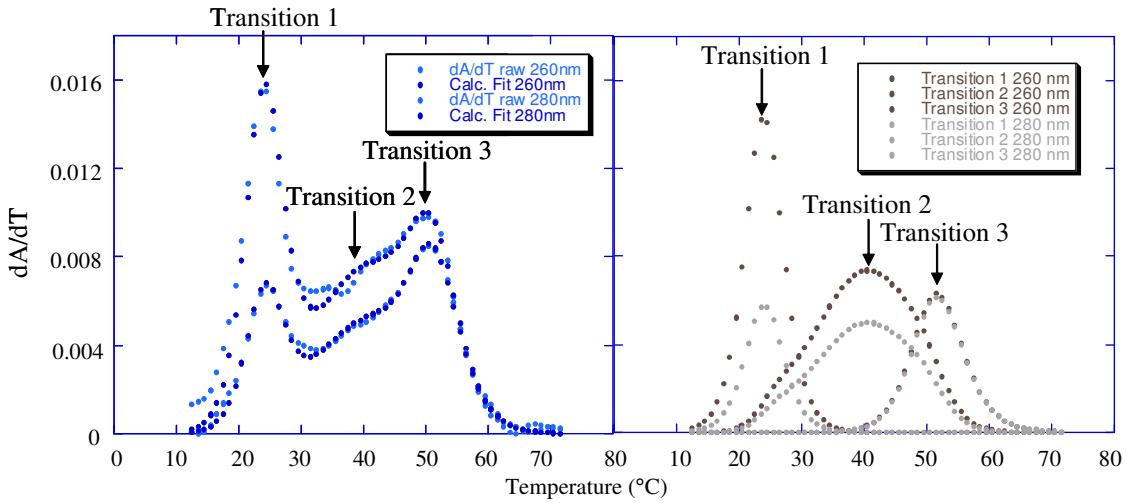

Figure 4-7: The melt profile and calculated fits of the hairpin ribozyme in the absence of divalent metal ions. The raw data are plotted on the left and the individual fits are plotted on the right. The solution conditions were 2 µM RNA, 5 mM TEA, pH 7.8, 25 mM NaCl.

Table 4-1: UV - detected thermal denaturation binding affinities of Mg^{2+} and Mn^{2+}. Solution conditions were 2 µM RNA, 5 mM TEA, pH 7.8, 25 mM NaCl.

	Mg^{2+}			**Mn^{2+}**		
Transition	**K_f (M^{-1})**	**K_u (M^{-1})**	**$K_{d\ app}$ (µM)**	**K_f (M^{-1})**	**K_u (M^{-1})**	**$K_{d\ app}$ (µM)**
1	4603 ± 400	1456 ± 150	217 ± 20	6786 ± 900	2548 ± 450	147 ± 17
3	3998 ± 200	660 ± 50	250 ± 13	12499 ± 600	3647 ± 200	80 ± 4

In comparison, the binding affinity of Mn^{2+} for the folded form is 6,786 ± 900 M^{-1}, and that for the unfolded form is 2,548 ± 450 M^{-1} for Transition 1. For Transition 3, K_f is 12,499 ± 600 M^{-1} and K_u is 3,647 ± 200 M^{-1}. The apparent dissociation constants of Mn^{2+} are 147 ± 17 μM and 80 ± 4 μM for Transition 1 and Transition 3, respectively. The binding affinities for both divalent metal ions are summarized in Table 4-1.

In addition, the assignment of the transitions to the unfolding events of each stem is supported by the extent of the shift in T_m as a function of metal concentration. This is due to the presence of stems with and without internal loops, which affects the stability of an RNA sequence.[53] Specifically, internal loops reduce the stability of RNA, which is manifested by a lower T_m than that of base-paired stems. This is another basis for designating the assignment of the melting of the loop-containing Stems A and B as Transition 1, which has the lowest T_m in the melt profile of the hairpin ribozyme. Another important characteristic is the greater metal-ion dependence of internal loops, which is generally manifested by a larger shift in melting temperature of a transition when compared to that of an RNA duplex lacking loops.[55] Therefore, Transition 1 has the largest shift in melting temperature consistent with its assignment as the unfolding event of the loop-containing stems, Stems A and B.

In summary, thermal denaturation metal dependence studies demonstrated an overall similarity in the apparent dissociation constants of divalent metal ions associated with each transition. The similarity indicates that Mg^{2+} and Mn^{2+} ions are able to stabilize the global structure of Stems, A, B, and D of the hairpin ribozyme in a similar manner. If the shift of the transition related to the destabilization of Stem C could be observed more clearly, a similar apparent dissociation constant may be determined.

Finally, the extent of shift in melting temperature as a function of divalent metal ion confirms the assignment of the transitions discussed in Chapter III.

Room-Temperature Mn^{2+} EPR Binding Isotherms

EPR spectroscopy has provided structural and mechanistic information for protein-based metalloenzymes, as well as for the hammerhead ribozyme[11, 12] and the group I intron.[56] Recently, in a background of 100 mM NaCl, the hinged construct was found to bind 24.2 $\pm$ 0.8 Mn^{2+} ions with an average binding affinity of 54.5 $\pm$ 7.3 μM.[41] Based on hammerhead studies in which high and low affinity sites were found with apparent K_d values of less than 10 μM and greater than 100 μM, respectively, an apparent K_d of ~ 54 μM for the hairpin ribozyme was obtained, suggesting a mixture of both tight and diffuse metal-binding sites is plausible.[12,41]

An EPR binding isotherm of the four-way junction construct of the hairpin ribozyme in a NaCl background concentration of 25 mM was obtained from fitting the data to one type of metal binding sites (Figure 4-8). The buffer solution was 5 mM TEA at a pH of 7.8. A sharp increase from 3 to 12 bound metal ions was revealed, suggestive of approximately 12 relatively tightly-bound Mn^{2+} ions in the hairpin ribozyme, and then the curve very gradually levels off to a total of 25 bound metal ions. Below 40 μM Mn^{2+}, there are no free ions, indicating that all metal ions are bound to the hairpin ribozyme. The apparent binding affinity of the metal ions yielded by the curve is ~ 45 μM, which is most likely an average of tight and weak metal binding affinities.

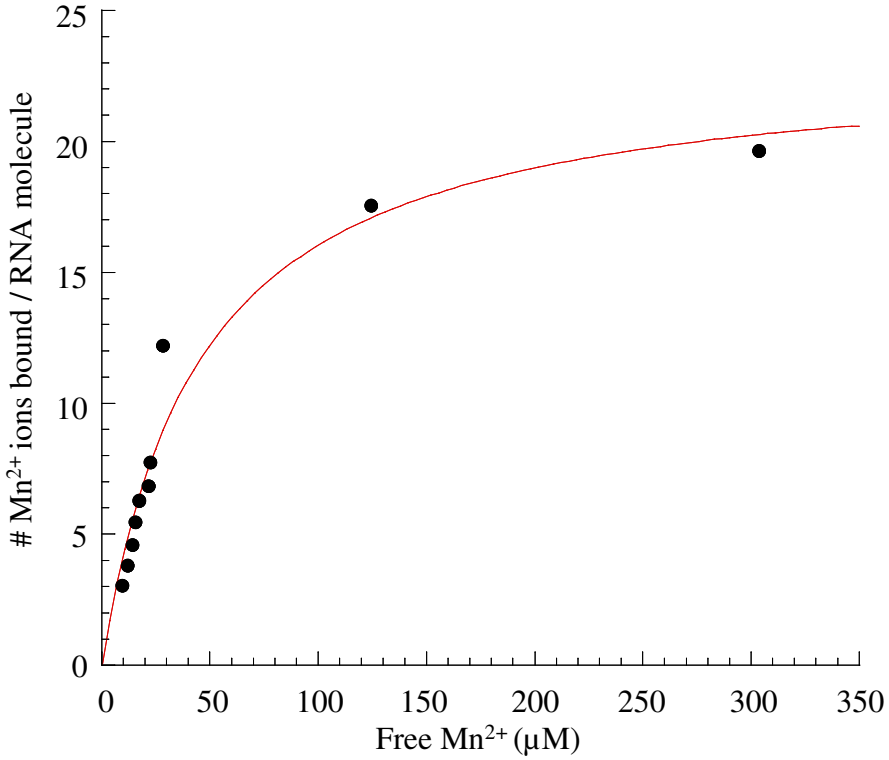

Figure 4-8: Mn^{2+} EPR binding isotherm of the four-way junction construct of the hairpin ribozyme in 25 mM NaCl. Solution conditions were 5 mM TEA, 25 mM NaCl, pH 7.8. The number of Mn^{2+} bound is 23.2 ± 1.7 and the apparent K_d is 45 ± 7.7 μM.

To attempt to isolate potential tight metal-binding sites in the four-way junction construct, EPR competition studies with higher concentrations of NaCl, from 50 mM to 500 mM, were conducted (Table 4-2). This was based on the principle that a larger concentration of Na^+ ions should displace "loosely" bound Mn^{2+} ions from their sites, with only the tightly bound Mn^{2+} remaining. This experiment was performed for the hammerhead ribozyme, which was found to have a single high affinity Mn^{2+} site with an apparent K_d less than 10 μM in 1 M NaCl.[12] Hence, EPR NaCl competition studies could be employed to detect a tight metal binding site, such as that suggested by the high-resolution crystal structure of the hairpin ribozyme. In 100 mM NaCl and only 50 μM

Mn^{2+}, approximately 2 Mn^{2+} ions were revealed to be bound. These two Mn^{2+} ions possibly correspond to the sites found within the crystal structure. However, it is important to note that these metal binding sites are not as tight as that found in the

Table 4-2: EPR NaCl competition study. Solution conditions were 5 mM TEA, pH 7.8, varied amounts of NaCl and $MgCl_2$.

Concentration of NaCl (mM)	**# Mn^{2+} ions bound in 150 µM Mn^{2+}**	**# Mn^{2+} ions bound in 50 µM Mn^{2+}**
25	12.19	3.81
100	8.54	1.44
200	2.23	0.88
500	-1.02	--

hammerhead ribozyme based on the absence of bound metal ions in 500 mM NaCl and 150 µM Mn^{2+} in the hairpin ribozyme.

Since two Mn^{2+} ions are bound in only 50 µM Mn^{2+}, the EPR experiments were performed in 100 mM NaCl, the results of which can be directly compared with EPR studies of other RNA systems in the same salt concentration. The EPR binding isotherm can be fit to one type of metal-binding sites, which also has about 25 Mn^{2+} ions bound with an apparent K_d of 215 µM. However, the binding isotherm can be fit to two types of metal-binding sites, which indicates the presence of both high- and low-affinity sites. The two fits are almost identical; however, the error of the apparent binding affinity of the tight metal binding sites is at least 200% (Figure 4-9).

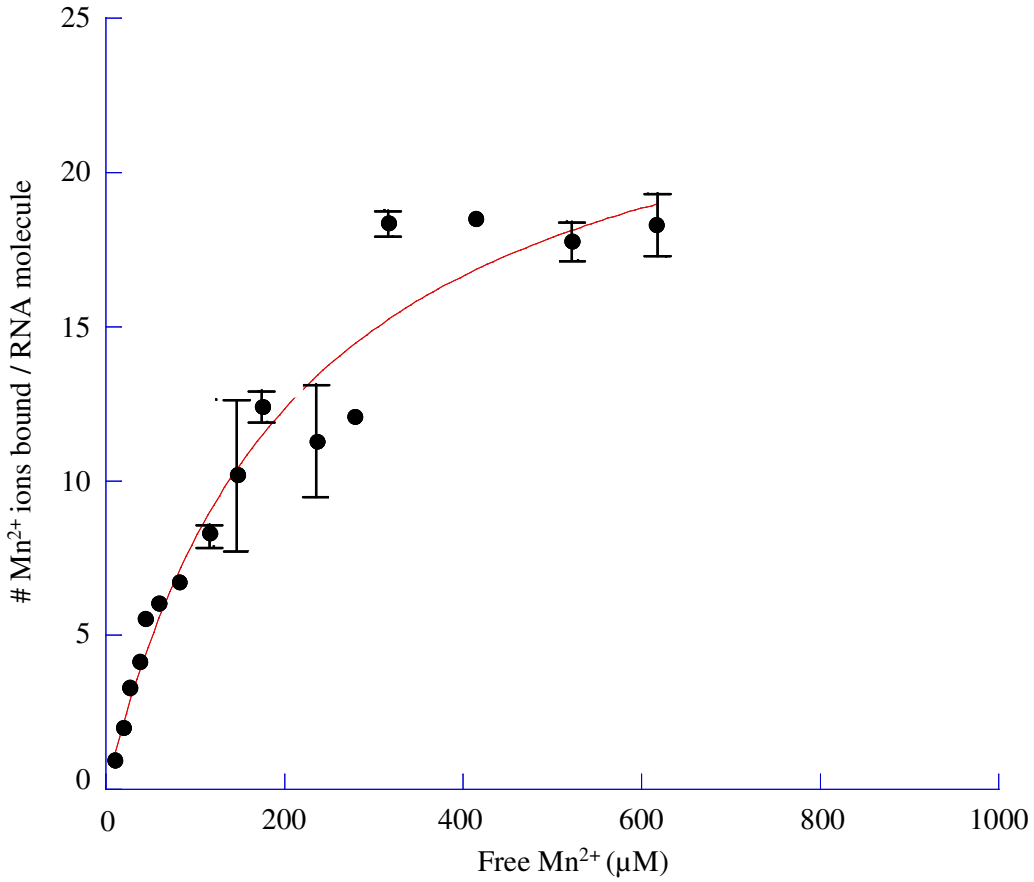

Figure 4-9: Mn^{2+} EPR binding isotherm of the four-way junction construct of the hairpin ribozyme in 100 mM NaCl. Solution conditions were 5 mM TEA, 100 mM NaCl, pH 7.8. The points are an average of 3 to 4 trials. The number of Mn^{2+} bound is 25.6 ± 2.3 and the apparent K_d is 214.8 ± 44 µM.

In comparison, the EPR binding isotherm of the mutant is very similar to that of the hairpin ribozyme (Figure 4-10). However, the two isotherms diverge slightly, which is expected based on the difference of the internal loops between the two hairpin structures. The inability of the mutant to dock in the absence of the internal loops is most likely the cause for the higher number of low-affinity sites. The missing loop-loop interaction cannot expel any metal ions that may have been loosely bound preceding docking. Therefore, the slight deviation between the two isotherms can be explained and

the overall qualitative resemblance of the slopes of both isotherms highlights comparable metal-binding properties between the two hairpin structures. This similarity is most likely due to the same electrostatic metal-RNA interactions within or in the vicinity of the four-way junction.

Based on the native gels, there are other minor species, such as uncomplexed

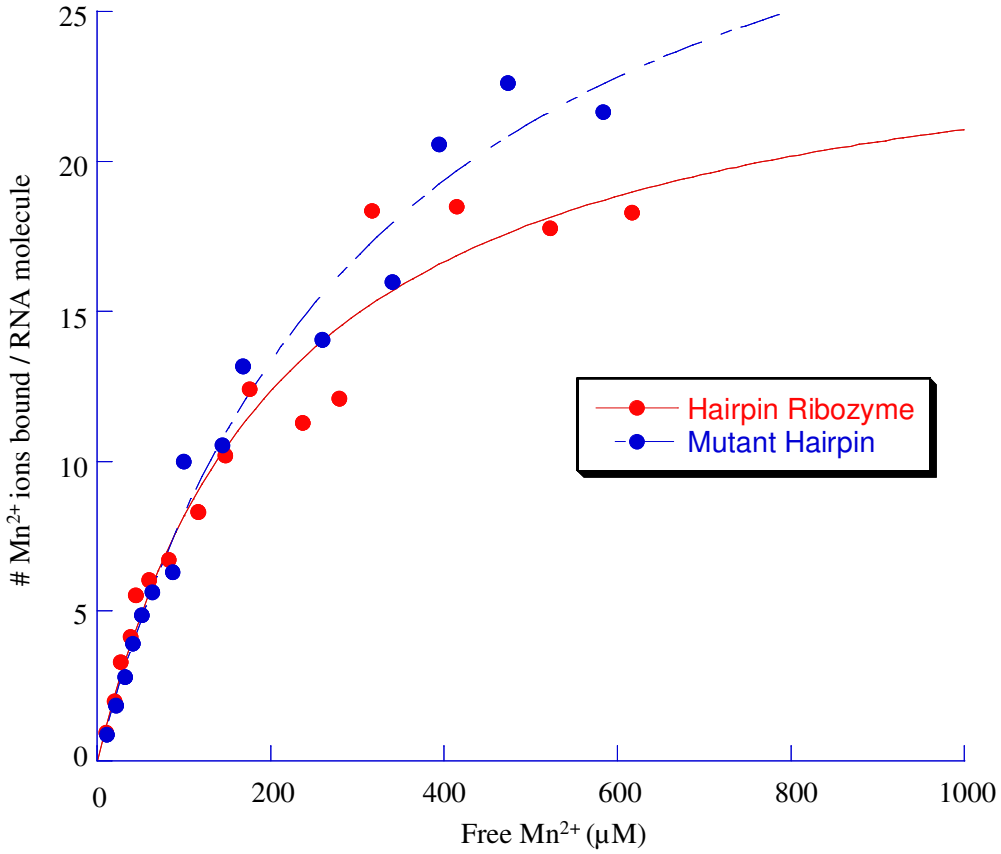

Figure 4-10: Comparison of Mn^{2+} EPR binding isotherms of hairpin ribozyme and its mutant in 100 mM NaCl. Solution conditions were 5 mM TEA, 100 mM NaCl, pH 7.8. The number of Mn^{2+} bound in the mutant is 35.4 ± 3.2 and the apparent K_d is 330.4 ± 59 µM.

RNA strands, and 2-stranded and 3-stranded complexes, in solution. On average, there is only about 20% of these species in solution. Therefore, the heterogeneity of the solution

may affect the EPR results, but ideally not in a significant manner. For example, if these species have solely diffuse electrostatic interactions, then they would cause the overall apparent binding affinity to be only slightly weaker.

Broadening of the EPR Lineshape of a Mn^{2+} Ion Bound to the Hairpin Ribozyme

Low temperature EPR spectroscopy decreases rotational motion of molecules, enhancing the anisotropy of the system. As a result, distinctive characteristics of inner-sphere binding of Mn^{2+} to a particular hairpin ribozyme may be observed. For example, a distinct feature in the sixth hyperfine line has been noticed in the hammerhead ribozyme. On the other hand, the lineshape may only broaden, but is also indicative of asymmetry as a result of the Mn^{2+} binding to the hairpin ribozyme.[55, 57]

In the case of the four-way junction construct of the hairpin ribozyme, a specific lineshape change in not observed, but line broadening and reduction in signal intensity points to asymmetry around a Mn^{2+} ion (Figure 4-11). Therefore, the Mn^{2+} ion bound with the highest affinity has inner-sphere coordination to the RNA within a site in the hairpin ribozyme. The substoichiometric ratio of Mn^{2+}:RNA of 0.75:1 was used to ensure the observed Mn^{2+} signal is a result of one Mn^{2+} ion bound to the highest-affinity site (Figure 4-11(a.)). However, the possibility of 75% hairpin ribozyme formation in solution based on the native gels may render the true ratio to be 1:1. Therefore, to ensure a substoichiometric ratio of Mn^{2+}:RNA, the ratio was decreased to 0.5:1. As a result, the low-temperature EPR spectrum of bound Mn^{2+} reveals an enhancement of line broadening and an even greater drop in signal intensity, thereby further pointing to the asymmetry around the Mn^{2+} (Figure 4-11(b.)).

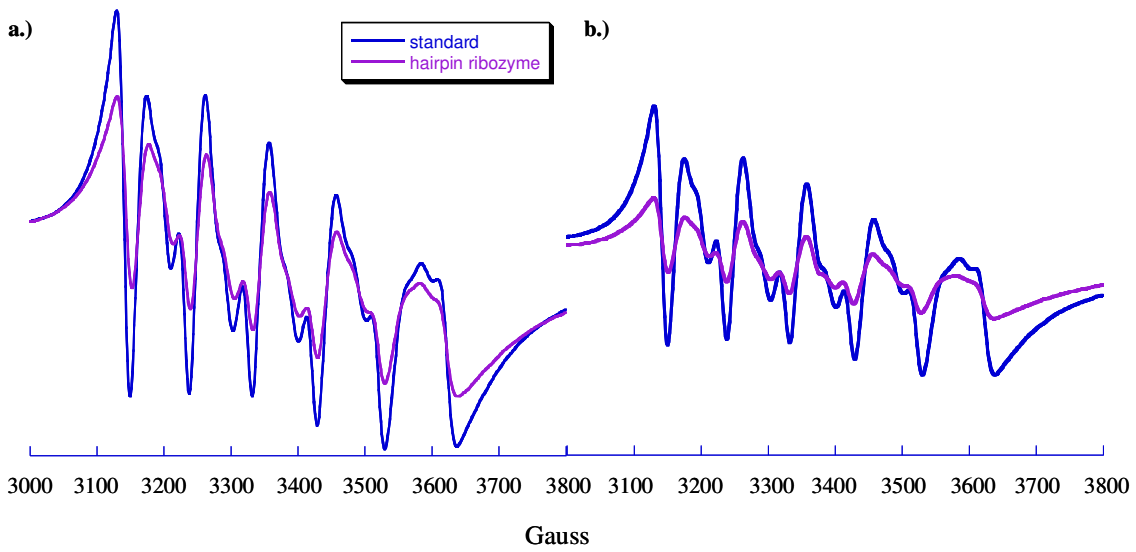

Figure 4-11: Comparison of low-temperature EPR spectra of Mn^{2+} in buffer and Mn^{2+} in the presence of the hairpin ribozyme. Solution conditions were 5 mM TEA, 100 mM NaCl, pH 7.8, 20% ethylene glycol. a.) 0.75:1 Mn^{2+}:RNA, 200 µM Mn^{2+}, 260 µM RNA, b.) 0.5:1 Mn^{2+}:RNA, 150 µM Mn^{2+}, 300 µM RNA.

Interestingly, the EPR spectrum of Mn^{2+} bound within the hairpin ribozyme and that of Mn^{2+} coordinated to the nucleotide, guanine monophosphate (GMP), overlay closely (Figure 4-12). Crystal structures of the hairpin ribozyme reveal that a water ligand of Mn^{2+} is replaced by the N7 heteroatom of the guanine.[58] Therefore, this suggests that the bound Mn^{2+} is directly coordinated to the N7 of a guanine in the hairpin ribozyme. All three regions of potential metal-binding sites, Loop A, Loop B, and the four-way junction, contain one or more guanines.

The low-temperature EPR spectrum of the loopless mutant should ideally suggest whether or not the possibility of a Mn^{2+} ion is bound within the four-way junction. Under the same substoichiometric ratio conditions, if the EPR spectra of the hairpin ribozyme and the mutant match well, then one could postulate that the high-affinity metal-binding site within the hairpin ribozyme is in the vicinity of the four-way junction.

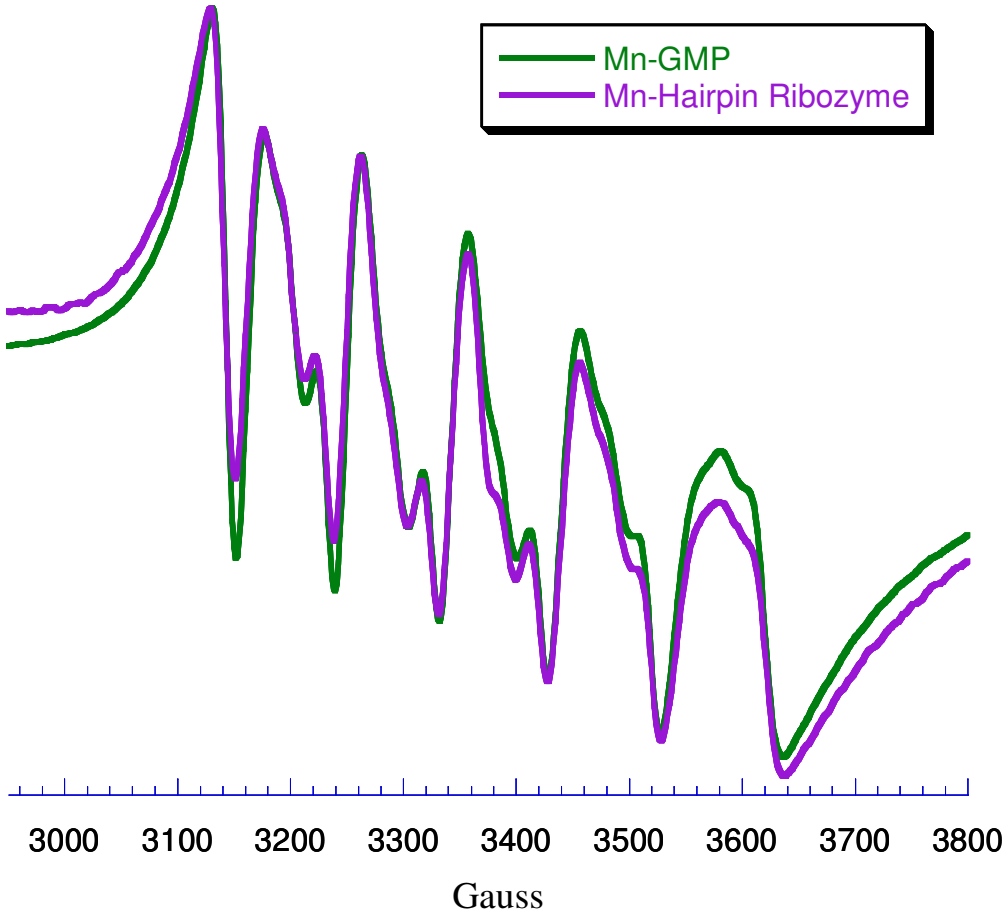

Figure 4-12: Comparison of low-temperature EPR spectra of Mn^{2+}-GMP complex and Mn^{2+}-hairpin ribozyme complex. Solution conditions for the Mn^{2+}-hairpin ribozyme were 5 mM TEA, 100 mM NaCl, pH 7.8, 20% ethylene glycol, 0.5:1 Mn^{2+}:RNA, 150 µM Mn^{2+}, 300 µM RNA. The solution conditions for Mn^{2+}-GMP is 500 µM Mn^{2+}, 2.5 mM GMP (1:5 ratio). The two spectra were normalized to match signal intensity for comparison.

Unfortunately, the low-temperature EPR spectroscopic experiments of the mutant encountered some technical difficulties; thus, the experiment needs to be repeated for future work.

Conclusion

In conclusion, the qualitative resemblance of the EPR binding isotherms of the hairpin ribozyme and its loopless mutant suggests that there are similar electrostatic metal-RNA interactions within or in the vicinity of the four-way junction of the hairpin ribozyme. However, a high-affinity metal-binding site could not be determined by these room-temperature EPR binding isotherms. In contrast, low-temperature EPR spectroscopy suggests inner-sphere coordination of a Mn^{2+} ion to the hairpin ribozyme, possibly to the N7 of a guanine. However, the possibility of direct Mn^{2+} coordination to specifically the four-way junction or its vicinity could not be confirmed.

Another novel result to note is the activity of the four-way junction construct of the hairpin ribozyme in the presence of Mn^{2+}. Previously, Mn^{2+} ions were reported to have the sole ability to promote the docking of the four-way junction construct of the hairpin ribozyme. However, this divalent metal ion did not support cleavage.[32] This observation was not the case in the experiments presented in this chapter and the discrepancy could be explained by the different buffer conditions. The apparent binding affinity of catalytically relevant Mn^{2+} ions is very similar to that of Mg^{2+}, confirming the nondiscriminatory nature of the activity of the hairpin ribozyme. On a similar note, UV thermal denaturation metal dependence studies reveal an overall similarity in the apparent binding affinities of divalent metal ions associated with each transition. In other words, Mg^{2+} and Mn^{2+} ions are able to stabilize the global structure of each stem of the hairpin ribozyme in a similar manner.

CHAPTER V

A LIGAND-TO-METAL CHARGE TRANSFER BAND BETWEEN SULFUR OF AMPS AND CD^{2+}

Introduction

Phosphorothioate substitution into nucleic acids, which results in the replacement of a non-bridging phosphate oxygen with a sulfur atom in either the pro-R or pro-S position, has proven to have extensive applications over the years (Figure 5-1). For example, the chiral phosphorothioate incorporated into RNA has been used to determine

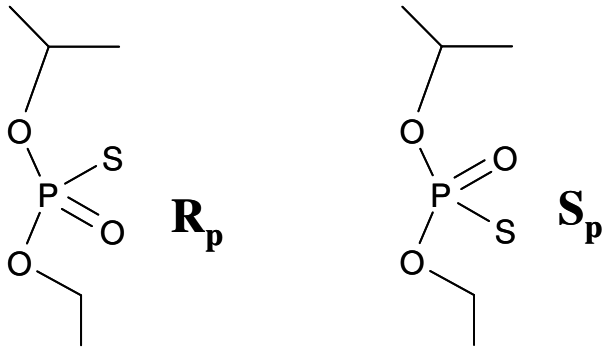

Figure 5-1: Pro-R and pro-S isomers arising from phosphorothioate substitution. Phosphorothioate substitution into nucleic acids results in the replacement of a non-bridging phosphate oxygen with a sulfur atom in either the pro-R or pro-S position.

the inversion of configuration at the phosphorus resulting from transcription by T7 RNA polymerase.[59] In addition, phosphorothioate-substituted DNA is important for gene therapy due to its ability to aid in drug targeting, suppress protein synthesis, and serve as an antisense therapeutic agent.[60, 61] In addition, phosphorothioate metal-rescue

experiments have been used extensively as a biochemical probe for locating metal-binding sites in functional RNAs. If a critical Mg^{2+} ion was directly coordinated to the oxygen that was replaced by the sulfur of the phosphorothioate, the activity should decrease. Activity may then be restored upon addition of a soft, thiophilic metal ion, such as Cd^{2+} or Hg^{2+}.[31] For example, Cd^{2+} has been observed by ^{31}P NMR to bind to the pro-R and pro-S sulfur of a phosphorothioate at the functionally important A9 site of the hammerhead ribozyme.[13] Even UV-vis spectroscopy has revealed a charge transfer band resulting from the coordination of a Hg^{2+} ion to the sulfur of a phosphorothioate at the active site of the hammerhead ribozyme.[14]

However, phophorothioate-Cd^{2+} interactions had not been studied in detail by UV-vis spectroscopy. It is already well-known that Cd^{2+} coordinates strongly to thiolates as their interaction absorbs intensely between 230-250 nm. Therefore, time-dependent density functional theory vertical excitation calculations using dimethyl thiophosphate to model phosphorothioates were performed, and predicted a detectable charge transfer band between the phosphorothioate and Cd^{2+} at ~235 nm. The calculations identified the transition as a ligand-to-metal charge transfer (LMCT) band due to the electron excitation from a molecular orbital predominantly sulfur in character into one that is mostly Cd-based.[62]

Results and Discussion

The major goals of the study presented in this chapter include the comparison of the wavelength of the LMCT predicted by these calculations to that derived from experimental results, and the determination of the apparent K_d values of Cd^{2+}-phosphorothioate complexes as models for RNA systems using UV-vis spectroscopy. A

boric acid/NaOH buffer was utilized due to its lack of absorbance in the high-energy region. A solution of Cd^{2+} (0.1 eq to 50 eq) was titrated into a solution of adenosine thiomonophosphate (AMPS) and an increase in absorbance at ~208 nm was clearly observed upon addition of increasing amounts of Cd^{2+}. Each individual spectrum was corrected for dilution and the absorbance of uncomplexed AMPS was subtracted. The resulting absorbance difference plot reveals an evident 208 nm feature as well as a smaller one at about 270 nm (Figure 5-2).

A binding affinity of Cd^{2+} for AMPS was determined by plotting the absorbance difference at 208 nm as a function of concentration of Cd^{2+} (M). The data were then fit to the following 1:1 binding model: [63]

$$A = \frac{A_{max}([Cd^{2+}]_{tot} + K_d + [AMPS]_{tot}\,b - (([Cd^{2+}]_{tot} + K_d + [AMPS]_{tot}\,b)^2 - 4b[AMPS]_{tot}[Cd^{2+}]_{tot})^{1/2}}{2b[AMPS]_{tot}}$$

where A_{max} is the maximum absorbance difference between the solution with the maximum concentration of Cd^{2+} with AMPS and the solution without AMPS, $[AMPS]_{tot}$ is the total concentration of AMPS, $[Cd^{2+}]_{tot}$ is the total concentration of Cd^{2+}, K_d is the apparent dissociation constant of Cd^{2+}, and b is the binding fraction, which is the number of bound Cd^{2+} compared to the total Cd^{2+}. An apparent K_d of ~ 3.7 ± 0.8 μM (10°C, pH = 8.0, 10 mM boric acid/NaOH buffer) was determined and compares relatively well with a previously reported value of 23 μM (25°C, pH = 7.5, 0.1 M $NaNO_3$) determined by potentiometric pH titrations.[64] In comparison, an apparent K_d of 400 μM (pH = 6.0, 0.1 M NaCl) was revealed by a Cd^{2+}-induced ^{31}P chemical shift change.[13] The stoichiometry of the AMPS-Cd complex was found to be 1:1 and its apparent extinction coefficient is ~ 4700 $M^{-1}cm^{-1}$ (Figure 5-2).

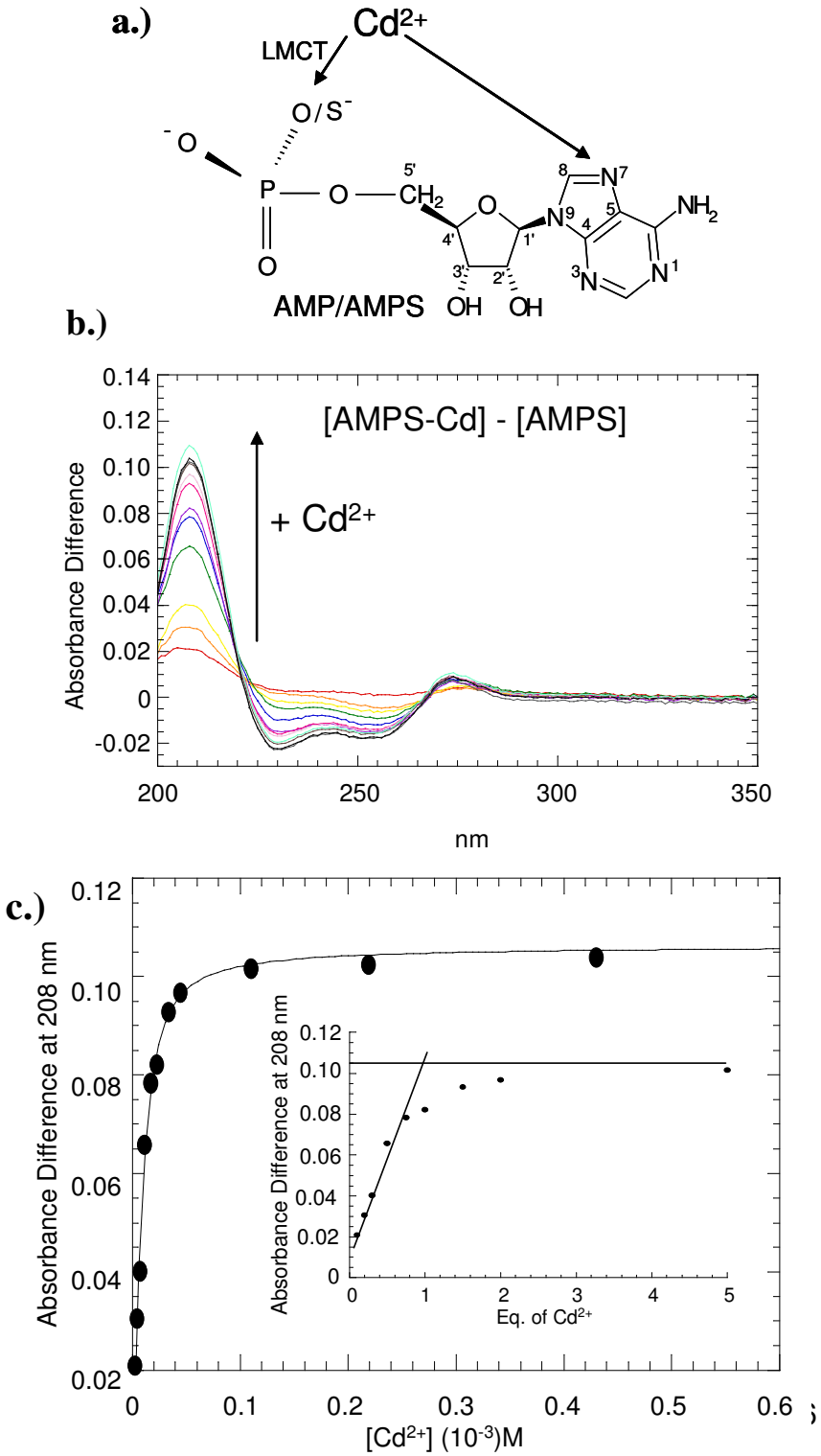

Figure 5-2: UV titration of Cd^{2+} to form AMPS-Cd complex. a.) AMPS-Cd complex b.) Plot of absorbance difference as a function of wavelength. Feature at 208 nm is proposed to be due to a ligand-to-metal-charge transfer band between the sulfur of the phosphorothioate-substituted mononucleotide and Cd^{2+}. c.) Binding curve of absorbance difference at 208 nm as a function of Cd^{2+} concentration. Data fit to equation 1 to yield $K_{d\ app}$ of ~3.7 $\pm$0.8 µM. $CdCl_2$ was added to 23 µM AMPS in 10 mM boric acid/NaOH, pH of 8.0 at 10°C. The inset of the plot of the absorbance difference at 208 nm as a function of equivalents of Cd^{2+} reveals the 1:1 binding ratio.

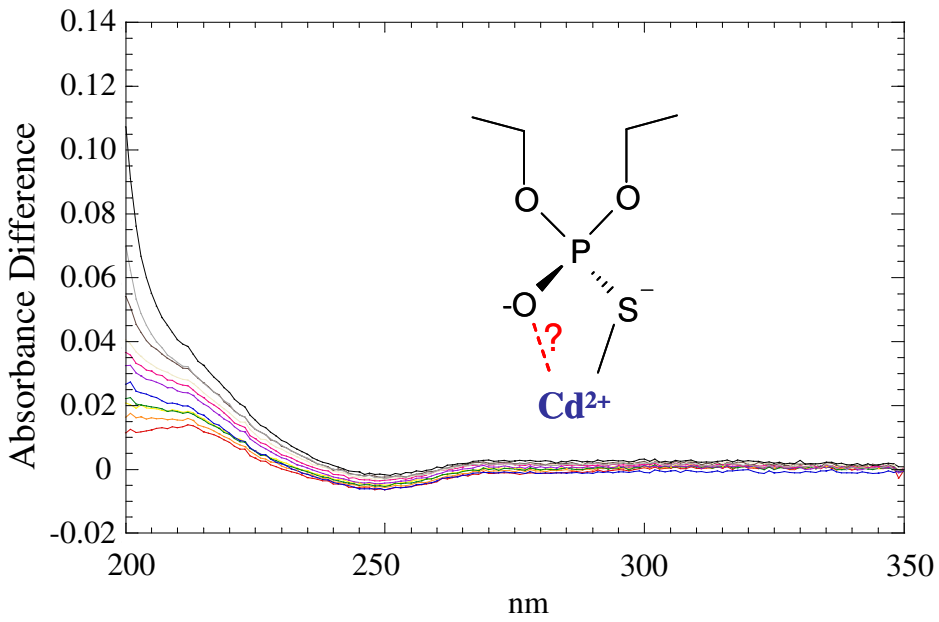

Figure 5-3: UV titration of Cd^{2+} to form DETP-Cd complex. a.) DETP-Cd complex Plot of absorbance difference as a function of wavelength of the DETP-Cd complex. The absorbance difference spectrum reveals a charge transfer band at ~ 208 nm. However, due to the absence of a clear peak at 208 nm upon an increasing amount of Cd^{2+}, a binding curve could not be generated. DETP-Cd complex shown in inset.

A control experiment in which Cd^{2+} was titrated into a solution of adenosine monophosphate (AMP) revealed no increase in the absorbance, confirming the assignment of the 208 nm feature arising from a cadmium – sulfur interaction (Data not shown). For comparison, variations on the phosphorothioate compound and its interactions with Cd^{2+} were studied. Complexation of diethyl thiophosphate (DETP) with Cd^{2+} was shown by an increase in the absorbance as well; however, due to the absence of a distinctive peak, a $K_{d\ app}$ could not be determined (Figure 5-3). Adenosine 5'O-3-thiotriphosphate (ATPγS) and Cd^{2+} were revealed to have an extremely tight apparent dissociation constant of 0.4 μM and the stoichiometric ratio of ATPγS:Cd is 1:1 as well. The apparent extinction coefficient is ~ 4450 $M^{-1}cm^{-1}$ (Figure 5-4).

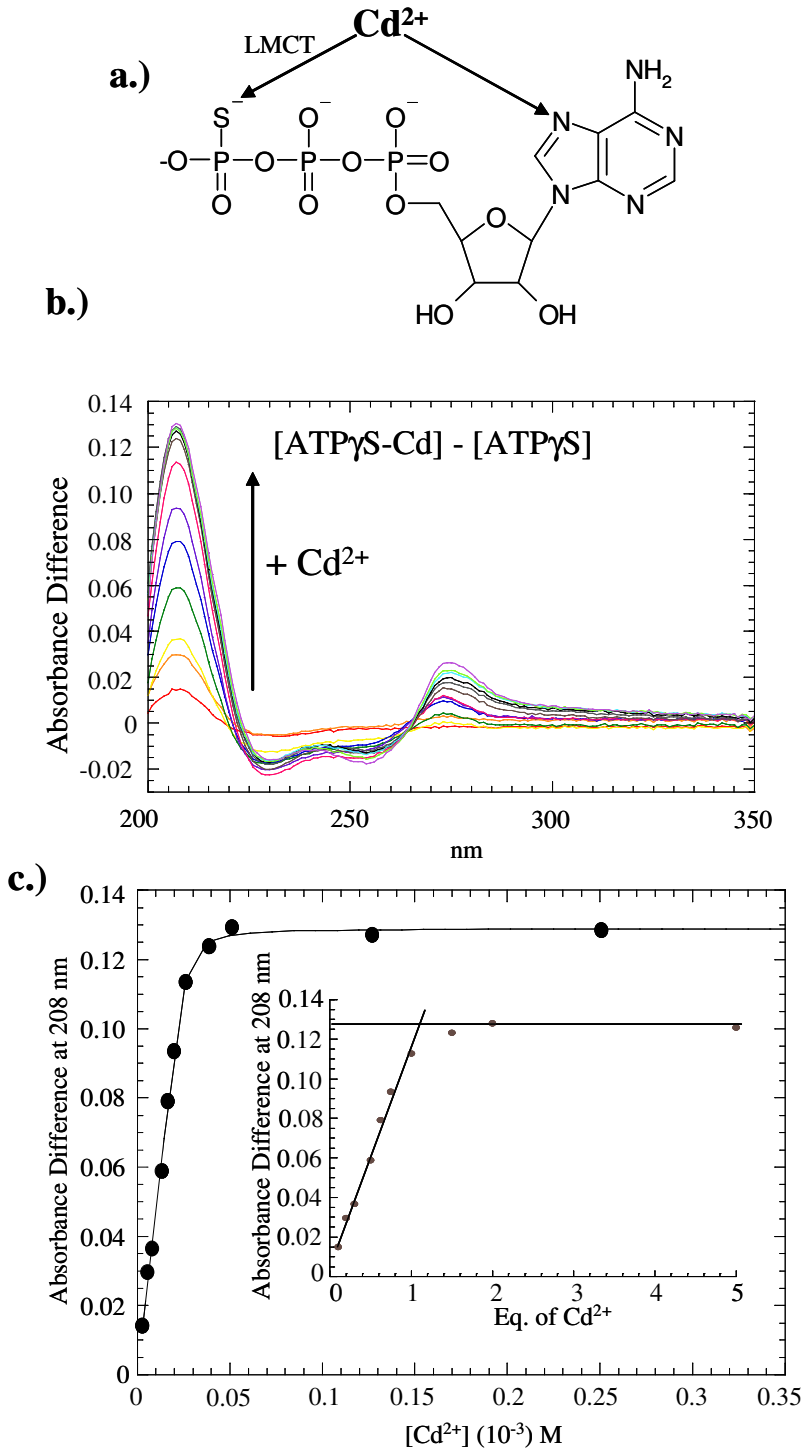

Figure 5-4: UV titration of Cd^{2+} to form ATPγS-Cd complex a.) ATPγS-Cd complex b.) Plot of absorbance difference as a function of wavelength of the ATPγS-Cd complex. The absorbance difference spectrum reveals the same features at 208 nm and 270 nm. c.) Binding curve of absorbance difference at 208 nm as a function of Cd^{2+} concentration. Data fit to equation 1 to yield $K_{d\ app}$ of ~ 0.4 µM. $CdCl_2$ was added to 26.7 µM ATPγS in 10 mM boric acid/NaOH, pH of 8.0 at 10°C. The inset of the plot of the absorbance difference at 208 nm as a function of equivalents of Cd^{2+} reveals the 1:1 binding ratio.

The apparent binding affinities may be explained by the extent of coordination of the Cd^{2+} ion with the various phosphorothioates. The Cd^{2+} ion most likely binds to the DETP molecule at only one site, the sulfur atom (Figure 5-3(a.)). However, in addition to the sulfur atom of the phosphorothioate group, AMPS provides the N7 of its adenine base for potential coordination of Cd^{2+} (Figure 5-2(a.)). A possible indication for this may be the small 270 nm feature observed in the difference spectrum since a bathochromic shift is observed upon the formation of a metal-purine coordinate covalent bond.[65] This additional coordination site may contribute to a tighter binding constant. ATPγS, consisting of two phosphates and one phosphorothioate group, has more potential binding sites, thereby leading to more complex and tighter binding with chelation from the triphosphate group (Figure 5-4(a.)).

To verify that the 208 nm feature arises from the formation of the AMPS-Cd complex, EDTA titrations were performed to observe the reversibility of the putative charge transfer band. The 208 nm absorbance feature decreased upon increasing additions of EDTA, indicating the source of the absorbance feature at 208 nm results from the LMCT band of the AMPS-Cd complex (Figure 5-5). In addition, this LMCT was not observed when AMPS was in the presence of either Mn^{2+} or Co^{2+} in solution.

Conclusion

In conclusion, this unique 208 nm feature arises specifically from a Cd^{2+}-phosphorothioate interaction and this could be the first reported charge transfer band between Cd^{2+} and phosphorothioates. The calculated and experimental wavelengths are different, which could arise from the dependence of the calculated charge transfer band based on the geometry around the phosphorus.[62] This simple technique using UV-vis

spectroscopy may serve as a probe that confirms Cd^{2+}- S coordination, which is important in understanding metal sites in RNA. In addition, it may have a potential application in determining the affinity of Cd^{2+} for phosphorothioate-substituted oligonucleotides.

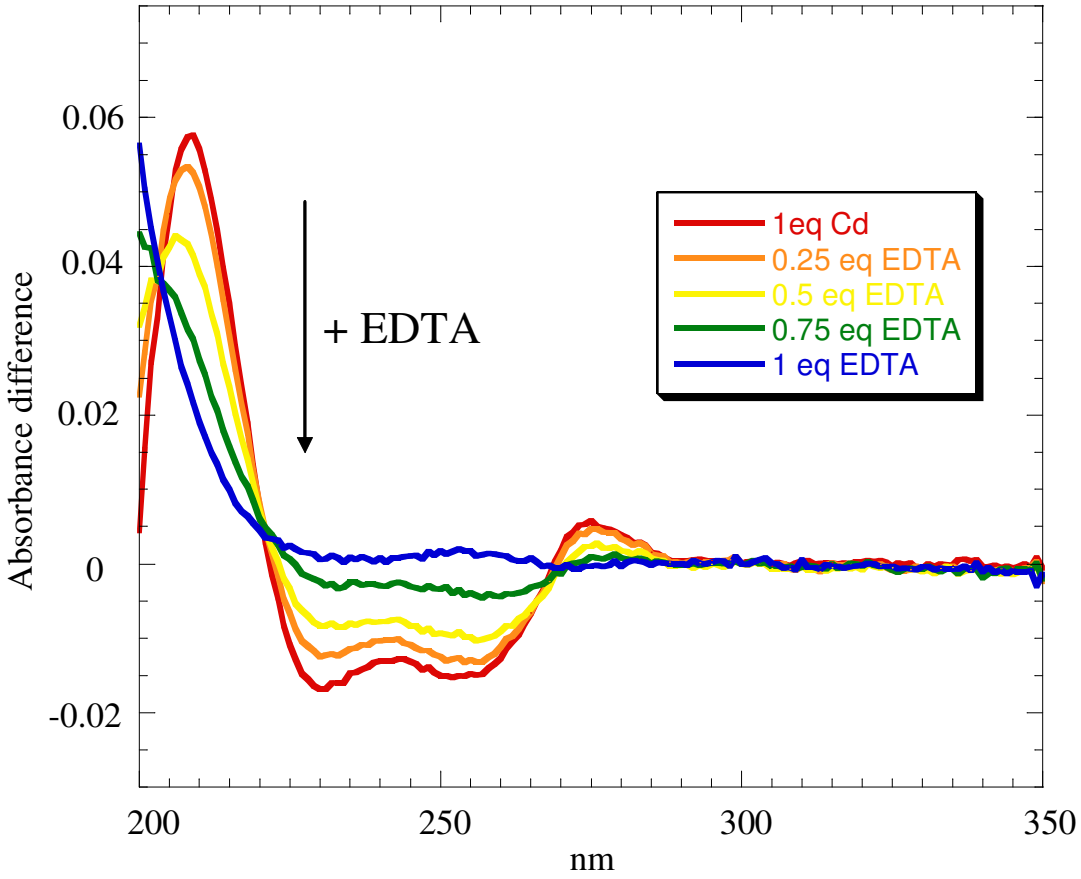

Figure 5-5: EDTA – AMPS-Cd complex competition studies. The feature at 208 nm is reversible, precluding the possibility of disulfide bond formation as the source of the feature.

CHAPTER VI

CONCLUSION

Summary

The research described in this thesis focused on the four-way junction construct of the hairpin ribozyme, since it is a better representation of the native conformation in the viral RNA genome, it is catalytically active under physiological conditions, and it is more stable than the simpler hinged construct. The goals of the work presented in this thesis are the characterization of this four-way junction construct of the hairpin ribozyme and the investigation of a putative metal-binding site within the four-way junction to further clarify the catalytic/structural role of metal ions in the hairpin ribozyme. Native gels, UV-detected thermal denaturation, kinetics, and EPR spectroscopy were employed in the investigation.

The full characterization of the four-stranded four-way junction construct of the hairpin ribozyme and of the isolated four-way junction mutant hairpin ribozyme was achieved by a multi-lateral approach applying three techniques: native gels, thermal denaturation, and kinetics experiments.

The application of these three techniques provided consistent and valuable information. Each thermal denaturation melt profile of the hairpin ribozyme and of the mutant was unique and complex, and the transitions were assigned as specific unfolding events for each stem. For example, Transition 1 of the melt profile of the hairpin ribozyme is a result of the simultaneous unfolding of Stems A and B, Transition 2 indicates the unfolding event of Stem C, and finally Transition 3 results from the destabilization of Stem D. In addition, native gels revealed not only the homogeneity of

the hairpin ribozyme and the mutant in solution, but the presence of other possible strand combinations as well. In fact, the results from native gels and UV melts were consistent.

The melting temperatures of the individual stems in the absence of divalent metal ions underscored the sensitivity of the ribozyme to temperature and the need for metal ions in the native gel and running buffer for stabilization. The melt profile provided valuable information for optimizing conditions in native gel electrophoresis, which was used to determine the homogeneity of the hairpin ribozyme in solution. Therefore, the application of native gel electrophoresis for the complexation of four RNA strands was successful. Finally, activity studies confirmed the homogeneity of the hairpin ribozyme in solution based on the percent of cleaved product.

The final goal of investigating the divalent metal ion interactions with the four-way junction construct of the hairpin ribozyme, particularly within its four-way junction, was accomplished. The qualitative resemblance of the EPR binding isotherms of the hairpin ribozyme and its loopless mutant, all of which were fit to one type of metal-binding sites, suggests that there are similar electrostatic metal-RNA interactions within or in the vicinity of the four-way junction of the hairpin ribozyme. It appears that most of the metal binding is not within the loops, but instead is with the stems and four-way junction. These critical electrostatic interactions within the stems and four-way junction must aid in the positioning of the loops into the docked state. Despite the fit to one type of low-affinity metal-binding sites, low-temperature EPR spectroscopy suggests inner-sphere coordination of Mn^{2+} to the hairpin ribozyme, and possibly to the N7 of a guanine. However, the possibility of direct Mn^{2+} coordination to specifically the four-way junction or its vicinity could not be confirmed.

Another novel result is the activity of the four-way junction construct of the hairpin ribozyme in the presence of Mn^{2+}. Previously, Mn^{2+} ions were reported to have the sole ability to promote the docking of the four-way junction construct of the hairpin ribozyme. However, this divalent metal ion did not support cleavage under these conditions. This observation is not the case in the experiments presented in this thesis and the discrepancy is explained by the different buffer conditions. The apparent binding affinity of catalytically relevant Mn^{2+} ions is very similar to that of Mg^{2+}, confirming the nondiscriminatory metal dependence of the activity of the hairpin ribozyme. On a similar note, UV thermal denaturation metal dependence studies reveal an overall similarity in the apparent binding affinities of divalent metal ions associated with each transition. Therefore, Mg^{2+} and Mn^{2+} ions are able to stabilize the global structure of each stem of the hairpin ribozyme in a similar manner. At this point, it is important to caution that interpretations of thermal denaturation studies may not be accurate due to the inability of models to take into account the differing energetic contributions of diffuse and site-specific metal binding. As a result, a tight metal-binding site revealed by thermal denaturation may in fact be a collective group of nonspecific electrostatic interactions.[10]

The apparent binding affinities of the catalytically relevant metal ions are weaker than those of the metal ions that globally stabilize the structure of the hairpin ribozyme as indicated by thermal denaturation. This observation is consistent with that of the hammerhead ribozyme and the HDV ribozyme, both of which require a structurally important high-affinity metal-binding site. However, higher metal ion concentrations are required for catalysis, during which a second type of metal site must be occupied with a weaker affinity.[31] Therefore, in the case of the hairpin ribozyme, the population of

structurally-important metal-binding sites must occur to cause the large conformational change that promotes loop-loop interaction. However, the occupation of a weaker type of metal-binding site is required to promote cleavage, though it may only cause a small conformational change.

Finally, the first ligand-to-metal charge transfer band arising from the interaction of a Cd^{2+} ion with the phosphorothioate of a mononucleotide was reported in this thesis. The charge transfer band was manifested as a unique feature at 208 nm. This experimental wavelength is different than that calculated by time-dependent density functional theory. The difference could arise from the dependence of the calculated charge transfer band based on the geometry around the phosphorus.[62] This simple technique using UV-vis spectroscopy may serve as a probe that confirms Cd^{2+}- S coordination, which is important in understanding metal sites in RNA. In addition, it may have a potential application in determining the affinity of Cd^{2+} for phosphorothioate-substituted oligonucleotides.

Future Work

Despite the potential problems of annealing four strands, full characterization of these four strands in solution revealed a homogeneous solution of the fully functional hairpin ribozyme. Therefore, this four-stranded four-way junction construct of the hairpin ribozyme is an effective and reliable model for further investigating its interactions with divalent metal ions.

To confirm the catalytically/structurally significant metal binding site within the four-way junction of the hairpin ribozyme, site-specific modifications, such as phosphorothioate substitutions, deoxy-modifications, and base modifications, will be

necessary. Specifically, for phosphorothioate-substitution into a nucleic acid in conjunction with EPR or ^{31}P NMR could be ideal techniques for locating metal-binding sites in the phosphodiester backbone in the hairpin ribozyme. However, the chemical synthesis of phosphorothioate-substituted RNA results in an approximate equal ratio of Rp and Sp diastereomers. Therefore, the separation of these diastereomers is achieved by HPLC and is only practical for strands that do not exceed 40 nucleotides. As a result, a four-stranded hairpin construct was chosen that meets this critical limitation.

Low-Temperature EPR Spectroscopy of the Loopless Mutant

The low-temperature EPR spectrum of the loopless mutant should ideally suggest whether or not the possibility of a Mn^{2+} ion is bound within the four-way junction. Under the same substoichiometric ratio conditions, if the EPR spectra of the hairpin ribozyme and the mutant match well, then one could postulate that the high-affinity metal-binding site within the hairpin ribozyme is in the vicinity of the four-way junction.

Low-Temperature EPR Microwave Power Saturation Studies

Another technique that could be applied is low-temperature EPR microwave power saturation, which should detect a cluster of metal ions. Metal ions in close proximity (less than 20Å) increase the number of relaxation pathways, thereby requiring a greater amount of power to saturate the EPR signals. Upon addition of increasing equivalents of Mn^{2+}, the microwave power at half saturation should increase if there are metal ions in close proximity.[11]

According to the EPR binding isotherm four-way junction construct of the hairpin ribozyme in 25 mM NaCl, four Mn^{2+} ions are bound in 50 μM Mn^{2+}, 5 mM TEA, pH 7.8. Therefore, up to 4 equivalents of Mn^{2+} may be added to the hairpin ribozyme. Based on

the point at which a power increase is observed, the order of population of metal binding sites may be predicted. According to room-temperature EPR spectroscopy, the metal-binding site with the highest affinity should be within or in the vicinity of the four-way junction. If there is a sudden power increase upon the addition of 2 equivalents of Mn^{2+}, a second metal-binding site within the four-way junction may be a possibility. On the other hand, an absence of or a slight power increase would suggest a metal-binding site further away, perhaps within Loop B. A confirmation of this location would be demonstrated by a subsequent increase in power upon the addition of 3 equivalents of Mn^{2+}, which would point to another metal-binding site in close proximity to that of Loop B. This site may be contained either within Loop B or between the docked loops. Disadvantages of this technique, however, include ambiguity in determining the order of populating metal binding sites or their exact location. Nonetheless, examination of the microwave power saturation results in conjunction with results from other techniques, including ^{31}P NMR and EPR spectroscopy, should ideally provide invaluable insight to further the ongoing investigation on the role of metal ions within the hairpin ribozyme.

Probing for Specific Metal-Binding Sites by ^{31}P NMR and Phosphorothioate Substitution

To confirm the presence of a critical metal-binding site within the four-way junction of the hairpin ribozyme, phosphorothioate-substitution in conjunction with ^{31}P NMR spectroscopy may be employed. ^{31}P NMR spectroscopy can be used to monitor the signal shifts induced by the addition of thiophilic Cd^{2+} to the single phosphorothioate-modified hairpin ribozyme. The signal of a phosphorothioate can be easily observed by its downfield shift of ~50 ppm from the overlapping signals of unmodified phosphates. An upfield shift of 2-3 ppm with the addition of Cd^{2+} suggests direct coordination of the

Cd^{2+} ion to the sulfur of the phosphorothiate is occurring and confirms the presence of a metal binding site. The apparent dissociation constant, K_d, for one single bound metal will indicate its affinity for the binding region under study.[13]

This technique was applied to two sites in the hammerhead ribozyme.[13] Although a phosphorothioate modification is generally considered as a conservative change, there are a few reports of RNA structures sensitive to this alteration.[31] Therefore, it is necessary to verify whether the conformation of the hairpin ribozyme remains unaltered upon phosphorothioate modification. If the conformation of the hairpin remains constant, phosphorothioate-rescue experiments can be employed to test whether activity of the phosphorothioate-substituted hairpin ribozyme is rescued in the presence of Cd^{2+}, thereby suggesting a functional role of the metal binding site. Phosphorothioate substitutions in each of the three potential metal binding regions may reveal the role of metal ions.

REFERENCES

1. DeRose, V.J.; Burns, S.; Vogt, M.; Kim, N.-K. In *Comprehensive Coordination Chemistry II* J.A. McCleverty, T.J. Meyers, Eds., Elsevier: Oxford, 2003, p.787.
2. Tinoco, I.; Bustamante, C. *J. Mol. Biol.* **1999**, *293*, 271.
3. Pyle, A. M. *J. Biol. Inorg. Chem.* **2002**, *7*, 679.
4. Treiber, D.K., Rook, M.S., Zarrinker, P.P., Williamson J.R. *Science* **1998**, *279*, 1943.
5. Pan, J., Thirumalai D., Woodson, S.A. *J. Mol. Biol.* **1997,** *273*, 7.
6. Misra, V. K.; Draper, D. E. *Biopolymers*, **1998**, *48*, 113.
7. Thirumalai, D.; Lee, N.; Woodson, S.A.; Klimov, D.K. *Annu. Rev. Phys. Chem.* **2001,** *52*, 751.
8. Brion, P.; Westhof, E. *Annu. Rev. Biophys. Biomol. Struct.* **1997***, 26*, 113.
9. Feig, A.L.; Uhlenbeck, O.C. In *RNA World*, 2nd Edition; Gesteland, R. F.; Cech, T. R.; Atkins, J. F., Eds; Cold Spring Harbor Laboratory Press: Cold Spring Harbor, NY 1999, p. 287.
10. Draper, D. E. *RNA* **2004** *10*, 335.
11. Vogt, M.; DeRose, V.J. In *Paramagnetic Resonance in Metallobiomolecules*; J. Telser, Ed.; ACS Books, Washington D.C. 2003, p.193.
12. Horton, T.E.; Clardy, D.R.; DeRose, V.J. *Biochemistry* **1998***, 37*, 18094.
13. Maderia, M.; Hunsicker, L. M.; DeRose, V. J. *Biochemistry* **2000**, *39*, 12113.
14. Cunningham, L. A.; Li, J.; Lu, Y. *J. Am. Chem. Soc.* **1998**, *120,* 4518.
15. Walter N.G.; Yang, N.; Burke, J.M. *J. Mol. Biol.* **2000**, *298*, 539.
16. Feig, A. L.; Panek, M.; Horrocks, W. D.; Uhlenbeck, O. C. *Chem. Biol.* **1999**, *6*, 801.
17. Matzke, M.; Matzke, A. J. M. *Science*, **2003**, *301*, 1060.

18. Kruger, K.; Grabowski, P.J.; Zaug, A. J.; Sands, J.; Gottschling, D. E.; Cech, T. R. *Cell* **1982**, *31*, 147.

19. Guerrier-Takada, C.; Gardiner, K.; Marsh, T.; Pace, N.; Altman, S. *Cell*, **1983**, *35*, 849.

20. Doudna, J.A.; Cech T.R. *Nature* **2002,** *418*, 222.

21. Tanner, N.K. *FEMS Microbiol. Rev.* **1999***, 23*, 257.

22. Hampel, K. J.; Walter, N.G.; Burke, J.M. *Biochemistry* **1998,** *37*, 14672.

23. Fedor, M.J. *J. Mol. Biol.* **2000**, *297*, 269.

24. Buzayan, J.M.; van Tol, H.; Zalloua, P.A.; Bruening, G. *Virology* **1995,** *208*, 832.

25. Takagi, Y.; Warashina, M.; Stec, W.J.; Yoshinari, K.; Taira, K. *Nucl. Acid. Res.* **2001,** *29*, 1815.

26. Fedor, M.J. *J. Mol. Biol.* **2001***, 309*, 893.

27. Zhao, Z.; Wilson, T.J.; Maxwell, K.; Lilley D.M.J. *RNA* **2000***, 6*, 1833.

28. Tan, E.; Wilson, T.J.; Nahas, M.K.; Clegg, R.M.; Lilley, D.M.J.; Ha, T. *Proc. Natl. Acad. Sci.* **2003,** *100*, 9308.

29. Pljevaljčić G.; Millar, D.P.; Deniz, A.A. *Biophys. J.* **2004**, *87*, 457.

30. Young, K.J.; Gill, F.; Grasby, J.A. *Nucl. Acid. Res.* **1997**, *25*, 3760.

31. DeRose, V.J. *Curr. Op. Struct. Biol.* **2003,** *13*, 317.

32. Walter, F.; Murchie, A.I.H.; Thomson, J.B.; Lilley, D.M.J. *Biochemistry* **1998**, *37*, 14195.

33. Chowrira, B.M.; Burke, J.M. *Biochemistry* **1991**, *30*, 8518.

34. Cai, Z.; Tinoco, Jr. I. *Biochemistry* **1996,** *35*, 6026.

35. Ferré-D'Amaré, A.R.; Rupert P.B. *Nature* **2001***, 410*, 780.

36. Murray, J.B.; Sehyan, A.A.; Walter, N.G.; Burke, J.M.; Scott, W.G. *Chem. Biol.* **1998**, *5*, 587.

37. Nesbitt, S.; Erlacher, H.A.; Fedor M.J. *J. Mol. Biol.* **1999***, 286*, 1009.

38. Earnshaw , D.J.; Gait, M.J. *Nucl. Acid. Res.* **1998,** *26*, 5551.

39. Butcher, S.E.; Allain, F.H.T.; Feigon, J. *Biochemistry* **2000**, *39*, 2174.

40. Klostermeier, D.; Millar, D.P. *Biochemistry* **2000**, *39*, 12970.

41. Kirchner, A.J.; M.S. Thesis, Texas A&M University, College Station, TX, 2002.

42. Hohng, S.; Wilson, T. J.; Tan, E.; Clegg, R. M.; Lilley, D. M.; Ha, T. *J. Mol. Biol.* **2003**, *336*, 69.

43. Wilson, T.J.; Lilley, D.M.J. *RNA* **2002**, *8*, 587.

44. Silverman, S. K.; Cech, T. R. *Biochemistry* **1999**, *38*, 8691.

45. Hendry, P.; McCall, M.J.; Lockett, T.J. In *Ribozyme Protocols;* P.L. Turner, Ed Humana Press: Totowa, NJ, 1997, p. 221.

46. Christopher, J., *Tmelt* [computer program]; Texas A&M University, College Station, TX, 1998.

47. Theimer C.A.; Wang, Y.; Hoffman, D.W.; Krisch, H.M.; Giedroc, D.P. *Journal of Molecular Biology* **1998***, 278*, 545.

48. Klostermeier, D.; Millar, D.P. *Biochemistry,* **2002**, *41*, 14095.

49. Laing, L.G.; Gluick, T.C.; Draper, D.E. *Journal of Molecular Biology* **1994,** *237*, 577.

50. Misra, S. K. *Physica B* **1997**, *240*, 183.

51. Kuzmin, Y.I.; Da Costa, C.P.; Fedor, M.J. *J. Mol.Biol.* **2004**, *340*, 233.

52. Chowrira, B.M.; Berzal-Herranz, A.; Burke, J.M. *Biochemistry*, **1993**, *32*, 1088.

53. Meroueh, M.; Chow, C. S. *Nucleic Acids Res.* **1999**, *27*, 1118.

54. Zhuang, X.; Kim, H.; Pereira, M.J.B.; Babcock, H.P.; Walter, N.G.; Chu, S. *Science*, **2002**, 296, 1473-1476.

55. Vogt, M. J. Ph.D. Dissertation, Texas A&M University, College Station, TX, 2004.

56. Burns, S. Ph.D. Dissertation, Texas A&M University, College Station, TX, 2004.

57. Morrissey, S.R.; Horton, T.E.; DeRose, V.J. *J. Am. Chem. Soc*. **2000**, *122*, 3473.

58. De Meester, P.; Goodgame, D. M.; Jones, T. J.; Skapski, A. C. *Biochem. J.* **1974**, *139*, 791.

59. Griffiths, A. D.; Potter B. V.; Eperon I. C. *Nucleic Acids Res.* **1987**, *15*, 4145.

60. Kanaori, K.; Sakamoto, S.; Yoshida, H.; Guga, P.; Stec, W.; Tajima, K.; Makino, K. *Biochemistry* **2004**, *43*, 5672.

61. Agrawal, S.; Kandimalla, E. R. *Mol. Med. Today* **2000**, *6*, 72.

62. Hunsicker-Wang L. M.; PhD. Dissertation, Texas A&M University, College Station, TX, 2001.

63. Chen, X.; Chu, M.; Giedroc, D. P. *J. Biol. Inorg. Chem.* **2000**, *5*, 93.

64. Sigel, R.K.O.; Song, B.; Sigel, H. *J. Am. Chem. Soc.* **1997**, *119*, 744.

65. Orenberg, J. B.; Kjos, K. M.; Winkler, R.; Link, J.; Lawless, J.G. *J. Mol. Evol.* **1982**, *18,* 137.

APPENDIX

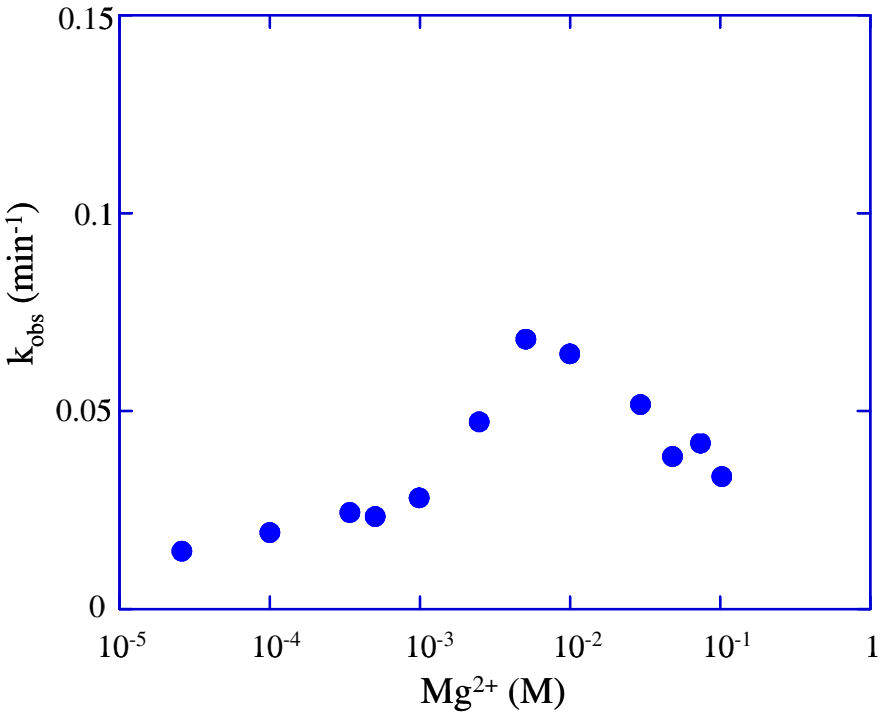

Figure A-1: Effect of ligation on the Mg^{2+}-dependent rate profile of the hairpin ribozyme with the shortened d substrate strand. A drop in observed activity was observed instead of a sigmoidal curve.

VITA

Aurélie L. Buckelew was born in Sacramento, California on August 14, 1979. She traveled all over the world and attended four different high schools in four years. She attended The Madeira School in McLean, Virginia in 10th grade, and studied in the International Baccalaureate program at the Bahrain International School the following year. She graduated from L.D. Bell High School in Hurst, Texas in 1997. She finally settled down in College Station, TX where she earned a B.A. in Chemistry and a minor in French at Texas A&M University. She graduated Magna Cum Laude in May 2001. She remained at Texas A&M University and joined the DeRose group in 2002. In May of 2005, she earned her M.S. degree in Chemistry. Aurélie can be reached through her parents at 3709 Woodmont Court, Bedford, Texas 76021.